SERS-Based Nanoparticle Biodetection Using Carbohydrate-Lectin Interactions

Jonathan Robert Henry Simpson

June 2016

This thesis is the result of the author's original research. It has been composed by the author and has not been previously submitted for examination which has led to the award of a degree.

Signed: Date:

Acknowledgements

I would like to thank all those who have helped and supported me throughout my postgraduate study. I would like firstly to thank Professor Duncan Graham and Professor Karen Faulds for their support and advice throughout my studies. Their patience and guidance have been invaluable both prior to, during and following completion of the research projects which I have been involved in and I greatly appreciate the opportunities they have given me in travelling abroad to conferences and visit other Universities.

While there are too many to name individually, I would like to thank all those members of the Centre for Molecular Nanometrology both past and present for making the group a great place to study. I would like to thank Dr Derek Craig for his support during the early parts of my studies. His inputs were always of great help and never without humour. I would also like to thank Dr Sarah McAughtrie, Dr Mhairi Harper and Mr Alan Hutton for providing invaluable insights into my research for putting up with my often awful chat, for that I am grateful.

I have been helped by a great number of post-doctoral researchers throughout my post-graduate studies. In particular I would like to thank Dr Lee Barrett, Dr Samuel Mabbott and Dr Stacey Laing for taking the time to not only answer my questions but also volunteer assistance throughout my postgraduate study.

I would also like to thank Christopher Steven. He has never tired of offering support, valued opinions and a helpful ear both as a fellow postgraduate student and as a friend.

I would like to thank my family and friends for all the support they have given me before, during and after my studies.

Finally though by no means least, I would like to thank my future wife, Rachel Black. Her support throughout my studies have meant everything to me and her positivity gives me strength in all I do.

Abstract

Endogenous biological processes including cellular recognition, motility and differentiation together with infection often result from carbohydrate-based interactions. Investigation into glycobiological interactions using sugar-coated nanoparticles are the basis for the research described herein.

Metallic nanoparticles were coated with a variety of thiol-based linker molecules. Heterobifunctional PEG (carboxyl/thiol) molecules were found to be most successful in preventing non-specific aggregation. The carboxylic acid functionality of the PEG molecules used allowed for subsequent coupling of a variety of carbohydrates to the nanoparticle surface. This resulted in the production of glyconanoparticles with unique surface functionality, for example, glucose or galactose. Additionally, functionalising the particles with Raman reporter molecules (RRMs) resulted in the measurement of surface enhanced Raman scattering (SERS) signals. Aggregation of the glyconanoparticles in the presence of a variety of carbohydrate-binding proteins (lectins) was measured *via* changes in the extinction profile, size and the SERS response of those particles. Nanoparticle aggregation was used for the sensitive detection of plant lectins, including the Concanavalin A and Jacalin lectin and also bacterial lectins including cholera toxin B subunit (CTB). CTB was detected sensitively, selectively and rapidly by using glyconanoparticles coated in a mixture of different carbohydrates (mixed-monolayers of galactose and N-acetylneuraminic acid). Detection was possible in both buffer and synthetic freshwater conditions, demonstrating the use of these glyconanoparticles in detecting a target in complex samples.

By exploiting the reversible nature of carbohydrate-lectin interactions, it was possible to use the glyconanoparticles together with the lectin ConA to develop a glucose sensor. This performed effectively across the physiological range and into the hypo/hyperglycaemic regions in buffer conditions.

Finally, the glyconanoparticles were used for the detection of plant and bacterial lectins on glass substrates by initially developing a sandwich SERS assay with a view to eventually creating SERS-based carbohydrate microarrays.

Abbreviations

The following are the abbreviated terms used throughout the report.

APGAP	– 4-Aminophenyl-β-D-Galactopyranoside
ATPEG	– Amine/Thiol Poly (Ethylene Glycol)
Asn	– Asparagine
Asp	– Aspartic Acid
ATP	– Adenosine Triphosphate
BSA	– Bovine Serum Albumin
cAMP	– 3',5'-Cyclic Adenosine Monophosphate
CCD	– Charge-Coupled Device
ConA	– Concanavalin A
CTB	– Cholera Toxin B Subunit
CAPEG	– Carboxyl/Amine Poly (Ethylene Glycol)
CTPEG	– Carboxyl/Thiol Poly (Ethylene Glycol)
DLS	– Dynamic Light Scattering
DMSO	– Dimethyl sulfoxide
DNA	– Deoxyribose Nucleic Acid
DTT	– Dithiothreitol
E. Coli	– Escherichia Coli
EDC	– 1-Ethyl-3-(3-dimethylaminopropyl)carbodiimide Hydrochloride
ELISA	– Enzyme Linked Immunosorbent Assay
Gal	– Galactose Functionality
Glu	– Glucose Functionality

Abbreviations

Gly	– Glycine
HEPES	– 4-(2-Hydroxyethyl)-1-Piperazineethanesulfonic Acid
HIV	– Human Immunodeficiency Virus
IR Spectroscopy	– Infra-Red Spectroscopy
Leu	– Leucine
LOD	– Limit Of Detection
LSPR	– Localised Surface Plasmon Resonance
Man	– Mannose Functionality
MAPEG	– Methoxy/Amine Poly (Ethylene Glycol)
MHA	– 6-Mercaptohexanoic Acid
MHL	– 6-Mercapto-1-Hexanol
MTPEG	– Methoxy/Thiol Poly (Ethylene Glycol)
NPs	– Nanoparticles
PA	– Pseudomonas Aeruginosa
PCR	– Polymerase Chain Reaction
PEG	– Poly (Ethylene Glycol)
Phe	– Phenyl Aniline
RRM	– Raman Reporter Molecule
SEM	– Scanning Electron Microscopy
SERS	– Surface Enhanced Raman Spectroscopy
SERRS	– Surface Enhanced Resonance Raman Spectroscopy
Sia	– N-acetyl Neuraminic Acid (Sialic Acid) Functionality
SPR	– Surface Plasmon Resonance

Abbreviations

sNHS	– N-hydroxysulfosuccinimide sodium salt
TFA	– Trifluoroacetic Acid
Tris	– Tris(hydroxymethyl)aminomethane
Trp	– Tryptophan
Tyr	– Tyrosine
UV-vis.	– UV-visible

Abbreviations

The following are the abbreviations of units used throughout the report.

au	– Arbitrary Unit
nm	– Nanometre
µL	– Microlitre
mL	– Millilitre
L	– Litre
ng	– Nanogram
µg	– Microgram
mg	– Milligram
g	– Gram
kg	– Kilogram
pM	– Picomolar
nM	– Nanomolar
µM	– Micromolar
mM	– Millimolar
M	– Molar
min	– Minute
hr	– Hour
°C	– Degree Celsius
Pa	– Pascal
rpm	– Revolution Per Minute

Table Of Contents

Introduction

Nanoparticles offer a versatile platform for a wide variety of applications including biosensing, targeted drug-delivery and catalysis.[1-4] The field of nano-chemistry has been rapidly expanding in recent times and the number of related publications has increased exponentially.[5, 6] Related research has included the development and subsequent application of nanoscale structures and features for biomedical purposes.[7] Nanoscale structures include nanoparticles for example spheres, rods and stars and have been used in research for imaging, mapping and target biosensing.[8-11] Nanoparticle biosensors are generated through surface functionalisation with species that have affinity towards particular targets.[12-15] The multivalency of the nanoparticles and, potentially, the target can result in the formation of aggregation of the particles which can subsequently be detected using a variety of spectroscopic techniques, including surface enhanced Raman spectroscopy (SERS) and extinction spectroscopy. Aggregation of particles in this way can be used to detect a target of interest.

Nanoparticle bioassembly formation has been used for the detection of a large number and variety of targets. Early research demonstrated the application of metallic nanoparticles to biosensing. In 1996, Mirkin *et al.* illustrated the formation of gold nanoparticle assemblies through complementary DNA-DNA interactions.[13] Nanoparticle aggregation was observed when thiolated DNA on the nanoparticle surface interacted with target DNA strands in solution. A change in extinction, notably a red-shift, was observed upon this interaction by UV-visible (UV-vis.) extinction spectroscopy.[13] This phenomenon has subsequently been exploited for the detection of DNA molecules specific to infection and disease.[15-17]

Nanoparticle functionalisation has also been achieved with proteins, for example antibodies and antigens. Zhang *et al.* functionalised gold nanoparticles with goat-anti-rabbit immunoglobin G for the detection of rabbit-anti-human immunoglobin G using inductively coupled plasma mass spectrometry.[18]

Investigations into carbohydrate-protein interactions and their applications in nanoparticle biodiagnostics have recently garnered interest. Barrientos *et al.* first used the term glyconanoparticles in 2003 to describe nanoparticles functionalised with carbohydrate molecules.[19] Surface tethering was achieved through metal-thiol interactions. Several review articles have subsequently highlighted the importance of carbohydrate-based interactions in nanoparticle bioanalysis.[20, 21]

Introduction

1. Carbohydrate Biosensing

1.1 Carbohydrates

Carbohydrates are naturally occurring organic molecules and are the most abundant of natural products. Simple sugars are one of four types of biomolecules found within cells, along with fatty acids, amino acids and nucleotides.[22] These essential molecules provide nutrition to living systems in the form of energy, for example starch for plants and glycogen for animals.[22, 23] Carbohydrates are also structurally important, being the main component in plant tissue matter and insect exoskeleton in the form of cellulose and chitin respectively.

Simple carbohydrates include mono and disaccharides. Monosaccharide structure can take two forms, termed anomers that are in equilibrium and form as a result of two possible hemiacetal ring closures. 1,6 ring closure gives rise to the pyranose anomer while 1,5 ring closure results in furanose anomer formation.

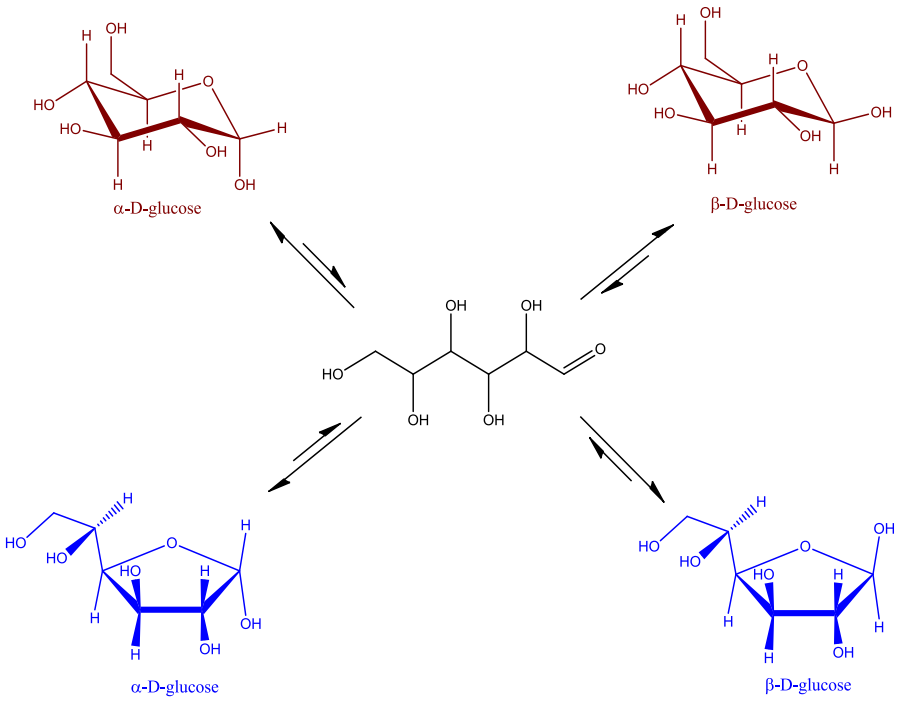

Figure 1. The structure of D-glucose pyranose (red) and furanose (blue) anomers.

Additionally, simple monosaccharide structure can exist in the α- or β- forms as shown in Figure 1. The process by which these structures interconvert is termed mutarotation and occurs only upon dissolution of the saccharide.[23] Each isomer is present in varying quantities in solution, for example at 25 °C, 1 atm, dissolved glucose exists in a 62:38 ratio of β- to α-forms.[23] In the case of mannose, this ratio is 35:65. The likelihood of the α-form predominating the β-form is determined by the anomeric effect. This effect describes the

tendency of heteroatomic substituents at C1 on the ring structure to adopt an axial orientation over the more sterically favoured equatorial position.[23] The anomeric effect is stereoelectronic and is caused by the overlap between an n-molecular orbital of the ring oxygen atom with the antibonding σ*-orbital of the C1 and axially orientated C1 substituent (C1-X) bond.[23, 24] This results in hyperconjugation where the non-bonding electrons are delocalised. If the C1-X bond is equatorially orientated, as is the case with β-glycosides, the same non-bonding electrons are delocalised into the high energy C1-H antibonding orbital (with respect to the C1-X σ*-orbital). A second reason for the anomeric effect is the occurrence of dipole-dipole interactions. Carbohydrates with electronegative substituents at the C1 position are subject to destabilising dipolar effects, from the polarized bond and from the lone pair on the ring oxygen, if this substituent is arranged equatorially. However, in the axial position the dipoles effectively cancel providing stabilisation.[23, 24] Other factors affecting the anomeric effect include the orientation of the C2 substituent. An equatorial orientation of the C2 substituent (in the case of glucose) weakens the effect whereas an axial orientation of the C2 substituent strengthens the anomeric effect (in the case of mannose).[23]

Oligosaccharides include disaccharides, which comprise monosaccharides linked together by a glycosidic bond, for example maltose (two linked glucose units) and lactose (linked galactose and glucose units). Many disaccharides arise naturally as a result of the hydrolysis of polysaccharides such as maltose which results from the breakdown of starch. The various possible combinations of different monosaccharides give rise to a large number and variety of oligosaccharides which can be linear, branched or cyclic; cyclic oligosaccharides include cyclodextrins.[23] Cyclodextrins are conical molecules that provide a hydrophilic exterior and lipophilic cavity where guest molecules may reside (as shown in figure 2).[23] The water solubility of compounds may be improved by using cyclodextrins, making these carbohydrates of particular interest to the pharmaceutical industry in formulation and drug delivery research.[25]

Introduction

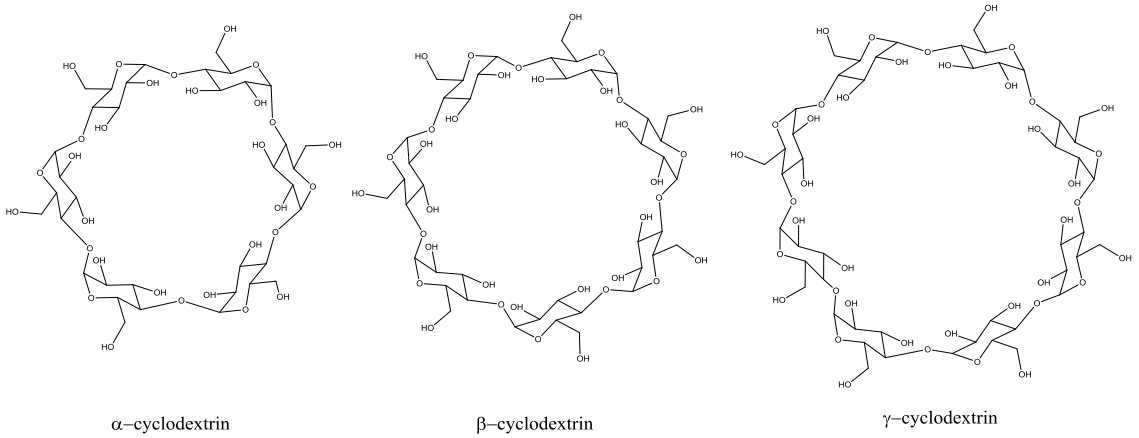

Figure 2. Cyclodextrins of increasing size (comprising 6, 7 and 8 sugar rings respectively from left to right).

Another important and diverse class of carbohydrates are polysaccharides; the majority of naturally produced carbohydrates are synthesised as polysaccharides. Starch is formed by the polymerisation of glucose units to give rise to two glucans, α-amylose and amylopectin.[23] Starch is comprised of a mixture of these and is used as energy storage and release for plants and animals respectively. Cellulose is a polysaccharide that is the major component in the cell wall of plants. The strength given to the cellulose macrostructure results from the multiple hydrogen bonds and van der Waals forces that form between parallel cellulose chains.[23] Chitin is another structurally important polysaccharide, giving strength to the exoskeleton of arthropods, for example scorpions, as a result of the structural similarity to cellulose.[23]

Carbohydrates are vital for the normal function of most organisms, providing energy and structural integrity to the cells of both plants and animals. The function of carbohydrates greatly extends beyond this and into the realm of biointeractions including carbohydrate-metal ion and carbohydrate-protein associations.[26, 27] The significance of the role of biological interactions cannot be overstated, as interactions are the basis for numerous vital process in living organisms. From the metabolism of native and xenobiotic species to the transportation of oxygen in blood throughout the body to the existence of genes through the DNA double helix, these are but a few examples from an extensive list of vital biological interactions.[22]

Introduction

1.2 Glycobiology

Carbohydrate-protein interactions are involved in a number of different processes including cell to cell adhesion, cell differentiation and fertilisation, through the interaction between complementary carbohydrate components found on both the sperm and egg.[23, 28, 29] Additionally, carbohydrate-protein interactions are key to the attachment of infectious species to host cells, allowing establishment of the pathogens and development of the infection in a living system[28, 30].

Carbohydrate to protein interactions can be either reversible or irreversible.[23] Irreversibly formed glycoconjugates include glycoproteins (macromolecules exhibiting a single carbohydrate), proteoglycans (discrete molecules exhibiting multiple carbohydrates) and glycolipids.[23] These molecules exist as a glycan coating on the surface of cells, termed the glycocalyx'.[23] The individual carbohydrate species of the glycocalyx are involved in processes such as cellular matrix cation and water transport, senescent erythrocyte clearance, leukocyte transport to a site of infection and the development of the nervous system.[23, 31]. The vast number of naturally occurring monosaccharides, oligosaccharides and polysaccharides means that the function of naturally formed glycoconjugates, of which there are many, is highly complex.

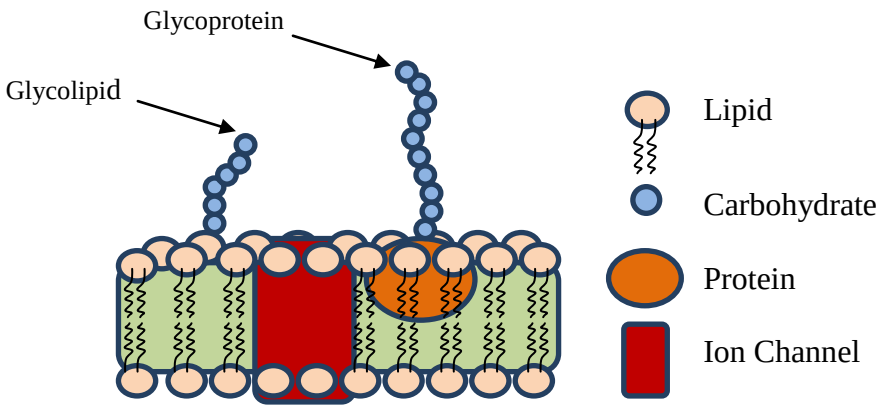

Figure 3. Section of cell wall illustrating the key components of the glycocalyx.

The glycocalyx is a vital part of cellular surface chemistry. Adhesion molecules expressed in the glycocalyx are key to cell motility during embryonic development.[32] Additionally, this molecular "coating" plays a crucial role in regulating vascular tissue and controlling capillary red blood cell volume.[33] Importantly, the glycocalyx is crucial to cell differentiation.[23] This can include identifying healthy from diseased cells but also pathogenic species, for example, viruses.

Introduction

The field of glycobiology has been growing in recent times with a particular focus being to better understand the precise role of the glycocalyx.[32, 34, 35] Part of the current research has involved the use of glyconanoparticles to further understanding on communication pathways of host-host and host-pathogen interactions involving the glycocalyx.[28, 30] It is hoped that by better understanding the specific relationship between each of the binding components, it will be possible to exploit these in bioanalysis. Such interactions include those reversible associations between carbohydrates and sugar-specific proteins called lectins.[23]

1.3 Lectins

Lectins are carbohydrate-binding proteins present throughout nature and produced by a host of organisms including animals, plants, bacteria and viruses.[36-38] In nature, they function as hemagglutinins; adhesion molecules in cellular recognition and differentiation. Both erythrocytes and lymphocytes possess surface glycoproteins and glycolipids which allow for interaction with lectins.[39]

As well as being involved in vital processes such as cell recognition, leukocyte transport and sperm-egg recognition, lectin-carbohydrate interactions can also have harmful consequences. Certain plant lectins behave as allergens, causing food intolerance reactions.[39] The interaction of dietary plant lectins with host cells activates the immune system by provoking antibodies, for example IgG, resulting in allergic reactions.[39] These reactions are caused by the inability of IgG to differentiate between native and foreign antigens.[39] This protein binds extensively and indiscriminately to host cells and target species alike leading to irritation and inflammation of host cells.[39] This can result in intestinal damage, vomiting and haemolytic anaemia.[39] Some lectins are incredibly toxic. Small amounts (20 ng/Kg) of *Ricinus communis* lectin (Ricin), found in castor beans, can cause a fatal reaction in humans.[40, 41] Lectin-carbohydrate interactions are also exploited by pathogens at the start of the infectious cycle; the association between host carbohydrates and pathogenic lectins or vice versa allows for establishment of the disease-related species.[28]

The carbohydrate recognition ability of lectins has previously been investigated and used in bioanalysis.[42, 43] Blood typing is one example of contemporary bioanalysis which utilises lectin-carbohydrate interactions. This method is stated to be reliable and more cost effective than the antibody equivalent.[43] Erythrocytes of different blood types express different carbohydrates on their surface.[23, 43] This allows only certain lectins, with affinity towards a particular sugar, to bind. This selectivity plays a key role in processes such as differentiating between distinct blood types such as A and B.[23]

Introduction

Lectins are important, naturally occurring species that are involved in a large number and variety of processes. Their diverse function comes as a result of the high number of lectin types and sub-types, which are distinct because of slight structural variations[23].

1.3.1 Lectin Structure

As shown in figure 4, lectins are composed of two or more subunits each made up of a variety of amino-acid containing sheets and loops.[44] In the case of plant lectin subunits, a six stranded β-sheet sits behind a second, seven stranded β-sheet with a five-stranded β-sheet located above these. Connecting this β-sheet "sandwich" are a variety of loops which differ in number and amino acid sequence depending on the type of lectin.[44] In the case of legume lectins there are four loops each containing one of four amino acids that are crucial in carbohydrate binding.[45] Two of these loops contain glycine and aspartic acid. A third loop, which greatly influences carbohydrate specificity, contains asparagine and either tryptophan, tyrosine, phenyl aniline or leucine (depending on the lectin).[46] These amino acids interact with carbohydrates through hydrogen bonding between the carbohydrate alcohol groups and appropriate acceptors on the protein. Other important interactions include hydrophobic associations and van der Waals forces which are responsible for the interactions between a fourth loop and the sugar backbone.[45]

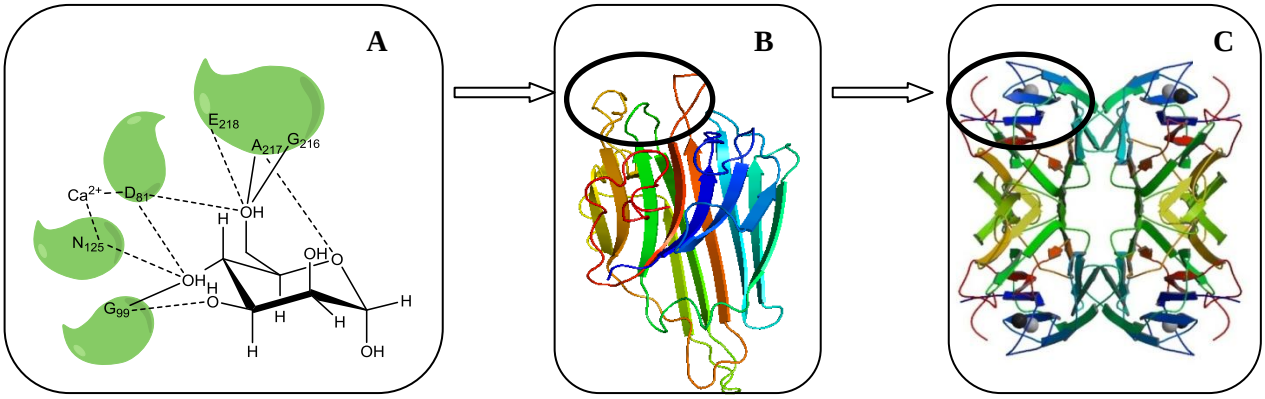

Figure 4. A) Interaction between mannose and the amino acid residues in the Concanavalin A (ConA) lectin binding pocket. B) ConA subunit with the binding pocket noted. C) Tetrameric ConA with binding pocket noted. PDB code is 3CNA.

Many lectins are metalloproteins, relying on metal ion coordination for carbohydrate binding activity.[47, 48] Calcium and manganese ions are implicated in the activity of certain lectins by coordinating to the amino acid residues within the lectin binding pocket, thereby keeping this open to incoming carbohydrates. These lectins are termed C-type lectins and include endocytic lectins, collectins (lectins attached to cell-bound collagen) and selectins (lectins with a cellular adhesion function).[23] An example of lectins reliant on these metal ions for

activity is Concanavalin A (ConA), shown in figure 4. Con A is a plant lectin that has been studied extensively for its carbohydrate binding properties. First isolated in its crystalline form in 1926 by James B. Sumner, it has been used in bioanalysis to better understand carbohydrate protein interactions, as well as in agglutination testing and glyconanoparticle biosensing.[14, 36, 49, 50]

1.3.2 Lectin Function

As previously stated, lectins are expressed by viral and bacterial species as agglutinins and toxins.[30, 51, 52] As adhesion molecules, toxins allow the attachment of a pathogen to host cells and subsequently for an infection to develop. The bacteria *Vibreo cholerae* express AB toxins (cholera toxin A and B) on the pili. The B subunit facilitates attachment of the bacteria to the pentasaccharide groups expressed on the intestinal cell glycocalyx by the glycosphingolipid, GM1.[53] The GM1-cholera toxin B subunit interactions play a crucial role in the development of the cholera infection. These binding interaction allow the A subunit to enter the intestinal cell membrane, initiating adenylate cyclase thereby raising cAMP levels.[53] Subsequently, the elevated levels in cells induce water, containing electrolytes, to flood the bowels causing life threatening diarrhoea and dehydration.[54]

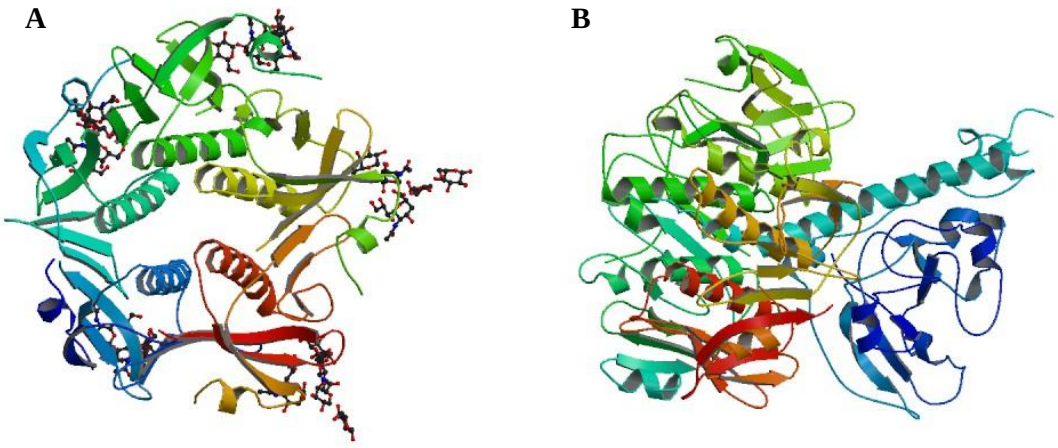

Figure 5. Structures of A) cholera toxin B-subunit and B) cholera toxin A- and B-subunits. PDB codes are 2CHB and 1XTC respectively.

A second example of a pathogen-related adhesion lectins is the influenza virus hemagglutinin (HA) expressed by the human influenza virus.[55] This lectin has affinity for the carbohydrate, N-acetyl neuraminic acid which is a type of sialic acid.[55] As these carbohydrates are expressed on the exterior of host cells, they allow the attachment of the

virus through HA. HA enables the fusion of the endosomal membrane, allowing endocytosis of the virus and subsequently initiating infection of the host by the influenza virus.[55]

In addition to the development of infection in a living system, lectins also play a crucial role in host defence against pathogens.[23, 56] Macrophages are white blood cells that ingest microorganisms including viral and bacterial species, thereby preventing infection. This type of first-line defence is termed innate immunity.[23] Mannose-macrophage receptors (MMRs) are present on the surface of lymphocytes and are composed of eight C-type lectin domains.[23] These lectins bind to the mannose and N-acetyl glucosamine residues on the surfaces of bacteria such as E.coli and viruses such as the human immunodeficiency virus (HIV).[57, 58] Additionally, host serum lectins provide defence against pathogenic species. One such lectin is the mannose-binding protein (MBP) which is present in mammalian serum. This lectin binds to the surface oligomannosides of pathogenic species. This activates the complement system (non-antibody), resulting in subsequent lysis of the pathogen. This has been shown to be effective against viruses such as the Ebola virus.[59] By binding to the Ebola virus, the MBP effectively prevents the virus from interacting with the mammalian cell surface lectin, DC-SIGN. This was demonstrated in mice by Olinger *et al.*[60] By increasing the levels of MBP seven times or over, the mice, dosed with the normally fatal level of Ebola virus, survived and subsequently became immune to the virus, as demonstrated with further viral dosing.[60] As demonstrated, carbohydrate-lectin interactions are key to the successful defence against pathogens through macrophages via MMRs and infection prevention via MBP.

The importance of carbohydrate-based interactions in living systems has driven research towards bioanalysis that exploits these associations. Though these interactions are weak, they are strengthened through multivalency, accommodated by the glycocalyx on cellular surfaces.[23, 28] Platforms that encourage multivalency are therefore of great interest when attempting to exploit sugar-lectin interactions for bioanalysis. The use of nanoparticles facilitates this multivalent approach, while also allowing for the use of a range of powerful spectroscopic techniques including UV-vis. extinction spectroscopy, dynamic light scattering (DLS) and surface enhanced Raman scattering (SERS).

2. Spectroscopy

The interaction of radiated energy with matter involves a number of processes. Light, consisting of photons, can transfer energy to a molecule resulting in a vibrationally excited state for that molecule. As these vibrations diminish and the molecule reverts to the ground state, the energy released can be measured by vibrational spectroscopy, for example infra-red (IR) spectroscopy.[61] Alternatively, light can be scattered. This process occurs when molecular oscillating charges, induced by oscillating electromagnetic energy, radiate at a particular frequency.[62]

2.1 Raman Scattering

Scattering involves the promotion of a molecule from a ground state to virtually excited states; levels arising from the oscillation of the molecular charges under the influence of oscillating electromagnetic radiation. This gives rise to a complex between the molecular electronic structure and the incident electromagnetic radiation that breaks down when the photons scatter.[1] The virtual states are greater in energy than the ground vibrational modes of the molecule but lower in energy than the excited electronic state.[1]

Scattering can either be elastic or inelastic. Elastic scattering arises from the oscillation of molecular charges at a frequency equivalent to that of the incident radiation.[61] For particles or molecules with a diameter smaller than the wavelength of the incident light, the elastic scattering is termed Rayleigh scattering.[61] Inelastic or Raman scattering occurs as a molecule attains a greater or lower vibrational mode following interaction with incident electromagnetic radiation, thereby gaining or losing energy from or to the photons respectively. Occurring for one in every million scattered photons, this event is rare.[1] Within inelastic scattering there are Stokes scattering events, where molecules gain energy from the incident light and anti-Stokes scattering, where molecules lose energy to the light. Stokes scattering begins from the ground vibrational state and therefore more commonly occurs at room temperature whereas, according to the Boltzmann distribution, anti-Stokes, occurring from the excited vibrational modes is more likely to be, and experimentally is, measured at higher temperatures.[1]

Introduction

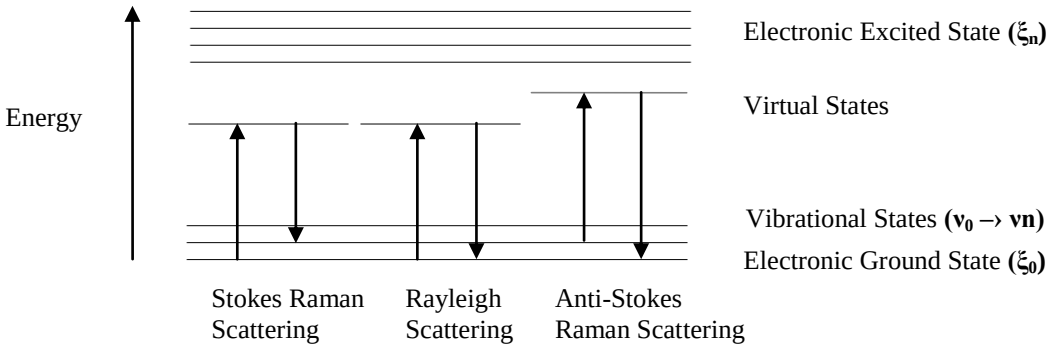

Figure 6. Jablonski diagram illustrating the possible scattering outcomes following irradiation of a sample.[1]

All molecules scatter light but some can absorb as well as scatter. In a centrosymmetric molecule, for example carbon dioxide, the mutual exclusion rule applies; no vibration will be both Raman and IR active. In this case, Raman and Rayleigh scattering occurs from a change in polarizability, arising from symmetrical stretching, and not from the formation of dipoles, arising from asymmetrical stretching.[1] For a non-centrosymmetric molecule, for example water, the mutual exclusion rule is relaxed; a vibration that is Raman active can also be IR active (for example the symmetric stretch mode of water at 3656 cm^{-1}). Experimentally, the intensity of this scattered light is measured by Raman spectroscopy.[1]

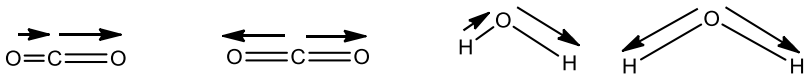

Figure 7. Asymmetric and Symmetric stretches of centrosymmetric CO_2 and non-centrosymmetric H_2O.

Raman spectroscopy measures these scattering events, providing a spectrum of peaks related to the different inelastic scattering events within a molecule. The technique requires little sample preparation, is non-destructive and can be used remotely.[1, 63] Although the signals obtained are often weak, the technique is molecularly specific, allowing multi-analyte detection.[1, 62, 64]

The intensity of Raman scattering if defined by equation 1.

Equation 1

$$I = Kl\alpha^2\omega^4$$

Where K is a constant comprising the speed of light, l is the laser power, α is the polarizability, and ω is the frequency of incident radiation.[1] To compensate for relatively weak Raman scattering, both the frequency and laser power can be controlled with the aim of increasing the intensity of the signal. However, photodegradation of the sample, as well as fluorescence, can arise as a result of using high powered lasers.[1] Fluorescence occurs when a

molecule absorbs energy from light, resulting in an excited state. Subsequent relaxation to the ground state results in emission of light that can mask Raman peaks, making result interpretation difficult.[1] Increasing the sensitivity of the technique requires minimizing background fluorescence while also increasing the analyte signal, particularly at low analyte concentration. This can be achieved by using resonance Raman spectroscopy.[1, 62]

By choosing a laser frequency to resonate with an electronic transition of the analyte, resonance Raman scattering may occur, increasing the scattering intensity by 10^3-10^4.[1] Chromophores are molecular functionalities key to this phenomenon; possessing electrons that are readily promoted to an electronic excited state following irradiation by a source. Examples include C=C and C=O functionalities. A major advantage of this technique is the increased Raman scattering to fluorescence signal intensity ratio, giving greater analyte response and hence greater sensitivity.[1] The increased scattering intensity obtained allows the use of lower power lasers which minimises sample degradation often encountered with conventional Raman spectroscopy. An alternative method of increasing the scattering intensity is by using a roughened metal surface to which the analyte is bound and irradiating this with a laser of appropriate frequency; this gives rise to surface enhanced Raman scattering (SERS).

2.2 SERS

Greater enhancement of scattering signals is possible when an analyte is bound to a metal substrate in a perpendicular fashion to the surface. The result is effective quenching of fluorescence as well as a 10^6 increase in Raman signal intensity.[1, 65] The phenomenon is termed surface enhanced Raman scattering (SERS). Originally discovered by Fleischmann, Hendra and McQuillan in 1973, the effect was thought to arise from the increased surface area of the metal to which the analyte could bind.[66] In 1977 two research groups proposed mechanisms simultaneously.[67, 68] Jeanmaire and Van Duyne proposed the electromagnetic enhancement effect, while Albrecht and Creighton proposed a charge transfer effect.

i) Electromagnetic Enhancement

For a bulk metal, the surface electrons are displaced from the constituent nuclei upon exposure to an applied field and return to their original position in the absence of this field due to the attractive force between the electrons and the nuclei. These coherent oscillations, called surface plasmons, occur at the frequency of the applied field and propagate as electromagnetic waves (surface plasmon polaritons) parallel to the metal dielectric interface.[69-71] With roughening of the surface, these oscillations transmit in directions both

parallel and perpendicular to the metal surface. Coupling of this transmission with an appropriate laser wavelength results in surface plasmon resonance.[69] An analyte within close proximity and perpendicular to a roughened metal surface is exposed to this enhanced field, increasing the scattering signal intensity obtained for that analyte.[1, 69, 72]

ii) Charge-Transfer Effect

An analyte bonded to a metal surface can receive or lose charge from or to the metal respectively. As a result, unique electronic states (Raman resonant intermediates) form, allowing radiation absorbed by the metal to be transferred to the analyte. As Raman scattering occurs, this energy is transferred back to the metal from where it is emitted[1, 69].

The electromagnetic enhancement effect applies long-range and so affects analytes that are remote from the metal surface. Conversely the charge-transfer effect is a short range mechanism applying to monolayer coverage of the metal surface where the analyte is in close proximity.[1] It is proposed that both mechanisms, along with molecular resonance, contribute to the overall enhancement of the scattering intensity.[73]

The molecular resonance contribution can be exploited by choosing a laser frequency that coincides with the excitation energy of a chromophore within the structure of the surface-bound molecule.[73] When this overlaps with the metal surface plasmon excitation energy, significant scattering enhancement can be achieved when compared with conventional Raman spectroscopy. This effect is called surface enhanced resonance Raman scattering (SERRS).[1] The sensitivity achieved when using this for measurement, rivals fluorescence, while the selectivity surpasses that achievable with UV-vis. extinction spectroscopy by only detecting the components with absorption maxima that coincide with the incident radiation frequency.[1, 74]

SERS and SERRS present numerous advantages over conventional Raman spectroscopy. The significant enhancement of scattering signal warrants investigation into the use of SERS and SERRS in biological component analysis at nanomolar and lower levels.[1] Quenching of fluorescence by the metal *via* resonance energy transfer further increases the sensitivity.[65, 75] The molecularly specific nature of SERRS is of great use in complex biological media, where multiple analytes can be detected simultaneously.[74]

Important factors in obtaining reproducible and accurate results by SERS and SERRS include the type and morphology of the metal substrate.[69] The substrate must be produced in

a reproducible way to encourage consistent results. A variety of metallic substrates exist including metal layers, electrodes and colloidal solutions of metal nanoparticles.[67, 76-78]

3. Metallic Nanoparticles

The SERS phenomenon was first observed for pyridine molecules in close proximity to a roughened silver electrode by Fleishmann *et al.* and has since been applied to metallic thin films and nanoparticles.[1] Nanoparticles, defined by a size of between 1 and 100 nm, are advantageous as high surface area probes in bioanalysis compared with bulk material equivalents and can be functionalised with a variety of species.[12, 79] Functionalisation with biomolecules of interest, for example DNA, proteins, sugars and sensing species, for example dyes and small molecules, give rise to intense Raman probes for use in the detection of targets of interest and in clinical diagnostics.[13, 80-84]

3.1 Preparation of Nanoparticles

Metals used in the production of nanoparticles include gold, silver and copper. A variety of different analytical techniques including UV-vis. extinction spectroscopy, SERS-based solution assays and biomedical imaging can be used with these particles as a result of their unique spectroscopic properties.[9, 15, 85-87] The generation of nanoparticles relies on the reduction of the metal salt in the presence of a reducing/capping agent.[88] Silver nanoparticles can be generated following the Lee and Meisel method, using citrate for both the reduction of the silver salt and the capping of the nanoparticles generated.[89] A solution of silver nitrate is heated to boiling followed by the addition of a solution of sodium citrate. Through the action of heat and water, the citrate is oxidised to acetone dicarboxylic acid which then reduces the Ag^{+} to Ag^{0}.[90] The precipitated nanoparticles are capped by citrate thereby preventing aggregation. Alternative methods of silver nanoparticle preparation include the use of sodium borohydride, hydroxylamine, ethylenediaminetetraacetic acid (EDTA) or glucose as reducing agents.[91-94] Similarly to silver, gold nanoparticles can be generated from the reaction of a gold salt and sodium citrate with a widely used method originally devised by Turkevich *et al.* in 1951.[88] Here an aqueous solution of chloroauric acid is heated to boiling after which time, an aqueous solution of citrate is added, simultaneously reducing and capping the precipitated nanoparticles in a similar way to the aforementioned Lee and Meisel method.[88, 90] By varying certain conditions, for example, altering the ratio of reducing agent to metal salt or changing the type of reducing agent, it is possible to generate nanoparticles of different sizes and shapes.[88, 95, 96]

3.2 Properties of Nanoparticles

The use of metallic nanoparticles in bioanalysis often stems from the absorptive and radiative characteristics of these particles; this is demonstrated by the colours obtained for silver nanoparticles which range from green, yellow and brown, and for gold nanoparticles, ranging from pink, ruby, red and purple. This arises as a result of the interaction between incident light and the nanoparticle surface plasmon and varies due to a number of factors including composition, size, shape.[72, 97]

3.2.1 Surface Plasmon Resonance

In the case of metallic nanoparticles, the fundamental optical properties arise from the field-induced collective oscillation of the valence electrons of the metal called the surface plasmon which propagate as electromagnetic waves in a parallel direction to the metal-dielectric interface (see figure 8).[70, 97] If the excitation wavelength is larger than the nanoparticle size (for example 200 - 800 nm), this allows the surface plasmon to oscillate in resonance with the excitation and hence allows extinction (absorption and scattering) as a result of this localized surface plasmon resonance (LSPR) effect.[72, 98] This results in a plasmon extinction band arising in the visible region of the electromagnetic spectrum and hence a colour not observed for the bulk material, which is larger than the excitation wavelength.[72]

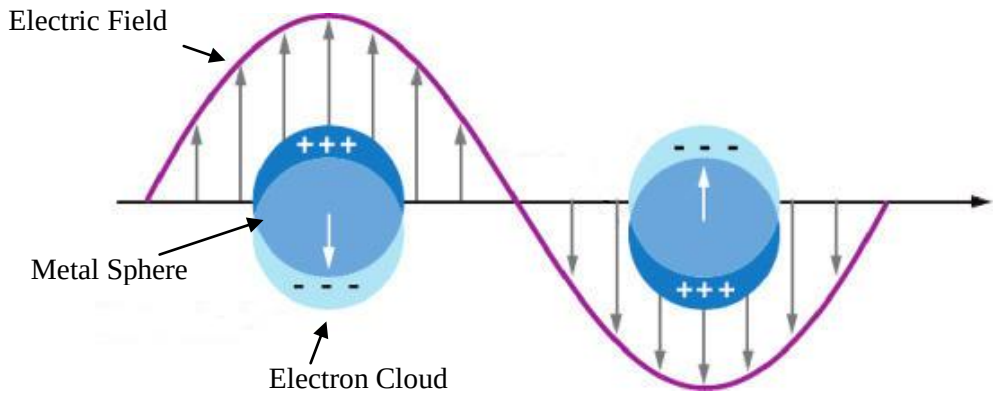

Figure 8. Light interacting with the oscillating surface plasmon of the metal nanoparticle.[99]

An explanation of surface plasmon resonance phenomenon was given by Gustav Mie who applied Maxwell's equations (used to explain the generation and behaviour of electromagnetic fields) to the scattering of electromagnetic radiation by spherical particles of a similar diameter to the wavelength of visible light.[100] Dipole oscillations of the electrons in the conduction band of the metal, present at energy levels slightly above the Fermi level give rise to the plasmon band obtained for spherical particles (for example gold or silver

nanoparticles).[101] Factors affecting the plasmon band include the type of metal, the size, shape of the particles and nature of the dielectric medium and the proximity of adjacent nanoparticles.[102] As an example, 30 nm gold and 40 nm silver nanoparticles exhibit extinction maxima at approximately 530 nm and 400 nm respectively. The charge density of silver atoms is greater than that of gold as a result of their being fewer electronic shells in silver and hence lower screening of the nuclear charge. This results in a plasmon which is less diffuse than that of gold and hence requires greater energy (higher frequency, shorter wavelength) for excitation.[103] Size is a major contributing factor to the colour of the nanoparticle colloid. As the nanoparticle size increases, the surface plasmon becomes more diffuse, resulting in a lower energy requirement for excitation, and hence a "red-shift" of the wavelength at maximum extinction.[72, 80, 97]

Figure 9. Samples of 30 nM gold (left) and 40 nM silver (right) colloid illustrating the lower energy gold emission compared with silver.

3.3 Stability and Aggregation

The mono-dispersity of nanoparticles in a solution relies on their being repulsion between neighbouring particles. Aggregation of nanoparticles occurs readily under a variety of conditions including changes to the ionic composition of the nanoparticle medium or the interaction between complementary species, either on different nanoparticles or free in solution in the presence of nanoparticles.[104, 105] This process can be monitored by UV-vis. extinction spectroscopy and Raman spectroscopy. Functionalising nanoparticles with a Raman reporter molecule, results in enhancement of the molecule signal when compared with the signal obtained from a solution of the reporter molecule.[1, 69] It is then possible to monitor the Raman signal obtained when a target of interest interacts with a complementary nanoparticle surface moiety, resulting in aggregation.[69] A corresponding increase in the Raman dye signal arises as a result of the position of the molecules in hot spots; regions of high surface plasmon density between neighbouring particles.[69]

Nanoparticle suspension relies on a number of factors that can be grouped into electronic or steric stabilisation.[79] Following nanoparticle colloid synthesis, the metal surface is coated

with a mixture of citrate, anions such as Cl^- and cations such as Na^+, which cause the nanoparticles to possess overall negative charges.[79, 106] These species contribute to the electronic stabilisation since, without them, the nanoparticles would experience van der Waals forces significant enough to cause aggregation.[79, 106] This is however a weak effect that can be overcome by an increase in the ionic strength of the solution as described by DLVO theory.[107, 108]

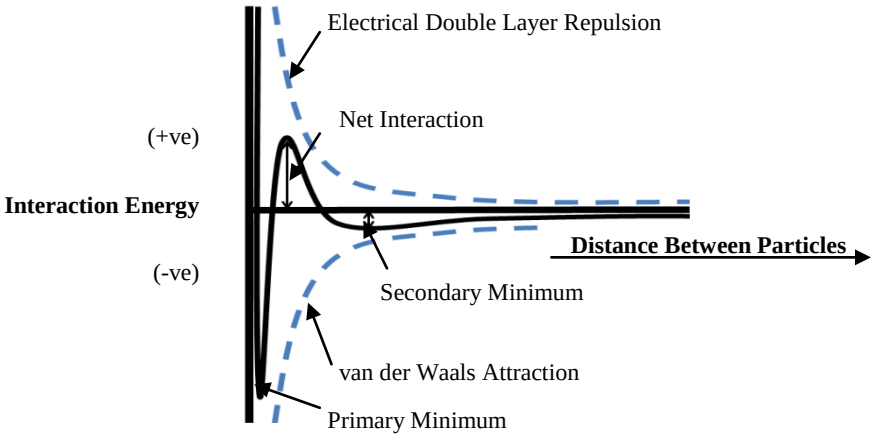

Figure 10. Plot of interaction energy as a function of interparticle distance. As the interparticle distance decreases a secondary minimum occurs as a result of van der Waals interactions. As the distance is decreased further, the electrical double layer repulsive force is dominant. Finally a primary minimum is observed signifying particle aggregate formation.

Derjaguin, Landau, Verwey, Overbeek, or DLVO theory states that the attractive forces arising from van der Waals interactions are balanced by the repulsive forces between charges on neighbouring particles that reside on what is termed the electric double layer.[107] The electric double layer comprises a stationary layer (stern layer) of ions, including water, that are tightly bound to the nanoparticle surface as well as a mobile layer of ions that are attracted to the charged particle (shown in figure 11).[108] This double-layer offers a form of protection to the nanoparticles from collisions that can result in aggregation. As the ionic strength of the solution is increased, the thickness of the double layer decreases, allowing neighbouring particles to break through the double layer, initiating aggregation.[107, 108]

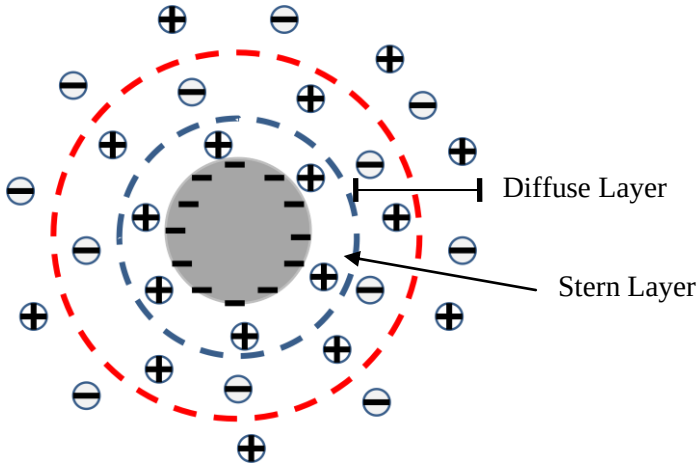

Figure 11. The electric double layer of a negatively charged silver nanoparticle.

The double layer offers little protection from aggregation since processes often used in functional nanoparticle preparation can easily disrupt it. These include centrifugation or the addition of ionic species like sodium chloride in biological buffers that effectively neutralise the surface and minimise any charge that is repelling the nanoparticles[109]. Nanoparticle stabilisation is often successfully achieved through the addition of steric bulk[79]. Following preparation of the nanoparticles, species such as citrate or borohydride ions will cap the surface and provide repulsion between particles[88, 89]. Alternative capping species can be added to the nanoparticle surface, to further increase the bulk. These include polymeric species, such as polyethylene glycol, proteins, such as bovine serum albumin or starch, which has recently been used for the preparation of biologically and environmentally friendly nanoparticles[72, 79, 81, 110-112]. The use of straight chain organothiol molecules, for example alkanethiols or thiolated polyethylene glycol, allows for the formation of self-assembled monolayers (SAMs) on the nanoparticle surface as shown in figure 12.[113, 114]

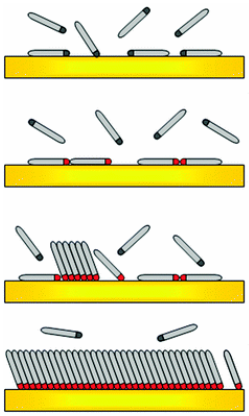

Figure 12. Illustration of SAM formation. This involves (from top to bottom) physisorption of molecules which subsequently take up a "lying down" orientation on the surface followed by the initiation and finally completion of the "standing up" phase.[115]

The use of heterobifunctional molecules in SAM formation, for example thiol/carboxyl polyethylene glycol (CTPEG), can subsequently allow attachment of biomolecules (*via* the carboxyl group) such as proteins, carbohydrates and peptides.[116] Alternatively, biomolecules can be thiolated prior to nanoparticle addition, allowing attachment to the surface without the need for subsequent conjugation.[13, 117] In both instances, the nanomaterials generated are suitable for biosensing due to both their unique optical properties and surface functionalisation with biomolecules that allow for interaction with targets of interest.

3.4 Nanoparticle Biosensing

Nanoparticles, for use in biosensing, are functionalised with biomolecules of interest, for example DNA, which, when binding multivalent complementary species, aggregate.[30] This phenomenon is used to indicate the presence of a biomolecule of interest, for example, a protein or DNA strand, specific to a particular pathogen.[12, 13, 30, 80] The benefit of this is that aggregation can be rapid, thus, providing a quick and reliable method of detecting a specific target. There are a number of analytical techniques that can be used to interrogate this aggregation including UV-vis. extinction spectroscopy, dynamic light scattering (DLS) and surface enhanced Raman or resonance Raman scattering. UV-vis. extinction spectroscopy can be used to record changes in the intensity and wavelength of the surface plasmon extinction peak. This type of analysis has been used previously by Mirkin *et al.* for the detection of complimentary DNA interactions.[13] Nanoparticles were functionalised with non-complementary DNA strands and then introduced to a solution containing DNA strands complementary to those tethered to the nanoparticle surface. The presence of the complementary DNA caused the nanoparticles to aggregate, resulting in changes to the extinction profile of the nanoparticles, which was measured spectroscopically.[13] Also using UV-vis. extinction spectroscopy, Schofield *et al.* have developed glyconanoparticles capable of detecting cholera toxin through aggregation.[30] Concentration dependent red-shifting was measured by UV-vis. extinction spectroscopy, highlighting the potential use of glyconanoparticles in a diagnostic setting. The benefits of using UV-vis. extinction spectroscopy include rapid detection and relative ease in the interpretation of the result obtained.[30] Drawbacks include a lack of sensitivity when compared with other techniques, including fluorescence and SERS, and the inability to detect multiple analytes at once (multiplexing). Multiplexing is often required in complex samples, for example, stagnant water, which can potentially contain a mixture of different waterborne pathogens.[118]

SERS and SERRS are promising analytical techniques that allow both sensitive and selective multianalyte detection.[1] Having been successfully used to simultaneously detect unique

Introduction

DNA sequences as well as different labels on proteins, they offer several advantages over conventional Raman and UV-vis. extinction spectroscopy.[69, 118, 119] Functionalising the nanoparticles with a Raman dye or small molecule, results in enhancement of that species. This is in comparison with the signal obtained from a solution of the dye or small molecule[1, 69]. It is then possible to monitor changes in the Raman signal following target-mediated aggregation of the particles. A corresponding increase in the Raman dye signal arises as a result of the position of the molecules in 'hot spots'; regions of high surface plasmon density between neighbouring nanoparticles.[1, 15, 120]

Examples of research utilising this phenomenon include work by Graham *et al.* involving the multiplexed detection of dye conjugated DNA with silver nanoparticles in a sensitive manner.[119] DNA sequences, including those from *E. coli* and the human papillomavirus, were conjugated to unique dyes, each giving an individually distinct Raman spectrum. Attraction between the positively charged bases and negatively charged nanoparticles allowed the dye to be positioned in close proximity to the metal surface, thereby resulting in the enhanced Raman signals and thus detection of the DNA.[119] The multiplexed detection was found to offer comparable sensitivity to that achievable with individual detection of each DNA type. This research highlights the advantages of SERRS in sensitive detection in samples that contain a variety of different analytes.

SERS and SERRS also have use in whole cell analysis. Vikesland *et al.* have demonstrated the use of gold nanoparticles, functionalised with malachite green or rhodamine B isothiocyanate dyes and antibodies, for the detection of waterborne parasites *C. parvum* and *Giardia lamblia (G. lamblia)* by SERRS[121]. This research provides one of the first reported examples of environmental analysis of pathogens by SERRS as they are found in nature. Research up until this point had focused on the detection of proteins and nucleic acids specific to these species. This illustrates an example of the successful use of SERRS in whole cell analysis which is an important step in imaging with SERRS and developing whole organism bioanalysis.

Introduction

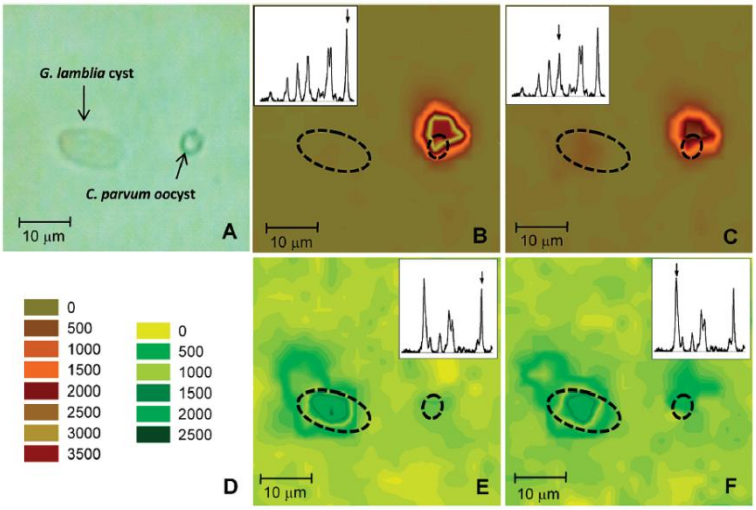

Figure 13. Raman maps of parasitic cysts of G. lamblia and C. parvum coated in MGITC and RBITC respectively.[121]

The past and present use of nanoparticles with SERS in bioanalysis was reviewed by Halvorson and Vikesland.[122] The benefits of sensitivity, and multi-analyte detection as well as differentiation between molecularly similar species by SERS are outlined[122]. Also discussed are the issues of result variability, arising from the slight differences between the surfaces of individual nanoparticles and uncontrolled aggregation. This is particularly important in complex samples taken from certain environments, such as bodies of water where a number of interfering, ionic species are present. Other issues such as degradation of the sample by the laser used also hamper reproducibility in analysis[1, 122]. However, the nanoparticle surface enhances the Raman signals of molecules close to the surface and therefore reduces the need for higher laser power[1]. Creating nanoparticles that are stable in a variety of conditions helps to control aggregation in the presence of an analyte of interest.

There are many challenges that exist in working towards creating relevant nanomaterials however, with the constant development in materials and methodologies, including the use of internal standards, the preparation of homogenous nanoparticles (both in terms of size and shape) as well as other factors, such as the use of microfluidic devices for the controlled mixing of nanosensor and analyte, this encourages greater reproducibility, providing greater contrast between the benefits and drawback of SERS/SERRS[122]. The use of unique SERRS labels on nanoparticles also allows for multiplexed detection. This, coupled with imaging of whole organisms (for example, entire parasitic cysts) highlights the use of SERRS in the analysis of samples, as received, from contaminated bodies of water. This is important in the rapid detection of an infectious species and the fast treatment of the contaminated body of water.

4. Glyconanotechnology

Recent developments in functionalised nanomaterials have included the preparation of glycofunctional, nanoscale materials for use in bioanalysis.[28] Multivalent glyconanomaterials for improved drug delivery and enzyme (protease) inhibition have been prepared as well as glycan, glycoprotein and lectin functionalisation of nanoparticles for use in molecular imaging and sensitive detection of biological species.[30, 38, 49, 123, 124]

4.1 Glyconanoparticles

Of particular interest in glycobiology is the investigation of carbohydrate-protein interactions by creating glycan-functionalised materials, for example nanoparticles, and interacting these with complementary species.[20, 28] Interactions of this type have been exploited by a number of groups for bioanalysis using nanoparticles. [110, 125-127]

Research by Ding *et al.*, involving gold glyconanoparticles, focussed on the detection and quantification of cell surface mannose residues.[128] The mannose-binding lectin, ConA, was introduced to the cells along with nanoparticles. Competitive binding between the lectin and the cellular mannose residues or the gold mannonanoparticles resulted in a decrease in the aggregation of the particles by ConA.

The gold nanoparticles then catalysed the reduction of ionic silver in the presence of a reducing agent, in this case hydroquinone. Unaggregated nanoparticles catalysed this reduction more successfully than aggregates, as shown by the greater concentration of silver nanoparticles produced in figure 14. This research demonstrates an example of effective, quantitative ways of analysing cellular glycans without the use of instrumentation.

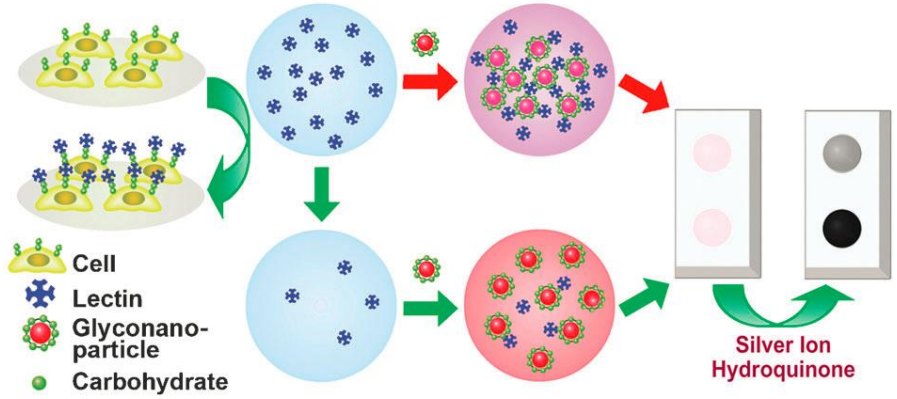

Figure 14. Cellular characterisation of cellular mannan residues using the competition between glyconanoparticles and cell surface. Resulting aggregation is visualised by silver reduction.

Research by Russell and co-workers has included the detection of leguminous and pathogenic lectins, ConA and cholera toxin B subunit (CTB), as well as metal ion sensing.[26,

[30, 49] The detection of ConA was achieved using mannose functionalised silver and gold nanoparticles which aggregated upon interaction with the lectin,. This aggregation was noted following characteristic changes in the extinction profile of the nanoparticles as observed by UV-vis. extinction spectroscopy.[49] Similarly, lactose functionalised nanoparticles were prepared for the detection of CTB (figure 15A).[30] Changes in the plasmonic extinction of the nanoparticles were monitored as an indicator of aggregation and a limit of detection of 54 nM was calculated.[30] Lactose functionalised nanoparticles were also used in the detection of Ca^{2+} ions, highlighting the important role of both glucose and galactose in calcium binding (figure 15B).[26]

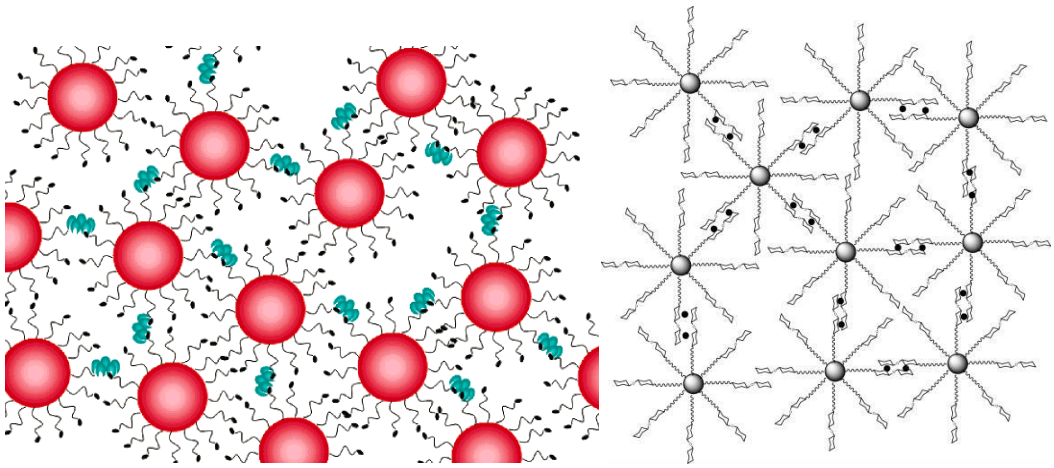

A) **B)**

Figure 15. Examples of glyconanoparticle arrays formed by the interaction between lactose coated gold nanoparticles and A) CTB or B) calcium ions.

In the examples shown in figure 15, detection was achieved by using UV-vis. extinction spectroscopy to measure nanoparticle aggregation. While this technique is rapid and allows clear differentiation between aggregated and unaggregated nanoparticles, the technique can lack sensitivity and does not allow for the detection of multiple analytes simultaneously that can often be useful and necessary in test samples.

Surface enhanced Raman spectroscopy (SERS) is a technique that offers the possibility of sensitive detection together with multiplexing capability. In addition to carbohydrates, nanoparticles can be functionalised with Raman reporter molecules (RRMs) giving characteristic spectra that can be monitored using Raman spectroscopy. The normally weak Raman scattering effect can be enhanced by the interaction between the molecule and the surface plasmon of the nanoparticles.[1, 129] This can allow sensitive detection of an analyte of

interest; the aggregation caused by the interaction of functional nanoparticles with that analyte results in enhancement of the Raman peaks associated with the RRM bound to the nanoparticle surface.[1] By functionalising nanoparticles with different RRMs, it is possible to design a multiplexed assay, capable of detecting multiple, unique analytes.[1, 82] This is of particular interest in biological or environmental samples where a plethora of potentially relevant analytes can exist.[122] The use of SERS-active glyconanoparticles for the detection of lectins has been successfully demonstrated by Graham *et al.* as shown in figure 16.[14] Using mixed monolayer nanoparticles, coated with both RRM and thiolated lactose, the sensitive detection of the lectin ConA was achieved. The detection limit obtained through the use of SERS in this study (40 pM) surpassed those previously possible with UV-vis. extinction spectroscopy or DLS (40 and 2.9 nM respectively).[14, 49, 110] This was the first example of the use of SERS-active glyconanoparticles for the detection of lectins.

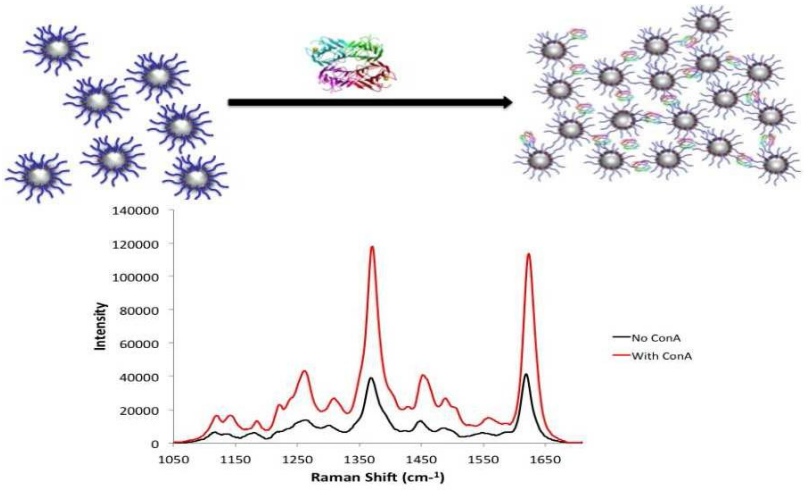

Figure 16. Raman reporter-coated lactonanoparticle assembly formation following addition of ConA and corresponding increase in RRM Raman intensity.[14]

Glyconanoparticles have also been used in imaging of a target species. Tseng *et al.*, prepared mannose functionalised nanodots for the detection of *Escherichia coli* (*E. coli*) by luminescence.[38] The lectin FimH, is expressed on the surface of E. coli, binding to terminal mannose residues on cellular surfaces. Not only was the detection of E. coli successful, the attachment of the nanodots to the bacteria resulted in growth inhibition.[38] This example highlights the various useful properties afforded by nanoparticles; simultaneously, detection and destruction of the pathogen are achieved.

Nanoparticles can be functionalised with carbohydrates, glycans or lectins. Lectin functionalised nanoparticles have been used for investigating the interaction of lectins with cell surface carbohydrates and to aid in drug delivery.[130, 131] They have also been used for

characterising the carbohydrate coverage of cells for the purpose of oncology.[10, 132] Characterising cellular surfaces is of interest to oncologists; certain carbohydrates and glycans have been identified as cancer biomarkers where the concentration and localisation of these can be used to track the progression and/or indicate the risk of cancer. Elevated levels of particular glycans, including those terminated with fucosyl, sialyl and N-acetylglucosamine residues, along with other carbohydrate antigens found on tumorous cell surfaces can be used as indicators for a variety of different cancer types.[132-134] Consequently, research has been directed towards better understanding cancer pathways from a glycan perspective. This is leading to the discovery and development of new detection and treatment strategies.[135-138]

Russell *et al.* used gold nanoparticles coated with the Jacalin lectin to successfully target the Thomsen-Freidenreich disaccharide antigen (T-antigen) expressed on HT-29 cancerous colon cells.[132] As shown in figure 17, the Jacalin lectin was shown to allow successful and selective attachment and uptake of the nanoparticles into the cells followed by subsequent detection using merged differential interference contrast (DIC) and confocal fluorescence (CF) microscopy. Along with Jacalin lectin, the nanoparticles were coated with phthalocyanine, which, upon interaction with an appropriate source of light, can be used to destroy the cancerous cells. This therapy is termed photodynamic cancer therapy (PDT). The system developed proved to be an effective way to both seek and destroy cancerous colon cells.

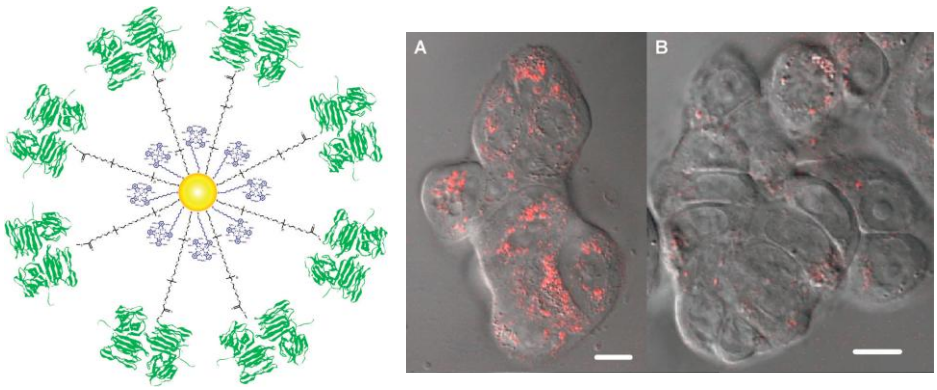

Figure 17. (Left) Jacalin lectin-PEG phthalocyanine gold nanoparticles. (Right) DIC/CF microscopy cell Image A) HT-29 cells with Jacalin lectin functionalised gold nanoparticles. DIC/CF microscopy cell Image B) HT-29 cells with unfunctionalised gold nanoparticles.

Graham *et al.* prepared lectin functionalised nanoparticles as molecular imaging agents to map the carbohydrate coverage of mammalian cells by SERS.[10] A number of lectins were used in functionalisation including ConA, *Lens culinaris* (LC) and wheat germ agglutinin (WGA). By measuring the signal of RRM on the nanoparticles surface it was possible to

observe attachment to the cells and thus compare the carbohydrate content of different cell types. As shown in figure 18, more nanoparticles were found to bind to cancerous, HeLa, cells compared with non-cancerous, Chinese hamster ovarian (CHO) cells, as a result of the increased carbohydrate expression on their surface. One such sugar monitored was N-acetylneuraminic acid. As stated, this has been used as a biomarker for cancer and in this particular study was targeted by the WGA-coated nanoparticles. The WGA-coated nanoparticles were shown to bind effectively to prostate cancer cells (PC3) and not to healthy prostate cells (PNT2A). When compared with fluorescence microscopy, SERS screening with lectin-functionalised nanoparticles was found to provide greater discrimination between the cancerous and non-cancerous cells.

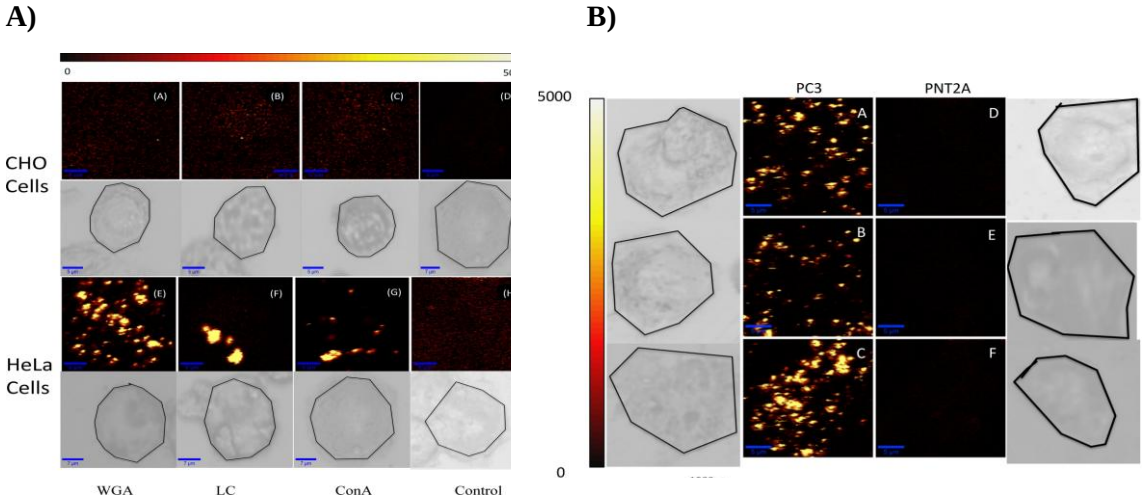

Figure 18. A) Confocal SERS map of HeLa and CHO cells following incubation with a variety of lectin-coated nanoparticles. B) Confocal SERS map of PC3 and healthy prostate PNT2A cells following incubation with WGA-coated nanoparticles.

Glyconanoparticles have the potential for use in bioassays as well as further developing the researcher's understanding of glycobiology which for a long time was a relatively underdeveloped area of biology.[23]

4.2 Carbohydrate Microarrays

Microarrays incorporate lab-on-a-chip technology and multiplexing capability on one substrate. Throughout the early 1990's, research groups across the globe set about developing high-throughput, low volume arrays to advance gene determination with the aim of achieving the human genome project's goals.[139] These began initially as macroarrays but were rapidly downscaled and in 1995 Schena *et al.* reported the first use of microarrays using robot printed DNA on microscopic glass slides to determine the expression of 45

Arabidopsis genes simultaneously in a high-throughput fashion.[140] Since then, microarrays have advanced considerably and are now used for a variety of different applications including high-throughput mini-sequencing, differential methylation hybridisation (DMH), and chromatin immunoprecipitation on microarrays (ChIP-on-chip).[141-143] Microarray platforms and applications have expanded to include cellular, tissue-based and microorganism microarrays, protein-based assays including antibody arrays and carbohydrate-based arrays including glycoprotein and lectin microarrays.[144-147] Additionally, microarray production and hence reproducibility and robustness have also benefited from improvements to the proprietary coatings of the glass slides. This yields better quality spots by ensuring consistent size and morphology.[148]

There are a variety of ways to interrogate the substrate and detect an analyte of interest. Commonly, fluorescence spectroscopy is used by tagging a protein, for example a lectin, of interest or by tagging a second species that can interact with the protein if it is bound to the surface glycans.[149, 150] Though this is a commonly used technique for glycan array interrogation there are limitations including the need to either tag the protein of interest or the need to obtain a fluorescent second species that will interact with the bound protein. Alternative methods of detection include surface plasmon resonance (SPR) and mass spectrometry. Mass spectrometry has been coupled with glycan microarrays to provide a powerful technique for the identification and characterisation of glycosyltransferase (biocatalytic enzymes involved in the production of oligosaccharides).[151] SPR has been used for real-time, label free detection of glycan interactions on microarrays. This has included the profiling of lectins and the determination of Ricin inhibitors.[152] Carbohydrate microarrays have been used to detect a variety of species including viral and bacterial proteins and whole cells, glycoaminoglycans, monoclonal antibodies and lectins and to measure immune response, towards cancer drugs.[153-158] It is hoped that the emerging technologies of functionalised nanoparticles and biologically applicable microarrays can be coupled together effectively. Their symbiotic use could drive research into both well and poorly understood biological interactions and associations while also advancing each technology significantly.

As described, the use of glyconanoparticles for detection of the legume lectin, Concanavalin A, by SERS has been achieved by Graham *et al.*[14]. This research allowed for an initial point from which to pursue further developments using SERS-active glyconanoparticles, including the development of a glucose sensor, waterborne bacterial lectin assay and surface-based assays (with a view to developing nanoparticle-based carbohydrate microarrays, coupled

with SERS detection). A significant challenge included ensuring the nanoparticles retained their colloidal form under the ionic conditions typical of samples, for example clinical or those taken from natural bodies of water. Overcoming this obstacle would allow a relevant and reliable glyconanoparticle to be developed for use in the stated applications.

Project Aims

Glyconanoparticles have value as tools in sensing and in developing a greater understanding of carbohydrate-carbohydrate and carbohydrate-protein interactions. This has previously been demonstrated by the research community with bacterial toxin detection, cancer cell screening and metal ion sensing, for example. The project sought to pursue development of glyconanoparticles for a variety of SERS-based applications including glucose sensing, bacterial toxin detection and the development of surface-based assays. The overall aims of the project were to:

- Generate stable, selective SERS-active glyconanoparticles, capable of being used reliably under salt conditions and react with a host of different plant lectins.
- Apply the technique used to generate these glyconanoparticles, in developing particles for use in glucose sensing, bacterial toxin detection and in the development of surface based lectin detection i.e. microarrays
- In each instance surface enhanced Raman spectroscopy (SERS) would be used as the primary measurement method, with UV-vis. extinction spectroscopy and dynamic light scattering also used to support findings.

The results described herein are based on these aims and are subsequently described in four chapters:

- Generating Stable, Lectin-Reactive Glyconanoparticles
- SERS-Based Glyconanoparticle Glucose Sensor
- SERS Detection of Cholera Toxin
- Developing Carbohydrate Microarrays

Generating Stable, Lectin-Reactive Glyconanoparticles

The sensitive and selective detection of biological species relies on the generation of stable yet responsive biosensors. Detection of a target often makes use of direct-labelling with fluorophores, for example. While these provide high sensitivity, they are susceptible to photo-bleaching and do not allow for multi-analyte detection.[159] Additionally, labelling requires treatment steps which, in the case of an unknown sample, may not work or might be time-consuming and potentially waste resources. Alternatively, an analyte can be detected using a secondary binding species which itself is labelled with a fluorophore (following reaction with a development agent) as is the case in enzyme labelled immuno-sorbent assays (ELISAs). However, this again requires additional time and resources for analyte detection along with the use of costly and difficult to obtain monoclonal antibodies, multiple wash and development steps and an uncertainty in the efficacy of blocking agents in effectively detecting novel or poorly understood analytes.[160] A rapid, selective and molecularly specific biosensing platform can be provided by SERS-active metallic nanoparticles. Particles, coated in RRMs, aggregate in the presence of a target of interest, increasing the associated RRM signal and giving an indirect measurement of analyte concentration. Alternatively, nanoparticles can be used to target specific analytes, for example intracellular species, giving rise to molecularly specific surface enhanced Raman signals for those species.[161] Both direct and indirect analyte detection by SERS allow for multi-analyte detection. Nanoparticles can be coded with different biomolecules and unique RRMs. In this way multiplexed detection is possible as unique SERS bionanosensors will aggregate with different targets simultaneously.[162]

The efficacy of these sensors relies on their selective and reliable activity towards a target. This is possible through the previously described stabilising surface species, including alkanethiol and polymeric coatings to which a target-binding molecule can subsequently be attached. Herein, the development of rapidly prepared alkanethiol- or PEG-coated, lectin-specific, silver glyconanoparticles is described. The research builds on work previously carried out using shorter (propyl) tethering units for glyconanoparticle preparation.[14]

Generating Stable, Lectin-Reactive Glyconanoparticles

1. Raman Reporter Molecule

Silver was chosen over gold as the Raman enhancing nanoparticle material because of the formers comparatively greater Raman scattering cross-section.[163] It was hoped that the coating strategy for the silver particles would offset their relative instability when compared with gold. The excitation wavelength of 40 nm silver nanoparticles is ~ 400 nm. To maximise SERS, a RRM should be chosen with chromophores that require close to this excitation. To undergo SERS, a molecule must be orientated perpendicularly to the metal surface. This is encouraged with either super-monolayer concentration of the RRM and/or with particular attachment motifs.

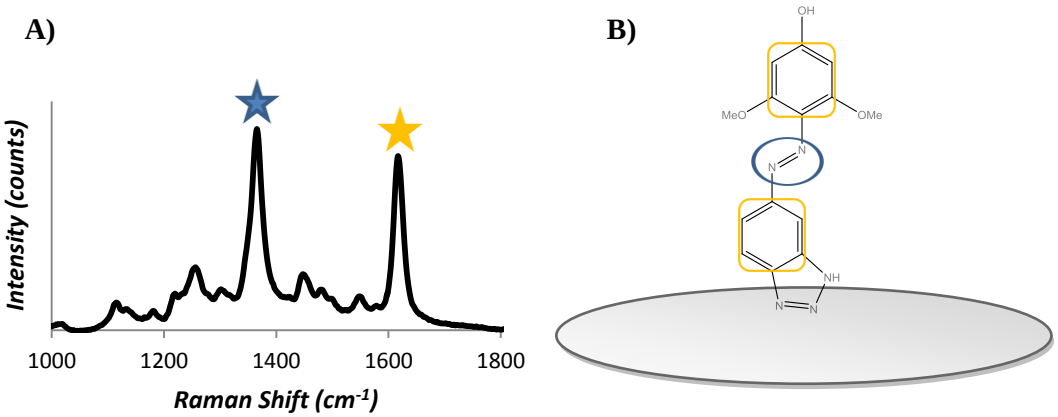

Figure 19. A) Raman (SERS) spectrum of the 4-((1H-benzo[d][1,2,3]triazol-6-yl)diazenyl)-3,5-dimethoxyphenol (RB1) dye, bound to 40nm silver nanoparticles and obtained by irradiation with a 514.5 nm laser B) RB1 molecular structure with peaks of interest indicated and corresponding to the coloured stars.

Benzotriazole-based molecules are suitable in this respect; the triazole unit encourages attachment to the metal surface in a perpendicular orientation while this and the aromatic units resonate with the metal plasmon frequency giving rise to effective enhancement of the Raman signal. In the case of RB1 (spectrum and structure shown in figure 19), the peaks between 1350 and 1450 cm^{-1} are attributed to aromatic ring and azo stretches (with the 1364 cm^{-1} peak (blue star) assigned to the azo stretches).[164] The peak at 1616 cm^{-1} (yellow star) is attributed to aromatic ring stretching and specifically a modified quadrant stretch.[164] The RRM, RB1 was chosen for project experiments, due to the well defined spectrum produced and the lack of aggregation caused to the nanoparticles it was added to as shown in table 1.

Table 1. λmax and 600 nm to plasmon extinction ratio results for silver citrate nanoparticles with different concentrations of RB1 added.

RB1 Concentration (μM)	λ max.	600 nm : Plasmon Extinction
0	405	0.089
1	408	0.102
10	407	0.100

Aggregation can be measured by monitoring changes to the ratio of the extinction intensity of the 600 nm region to that of the plasmon extinction peak together with the change in λ max.. As shown in table 1, minimal changes are measured both in the λmax. and 600 nm to plasmon extinction ratio indicating the stability of the particles coated with RB1. The concentration of RB1 used in subsequent experimentation was 10 μM.

2. Heterobifunctional Linkers

Previously, SERS-responsive glyconanoparticles have been prepared with carbohydrate linkers based on propionic acid.[14] These were produced *via* Steglich esterification between the primary hydroxyl of the desired carbohydrate and the carboxylate of 3-mercaptopropionic acid. Though this method proved successful for the preparation of glyconanoparticles and the detection of the lectin Concanavalin A, the linkers were prepared separately from the nanoparticles, requiring multiple, time-consuming steps to synthesise the linker and separate functionalisation of nanoparticles with those linkers. The incorporation of the nanoparticle coating step with carbohydrate functionalisation was pursued with an aim to reduce the preparation time to 1 day.

Heterobifunctional linkers possess a variety of different functionalities which generate versatile nanomaterials. An amine or sulfohydryl functionality allows attachment of the linkers to the silver nanoparticle surface through the soft-soft association between the metal and ligand. Following addition of an appropriate concentration, the linkers bind the nanoparticle surfaces, forming assembled monolayers and positioning the second functionality, for example carboxylate or amino group, away from the surface. This allows for covalent attachment of a target-binding molecule, for example protein, peptide or carbohydrate. The research herein makes use of thio/carboxyl linkers which decorate silver nanoparticle surfaces with amine reactive carboxyl groups. Water-soluble carbodiimides encourage amide coupling between amine-bearing carbohydrates, for example glucosamine and the surface-bound carboxyl groups (see figure 20).

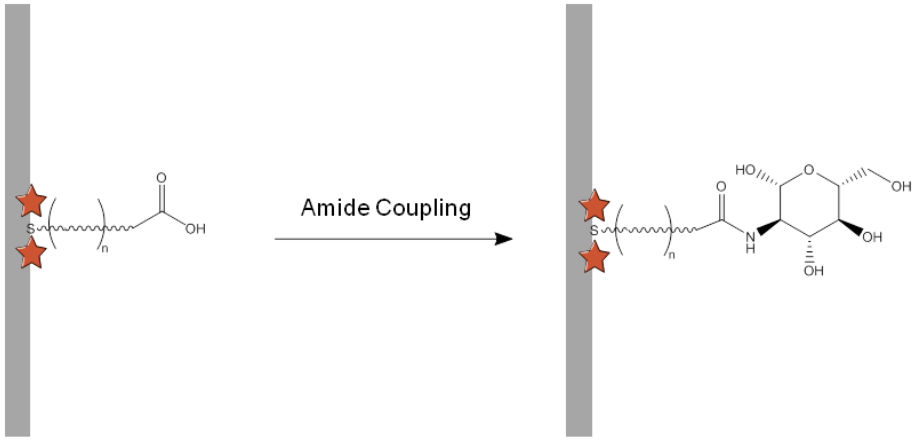

Figure 20. (Left) Functionalisation of the nanoparticle surface with heterobifunctional linkers for example, those with carboxyl/thiol functionalities, gives a surface presenting carboxylic acid groups. (Right) The carboxyl subsequently reacts, under appropriate amide coupling conditions to give a surface decorated with carbohydrates.

As shown in figure 4 of the thesis introduction, hydroxyl groups on C3, 4 and 6 (3-OH, 4-OH and 6-OH respectively) of mannose are involved in Concanavalin A binding. Previously, preparation of carbohydrate derivatives had relied on ester formation at the primary 6-OH of the sugar. Though this gives good regioselectivity in the generation of one type of sugar ester, it diminishes the possible binding between 6-OH and the lectin. It was therefore thought that by using the aminated version of the sugars of interest, where the 2-OH, not used in lectin interaction, is replaced by NH_2, it would be possible to generate glycoderivatives that would bind selectively to the lectins of interest. The use of water soluble 1-ethyl-3-(3-dimethylaminopropyl)carbodiimide (EDC) and N-hydroxysulfosuccinimide (sNHS) reduces the need for several different preparation or purification steps in the generation of glyconanoparticles. As with the 3-mercaptopropionic acid based carbohydrate derivative, the thiolated moiety of alkanethiols and PEG reagents allow facile, covalent attachment to gold or silver nanoparticles. This allows functionalisation of the nanoparticles with the desired coating followed by coupling to glucos- or galactosamine in two steps with only centrifugation and resuspension in the appropriate buffer required as additional steps.

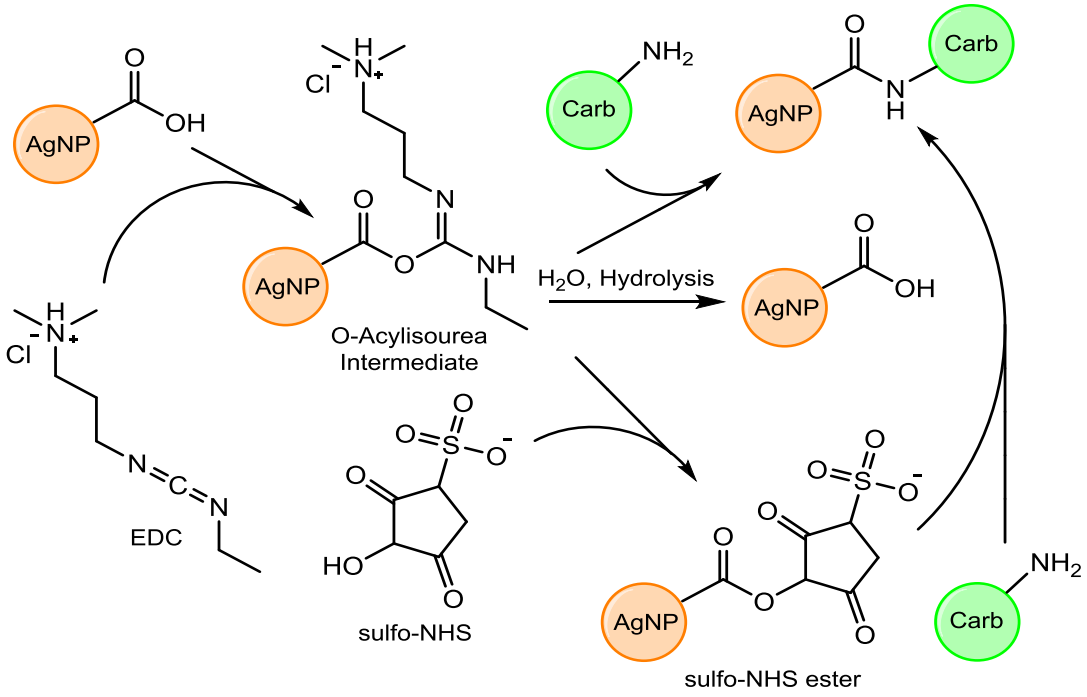

Figure 21. EDC/sNHS reaction cycle giving amide coupled, carbohydrate (Carb) coated nanoparticles (AgNP). The O-acylisourea intermediate normally undergoes one of three processes. Hydrolysis of the intermediate gives the original carboxyl group and deactivates the EDC. Presence of an amine can give formation of an amide however this is unlikely in aqueous conditions without the presence of sNHS.

The EDC/sNHS amide coupling procedure has been successfully used for a variety of procedures including, protein and peptide modifications and the functionalisation of nanoparticle surfaces.[165, 166] The sulfonic acid analogue of NHS is water soluble allowing coupling to be performed in aqueous environments. Careful consideration of the optimal pH for amide coupling using the EDC/sNHS system is required. MES buffer, at a pH of between 5 and 6, is typically used in the initial formation of the sNHS ester. The slightly acidic pH discourages hydrolysis of the sNHS ester prior to the addition of the aminated species.[167, 168] Upon addition of the amine, the pH of the mixture is increased to between 7.2 and 7.5 (depending on the pka of the amine).[169] A balance must be struck between activating the amine for nucleophilic attack and the rate of hydrolysis of the sNHS ester, as the half-life of the ester is 4-5 hours at pH 7, 1 hour at pH 8 and 10 minutes at pH 8.6.[167, 168] Non amine buffers, such as HEPES or phosphate, are typically used both for dissolution of the amine-bearing species and in pH adjustment. An additional consideration is the mixing of the EDC and sNHS prior to addition to the carboxy-coated nanoparticles, As shown in figure 21, hydrolysis of the O-acylisourea occurs rapidly in aqueous conditions to give the original carboxyl functionality and an inactive urea, 1-(3-(dimethylamino)propyl-3-ethylurea (EDU).[170] By pre-mixing the EDC and sNHS, this encourages the formation of the sNHS

ester before hydrolysis of the O-acylisourea can proceed. An additional consideration to ensure effective coupling is the ratio of the coupling components. Generally, the EDC should be at a >10x molar excess compared with the carboxyl-bearing species. When preparing the coupling mixture a minimum of 15x molar excess of EDC was used together with a 20x molar excess of sNHS and aminated carbohydrate. Silver nanoparticles were coated in either alkanethiols or PEGylated linkers to assess the suitability of each coating type in glyconanoparticle preparation.

3. Alkanethiol Coating

Alkanethiols provide a rapid way of coating nanoparticles for further functionalisation. By centrifuging the nanoparticles, it is possible to remove the supernatant and thereby readily discard any unbound thiol, giving only surface-bound carboxyl groups available for further functionalisation. Citrate-capped silver nanoparticles (prepared using the Lee and Meisel method) were coated with different concentrations of 6-mercaptohexanoic acid (MHA) to give silver (Ag)-MHA conjugates. Excess MHA was removed by a two-step centrifugation (slow speed spin and high speed spin) to ensure that changes in size and extinction results could only be attributed to single nanoparticle size increase and not aggregate formation. The preparation of these nanoparticles was monitored at each functionalisation stage by UV-vis. extinction spectroscopy and DLS to evaluate the extinction and size of the nanoparticles, thereby indicating if successful conjugation had occurred.

Table 2. Extinction and size data for silver colloid and 6-mercaptohexanoic acid conjugates of silver colloid (Ag-MHA).

Nanoparticle Coating	λmax. (nm)	Size (nm)
Citrate	404	45.90 ± 0.18
MHA (25 μM)	411	49.42 ± 0.25
MHA (50 μM)	410	50.17 ± 0.53
MHA (100 μM)	411	73.52 ± 0.80
MHA (200 μM)	414	66.93 ± 0.28

As shown in table 2, the size of the conjugates increased, following addition of MHA and a corresponding red-shift in the surface plasmon λmax. was also measured. This indicated successful functionalisation of the particles with MHA. The greater size increase at higher concentrations (100 and 200 μM MHA) could have also been caused by slight aggregation of the nanoparticles. To mitigate this, 6-Mercaptohexanol (MHL) was added as a stabilising

agent to block any sites not already bound by the 6-mercaptohexanoic acid. However, the use of this caused significant aggregation as shown in table 3.

Table 3. Extinction data for nanoparticles samples with varying ratios of 6-mercaptohexanoic acid/6-mercaptohexanol at a total concentration of 100 μM.

Nanoparticle Coating	λmax. (nm)	Extinction
Citrate	403	1.212
MHA/MHL (10/90 μM)	415	0.264
MHA/MHL (20/80 μM)	409	0.929
MHA/MHL (50/50 μM)	410	0.920

Increasing the proportion of MHL to MHA caused aggregation as shown in table 3 by the dramatic decrease in extinction when 90% of the component added was the alcohol. As mercaptohexanol is a neutral species, it was thought that its presence could decrease the electrostatic repulsion between nanoparticles. This combined with the lack of steric bulk provided by MHL or MHA allowed the nanoparticles to come into close proximity and, due to van der Waals interactions, aggregated.

Subsequently, the nanoparticles were functionalised with 6-mercaptohexanoic and the surface-blocking protein, bovine serum albumin (BSA). Successfully prepared silver-MHA particles were combined with EDC, sNHS and glucos- or galactosamine for amide coupling as indicated in figure 20. Following this, the samples were washed of any unbound carbohydrate by two-step centrifugation and resuspended in 10 mM HEPES buffer, pH 7.4, containing BSA to block any uncovered sites on the nanoparticles. These were then rinsed free of any unbound BSA and suspended in 10 mM HEPES buffer with 0.2 mM manganese nitrate and calcium nitrate at pH 7.4.

Table 4. Extinction and size data for glucosamine/galactosamine conjugated silver nanoparticles *via* 6-mercaptohexanoic acid.

Nanoparticle Coating	λmax. (nm)	Size (nm)
MHA(25 μM)-Glucose (80 μM)	414	70.87 ± 0.34
MHA(25 μM)-Galactose (80 μM)	415	90.97 ± 0.52
MHA(50 μM)-Glucose (80 μM)	413	116.73 ± 2.57
MHA(50 μM)-Galactose (80 μM)	413	67.37 ± 0.35
MHA(100 μM)-Glucose (80 μM)	413	75.91 ± 0.24
MHA(100 μM)-Galactose (80 μM)	413	86.49 ± 1.70
MHA(200 μM)-Glucose (80 μM)	413	73.69 ± 0.62
MHA(200 μM)-Galactose (80 μM)	413	104.23 ± 2.63

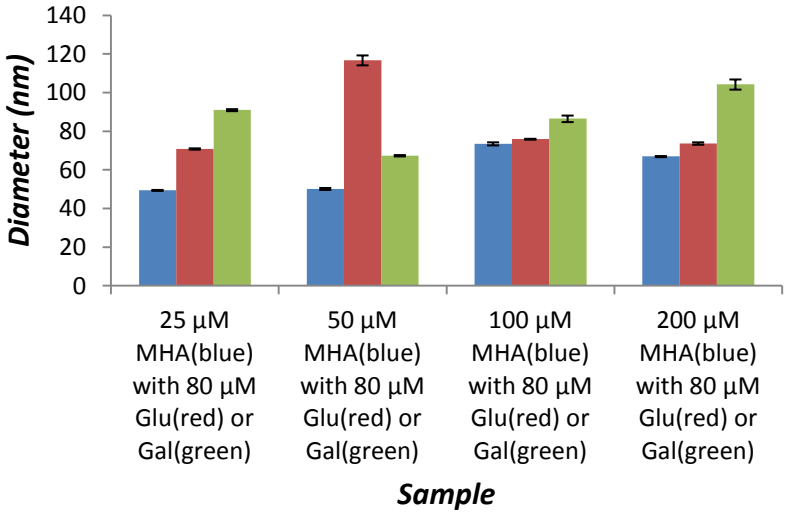

Figure 22. Size of nanoparticle conjugates with each stage of preparation when compared with an initial silver nanoparticle size of 46 nm.

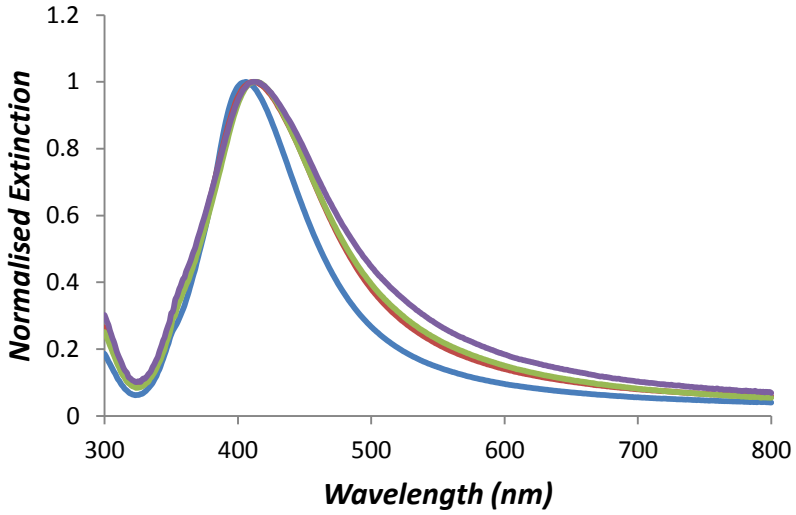

Figure 23. Normalised extinction spectra of silver nanoparticles (citrate) (blue), MHA-nanoparticles (100 µM) (red), MHA-gluconanoparticles (green) and MHA-galactonanoparticles (purple).

Table 4 demonstrates that the conjugates increase in size following coupling to glucosamine or galactosamine. A summary of the size and extinction changes of the conjugates with each preparation step are illustrated in figures 22 and 23 respectively. In general, the size and extinction maxima of the particles increased and red-shifted respectively with each new species conjugated to the surface in the order colloid < colloid-MHA < colloid-MHA-carbohydrate. The glucose and galactose-coated samples with 100 µM MHA were most similar in terms of size and extinction. At lower and higher concentrations there were significant changes in size measured which were attributed to aggregation. It was therefore

decided that the 100 μM MHA samples would be used. To assess the conservation of stability over time, the size and extinction profile of these particles were measured 72 hours after coupling. As noted from table 5 little change in size or extinction occurs when compared with the values in table 4.

Table 5. Extinction and size data for glucosamine/galactosamine-conjugated silver nanoparticles *via* 6-mercaptohexanoic acid.

Sample	λmax. (nm)	Size (nm)
Ag-MHA(100 μM)-Glu (72 hours)	413	71.28 ± 0.28
Ag-MHA(100 μM)-Gal (72 hours)	413	78.16 ± 1.55

3.1 Lectin Testing

In order to test the success of carbohydrate conjugation and hence the lectin-binding activity of each nanoparticle type, lectins, specific and non-specific to each sugar type, were added to the conjugates and changes in UV-vis. extinction spectroscopy monitored over 2 hours. The lectins tested were the glucose specific Concanavalin A and the galactose specific *Artocarpus integrifolia* lectin (Jacalin lectin).

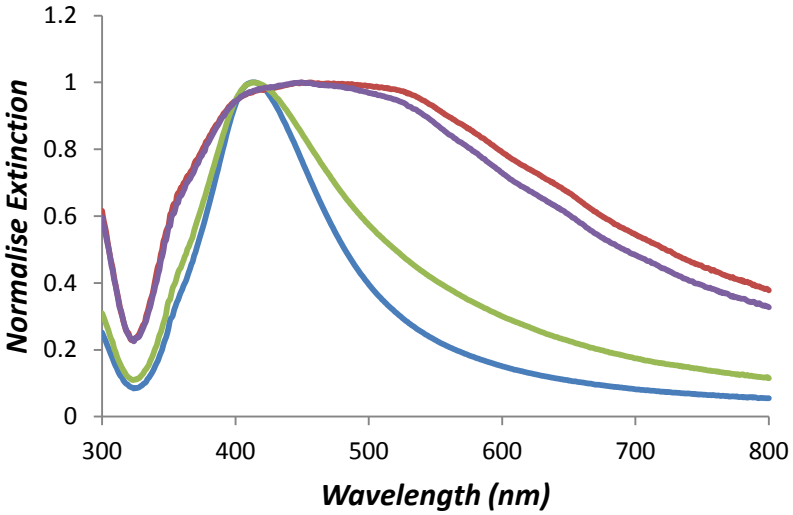

Figure 24. Extinction spectra of MHA-glyconanoparticle control (blue) MHA-gluconanoparticles with 600 nM ConA (red) MHA-galactonanoparticles with 600 nM ConA (green) and MHA-galactonanoparticles with 600 nM Jacalin lectin (purple) taken 30 minutes after lectin addition.

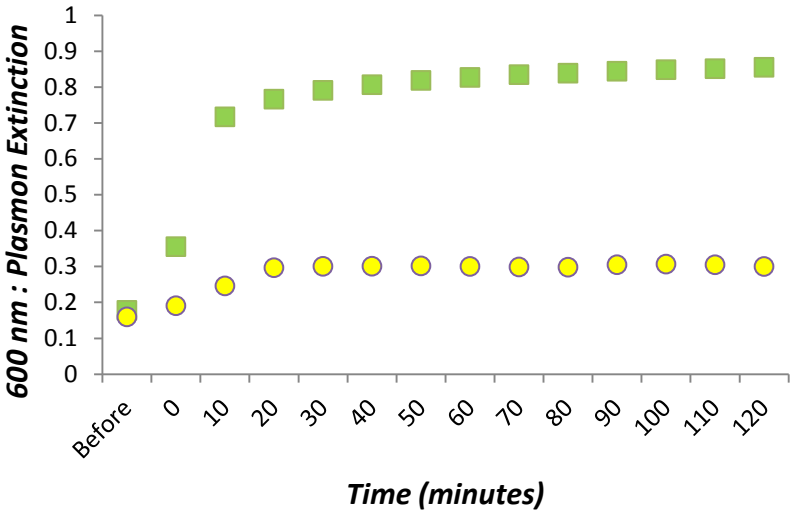

Figure 25. Ratio of the 600 nm to plasmon extinctions over time for the MHA-gluconanoparticles with 600 nM ConA (green) MHA-galactonanoparticles with 600 nM ConA (yellow).

Figure 24 illustrates the increased aggregation of the galactonanoparticles in the presence of Jacalin lectin when compared with Concanavalin A. There was still some aggregation of the galactonanoparticles with ConA as indicated by both figures 24 and 25, demonstrating a lack of selectivity with the MHA-based galactose-coated conjugates.

As stated, the ratio of extinction at 600nm to that of the surface plasmon can be used to monitor the aggregation of nanoparticles. The results in figures 24 and 25 demonstrate aggregation of the glyconanoparticles in the presence of target lectins. However, some unexpected aggregation was noted for the galactonanoparticles in the presence of Concanavalin A. One suggestion for this observation was that the MHA was providing insufficient protection for the particle from non-specific binding of the lectin. Additionally, the BSA, used to provide protection for the nanoparticles from non-specific binding, can be glycated and hence could possess carbohydrates to which Concanavalin A has affinity , namely glucose and mannose residues. These observation raised the need to test alternative linkers and blocking agents to BSA such as PEG-based linkers.

A change of blocking species was first tested. Having re-prepared MHA-based gluco- and galactonanoparticles, the final step of washing the nanoparticles with BSA was instead carried out with SH-PEG-OCH_3 (average M_n = 5000 g mol^{-1}) ($MTPEG_{90}$) at a final concentration of 10 μM. Subsequently the nanoparticles were resuspended in the lectin testing buffer and tested with Concanavalin A and Jacalin lectin. Changes to extinction were

measured by UV-vis. extinction spectroscopy to evaluate the use of PEG as a blocking agent for lectin-sensing glyconanoparticles.

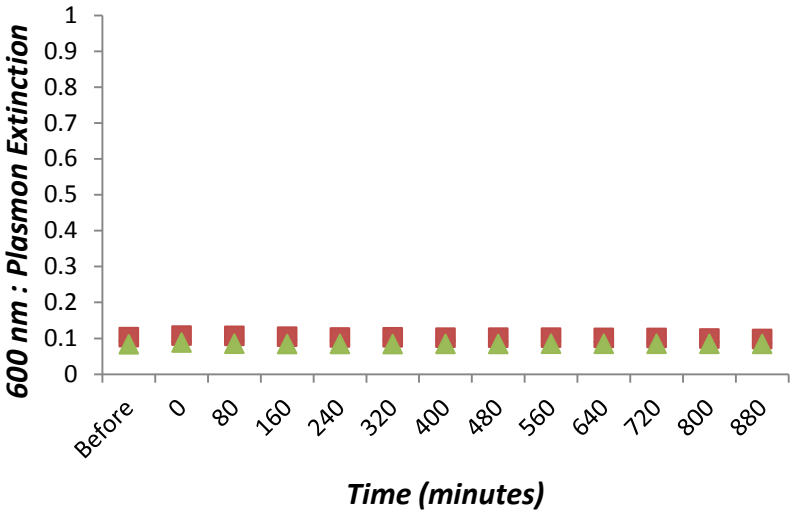

Figure 26. Ratio of the 600 nm to plasmon extinctions over time for MHA/ $MTPEG_{90}$-gluconanoparticle control (Blue) MHA/$MTPEG_{90}$-gluconanoparticles with 600 nM Jacalin lectin (Green) and MHA/$MTPEG_{90}$-gluconanoparticles with 600 nM ConA (Red).

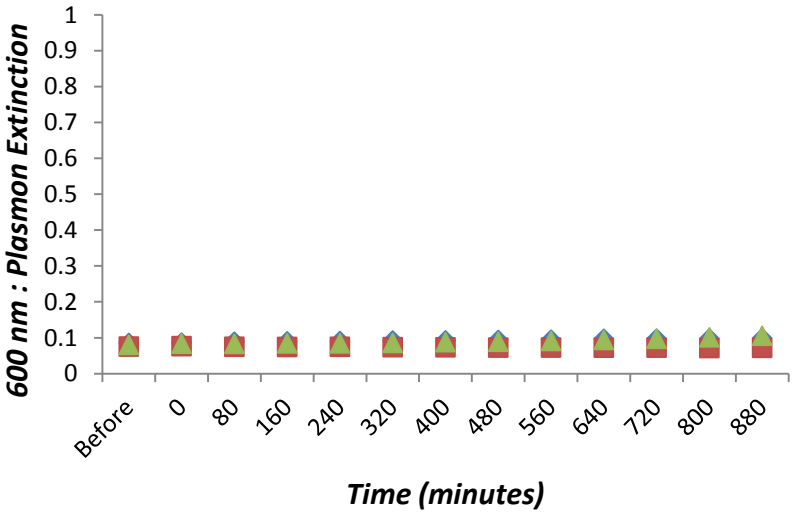

Figure 27. Ratio of the 600 nm to plasmon extinctions over time for MHA/ $MTPEG_{90}$-galactonanoparticle control (Blue) MHA/ $MTPEG_{90}$-galactonanoparticles with 600 nM Jacalin lectin (Green) and MHA/ $MTPEG_{90}$-galactonanoparticles with 600 nM ConA (Red).

Figures 26 and 27 illustrate the lack of aggregation in the modified system when using $MTPEG_{90}$ as a blocker. There was a slight increase in the ratio for the galactonanoparticle

sample with Jacalin lectin over time (after 880 minutes), indicating some gradual aggregation, however this detracted from the rapid detection desired. It was proposed that the $MTPEG_{90}$ molecules, being much larger than MHA, smothered the surface of the nanoparticle and blocked the carbohydrates from binding to the lectins through unfavourable sterics as a result of the mobile and extensive PEG chains. A proposed solution was to replace the MHA coating with carboxyl/thiol PEG (CTPEG) which could be used both to protect the surface and for further functionalisation with carbohydrates.

4. Thiolated PEG Evaluation

Heterobifunctional, $SH\text{-}PEG_n\text{-}CO_2H$ (CTPEG) linkers were investigated as an alternative to 6-mercaptohexanoic acid, with the hope that greater selectivity would be observed between glyconanoparticles and the target lectin compared with non-specific lectins.

4.1 $CTPEG_{90}$

Initial studies were carried out using the carboxyl/thiol $CTPEG_{90}$. The theoretical concentration of $CTPEG_{90}$ required for nanoparticle monolayer coverage was calculated as follows.

Equation 2

$$Area\ of\ nanosphere\ (\boldsymbol{ANS}) = 4\pi r^2$$

Equation 3

$$Number\ of\ PEG\ molecules\ per\ nanosphere\ (\boldsymbol{NPEG}) = \frac{ANS}{Area\ occupied\ by\ one\ PEG\ molecule}$$

Equation 4

$$Concentration\ of\ PEG\ (M) = Nanoparticle\ concentration(M) \times NPEG$$

A PEG footprint of $0.35nm^2$ was used together with equations 2-4 and a silver nanoparticle concentration of 4.04×10^{-10} M in calculating the minimum concentration required for coverage of 40 nm silver citrate nanoparticles as 8-10 μM.[171] A 10 times excess (100 μM) of this amount was used to ensure complete nanoparticle coverage. Any unbound PEG was then removed by rapid (15 minute) centrifugation steps. The prepared conjugates were evaluated by UV-vis. extinction spectroscopy and DLS.

Table 6. Extinction and size data for nanoparticles coated with either citrate, $CTPEG_{90}$ or $CTPEG_{90}$-glucose

Nanoparticle Coating	λ max. (nm)	Size (nm)
Citrate	401	45.90 ± 0.18
$CTPEG_{90}$	405	71.68 ± 0.80
$CTPEG_{90}Glu$	428	93.66 ± 6.96

The increase in size and considerable red-shift of the extinction maximum, shown in table 6, indicated the successful functionalisation and subsequent amide coupling between the $CTPEG_{90}$ and aminated carbohydrate. The larger increase in size and red-shift when compared with the MHA-glyconanoparticles was indicative of the increased length of the PEG when compared with MHA.

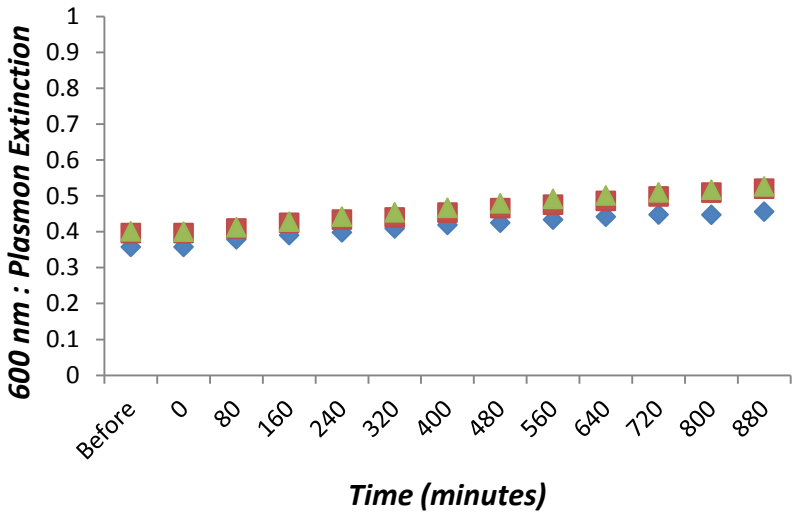

Figure 28. Ratio of the 600 nm to plasmon extinctions over time for PEG_{90}-glyconanoparticle control (blue) PEG_{90}-gluconanoparticle with 600 nM ConA (green) and PEG_{90}-gluconanoparticle with 100 nM ConA (red).

The lack of change in extinction demonstrated in figure 28 was attributed to the size of the PEG chains, which would distance the carbohydrates from the nanoparticles surface and reduce any coupling between the electromagnetic field of individual particles brought together *via* interaction with the lectin. For this reason, the shorter $CTPEG_{12}$ linker was tested. It was hoped that $CTPEG_{12}$ would provide greater stability to the nanoparticles from non-specific interferents than the MHA linker, while also enabling the particle extinction profile to change more predominantly when compared with $CTPEG_{90}$ as a coating.

4.2 $CTPEG_{12}$

Nanoparticles were coated with the same concentration of $CTPEG_{12}$ as $CTPEG_{90}$ (100 μM). The concentrations of coupling reagents and aminated carbohydrates were equivalent to that used with the $CTPEG_{90}$. The conjugates were characterised by UV-vis. extinction spectroscopy, DLS and by gel electrophoresis.

Table 7. Extinction and size data for nanoparticles with either citrate, PEG_{12}, PEG_{12}-glucose or PEG_{12}-galactose

Nanoparticle Coating	λ max. (nm)	Size (nm)
Citrate	403	45.9 ± 0.18
PEG_{12}	410	67.25 ± 0.16
$PEG_{12}Glu$	411	71.67 ± 1.09
$PEG_{12}Gal$	411	69.41 ± 0.24

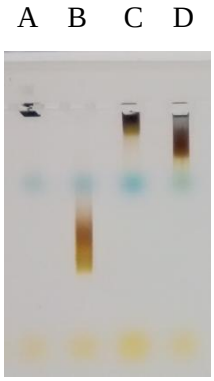

Figure 29. Agarose gel electrophoresis image showing transit of silver nanoparticles with various coatings; A) citrate, B) PEG_{12} C) PEG_{12}-glucose, D) PEG_{12}-galactose

The red-shift in extinction maximum and particle size increase indicated both the successful coating of the nanoparticles with $CTPEG_{12}$ and subsequent coupling of glucosamine or galactosamine to the particles. Figure 29 illustrates the changes in particle behaviour in the agarose gel, depending on the coating present. It was proposed that the PEG coating protected the surface of the particles, thereby preventing aggregation in the buffer used, allowing the particles to travel readily through the gel. It was also proposed that coupling of the carbohydrate to the nanoparticle surface encouraged these to interact with the agarose (a polymeric carbohydrate) *via* hydrogen bonding.

As with the Ag-MHA and Ag-PEG_{90} conjugates, the lectin reactivity of Ag-PEG_{12} conjugates was measured initially by changes in extinction spectroscopy.

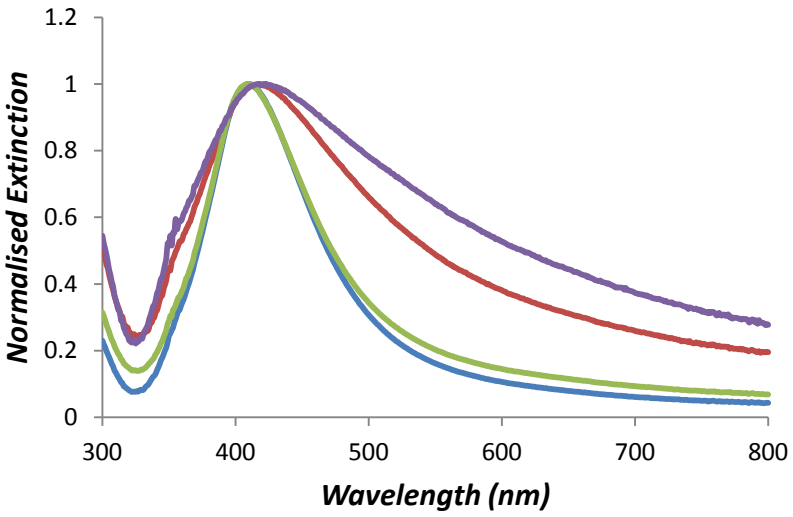

Figure 30. Extinction spectra of the $CTPEG_{12}$-glyconanoparticle control (blue) $CTPEG_{12}$-gluconanoparticles with 600 nM ConA (red) $CTPEG_{12}$-galactonanoparticles with 600 nM ConA (green) and $CTPEG_{12}$-galactonanoparticles with 600 nM Jacalin lectin (purple) taken 30 minutes after lectin addition.

The extinction spectra shown in figure 30 demonstrate the selective interaction between the glyconanoparticles produced and the lectins. In the case of the glucose nanoparticles, these interacted most strongly with ConA as shown by the spectrum measured 30 minutes after incubation with 600 nM ConA. There was only slight interaction measured between the galactonanoparticles and ConA, demonstrating the selectivity of the particles produced. To demonstrate the reactivity of the galactonanoparticles these were incubated with the galactose-binding lectin, Jacalin lectin. The extinction spectrum measured 5 minutes after incubation with lectin demonstrated aggregation and confirmed the reactivity of these particles towards galactose-binding lectins. It was hoped that this reactivity could eventually be used for the detection of galactose-binding toxins, for example the cholera toxin B subunit (CTB). Due to the success observed with $CTPEG_{12}$, this linker was used for subsequent glyconanoparticle preparation

To demonstrate the importance of pre-mixing the EDC and sNHS to ensure effective coupling, glyconanoparticles prepared with separate EDC/sNHS addition and mixed EDC/sNHS addition were incubated with 600 nM lectin and changes in extinction measured.

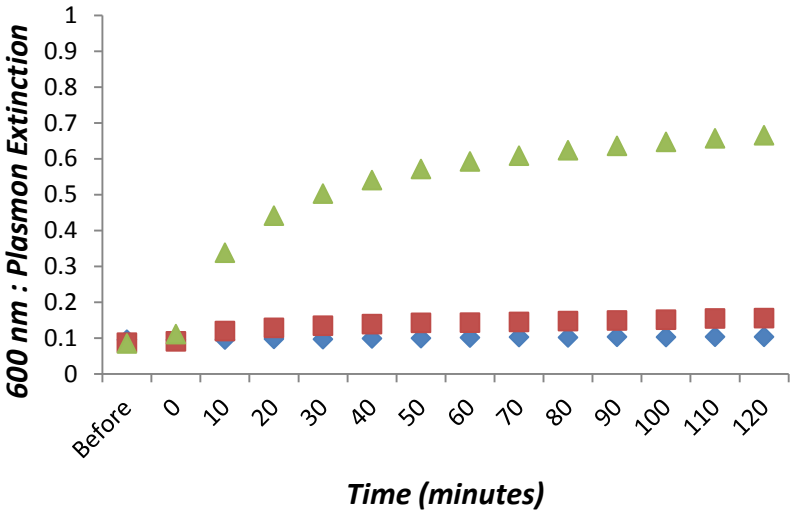

Figure 31. Ratio of the 600 nm to plasmon extinctions over time for gluconanoparticles (Blue) gluconanoparticles prepared using mixed EDC/sNHS addition with 600 nM ConA (Green) gluconanoparticles prepared using separate EDC/sNHS addition with 600 nM ConA (Red).

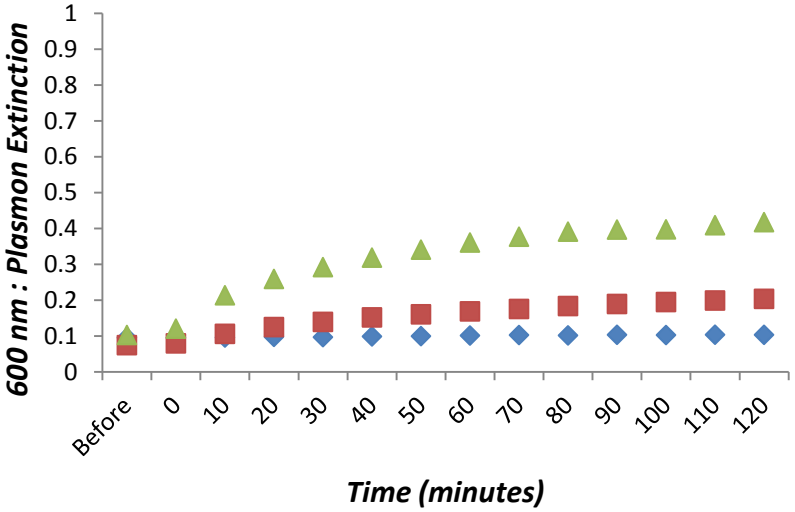

Figure 32. Ratio of the 600 nm to plasmon extinctions over time for galactonanoparticles (Blue) galactonanoparticles prepared using mixed EDC/sNHS addition with 600 nM Jacalin lectin (Green) galactonanoparticles prepared using separate EDC/sNHS addition with 600 nM Jacalin lectin (Red).

As demonstrated by figures 31 and 32, the changes in extinction, and hence aggregation were greatly enhanced when the EDC and sNHS were premixed. When mixed separately, it was proposed that a high proportion of the O-acyl urea was cleaved from the PEG by hydrolysis, preventing the formation of amine-reactive sNHS esters. This then reduced the amount of carbohydrate bound to the nanoparticle surface and hence the reactivity towards

the lectins. This was supported by observation of this experimentally for both gluco- and galactonanoparticles incubated with 600 nM ConA or Jacalin lectin respectively.

The lectin-mediated aggregation experiments were repeated using Raman reporter molecule (RB1)-coated nanoparticles (prepared according to section 6.2 of the experimental section) and changes in the SERS intensity of the surface-bound RB1, measured. It was hoped that an increase in the SERS intensity of RB1 would accompany the changes in extinction profile previously measured. Initially, experiments were carried out using only the gluconanoparticles with ConA. This and all subsequent SERS spectra measured (excluding those taken for the Developing Carbohydrate Microarrays chapter) were normalised against the SERS intensity of the 800 cm^{-1} peak of the spectrum of cyclohexane, measured prior to each experiment.

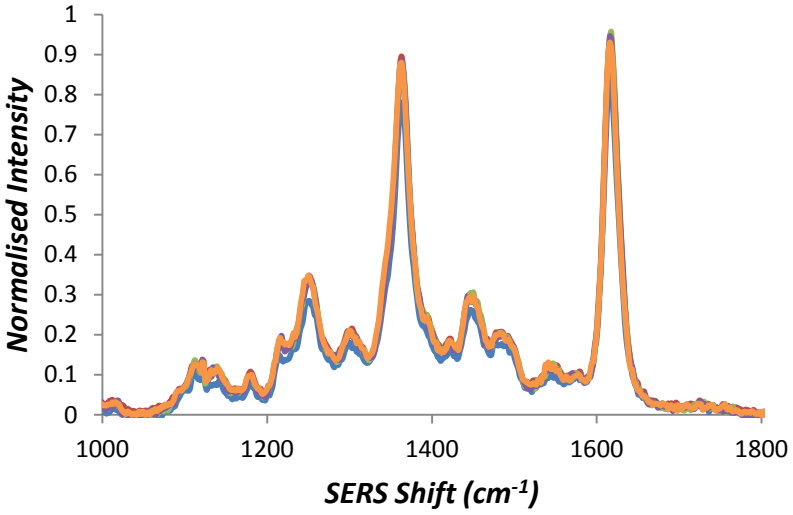

Figure 33. SERS spectra of RB1-coated gluconanoparticles taken 30 minutes after incubation with 0 nM (blue), 1 nM (red), 10 nM (green), 100 nM (purple) and 1μM (orange) ConA.

The measured changes in SERS intensity following incubation of the gluconanoparticles at different concentrations of ConA were minimal as demonstrated in figure 33. This was unexpected, given the changes measured by extinction spectroscopy. One explanation for this is the large variation in size and shape of the particles generated when using citrate as the reducing agent (demonstrated by the SEM image in figure 34). As increases in SERS intensity most commonly occur when single particles form dimers, the rational was that aggregates (including dimers) were already present, following preparation of the

nanoparticles., This could subsequently minimise any increase in SERS signal measured upon further aggregation.[172]

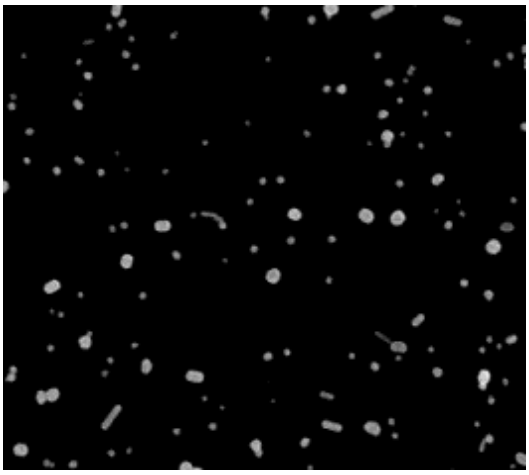

Figure 34. SEM of silver citrate nanoparticles illustrating the variation in size and shape of particles.

4.3 EDTA-Reduced Silver Nanoparticles

The silver nanoparticle preparation method was modified by using ethylenediaminetetraacetic acid (EDTA) as the reducing agent instead of citrate. Silver-EDTA particles are monodispersed in comparison to those prepared using the citrate reduction as shown in figure 35 and table 8.

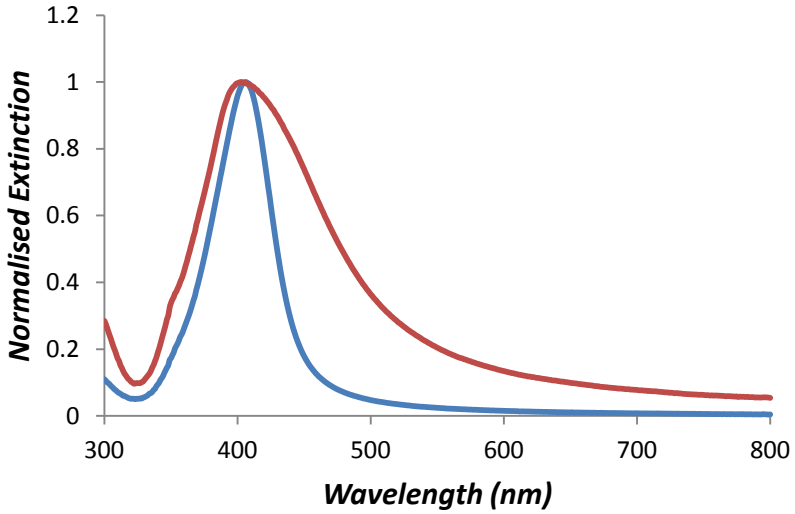

Figure 35. Normalised extinction spectrum of EDTA reduced (blue) and citrate reduced (red) silver nanoparticles.

Table 8. Summary of extinction ratio (600 nm to plasmon) and size measurements taken for the EDTA and citrate reduced nanoparticles.

Colloid Reduction Method	600 nm : Plasmon Extinction	Size (nm) /pdI
EDTA	0.015	56.2 ± 1.97/0.27
Citrate	0.140	39.2 ± 0.04/ 0.47

Figure 35 and table 8 demonstrate the relative polydispersity of the silver citrate particles when compared with those prepared using the EDTA reduction method (polydispersity index (pdI of 0.27 and 0.47 respectively). The ten-fold increase in extinction ratio for the citrate particles indicated the a greater proportion of aggregates (including dimers) were produced alongside the individual 39 nm particles.

It was hoped that the increased monodispersity of the EDTA colloid (indicating a greater proportion of individual particles present) would encourage lectin-mediated dimer formation, allowing better discrimination between the SERS signal of individual and aggregated particles.

Glyconanoparticles were prepared from the EDTA reduced silver particles in an analogous way to the citrate capped particles. The prepared particles were analysed by UV-vis. extinction spectroscopy, DLS and gel electrophoresis.

Table 9. Summary of extinction and size measurements taken for EDTA nanoparticles conjugates (functionalised with $CTPEG_{12}$ and subsequently coupled to glucosamine or galactosamine).

Nanoparticle Coating	λ maximum (nm)	Size (nm)
EDTA	407	55.05 (± 0.30)
RB1/$CTPEG_{12}$	414	61.19 (± 0.56)
RB1/$CTPEG_{12}$-Glucose	413	77.18 (± 0.23)
RB1/$CTPEG_{12}$-Galactose	413	75.89 (± 1.05)

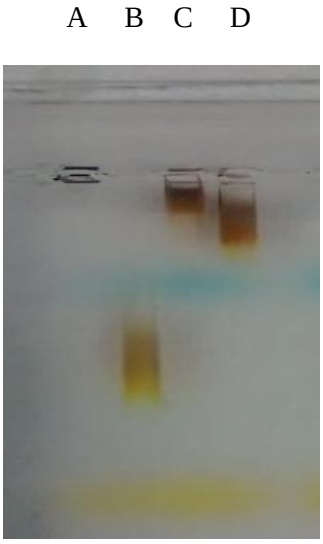

Figure 36. Agarose gel electrophoresis image showing transit of silver nanoparticles with various coatings; A) EDTA, B) PEG_{12}, C) PEG_{12}-glucose, D)PEG_{12}-galactose.

The results shown in table 9 and figure 36 (red-shift in λmax., increase in size and change of nanoparticle behaviour in the agarose gel) indicate the successful functionalisation of the particles with $CTPEG_{12}$ and subsequent coupling of glucose or galactose to this surface. The size variations measured indicated a change in surface coating, rather than dimer formation (as the size measured for the $CTPEG_{12}$-coated nanoparticles and the glyconanoparticles was less than double that of the individual particles). The newly prepared glyconanoparticles (EDTA reduced) were evaluated for reactivity with the lectin ConA.

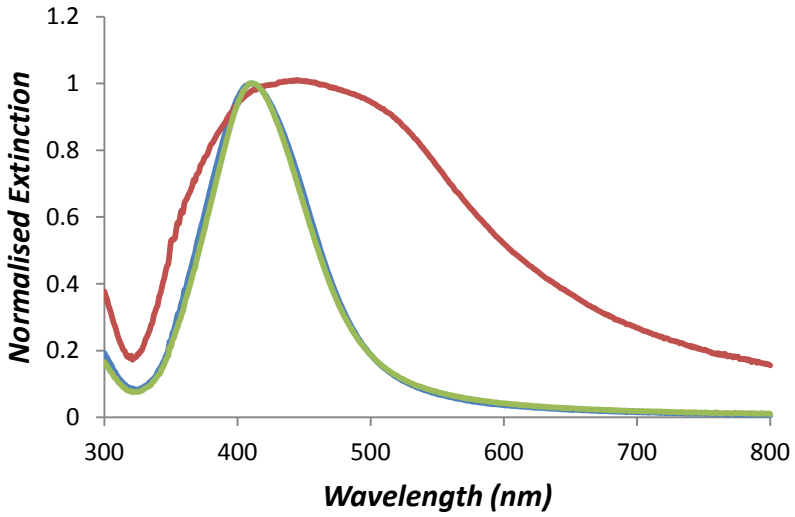

Figure 37. Normalised extinction spectra of the gluconanoparticles (blue), gluconanoparticles with 100 nM ConA (red) and galactonanoparticles with 100 nM ConA (green) taken 30 minutes after addition of the lectin.

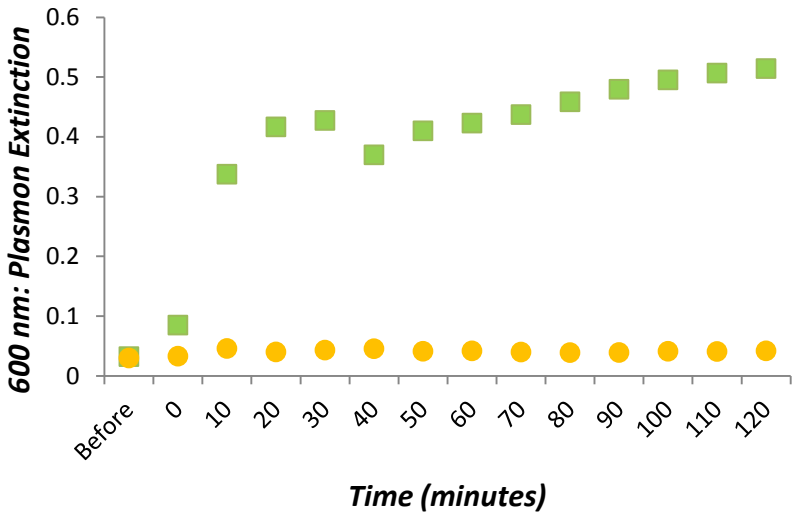

Figure 38. Ratio of 600 nm to plasmon extinction following addition of 100 nM ConA to gluconanoparticles (green) and galactonanoparticles (yellow).

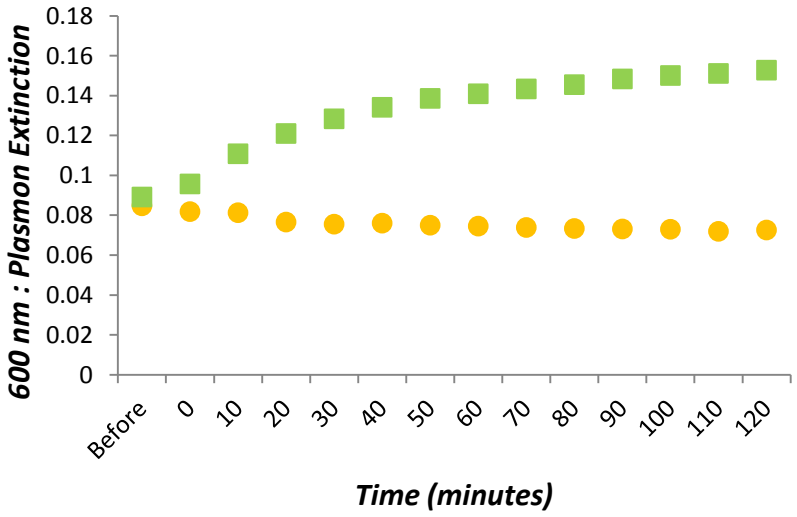

Figure 39. Ratio of 600 nm to plasmon extinction of galactonanoparticles alone (yellow) and 100 nM Jacalin lectin to galactonanoparticles (green).

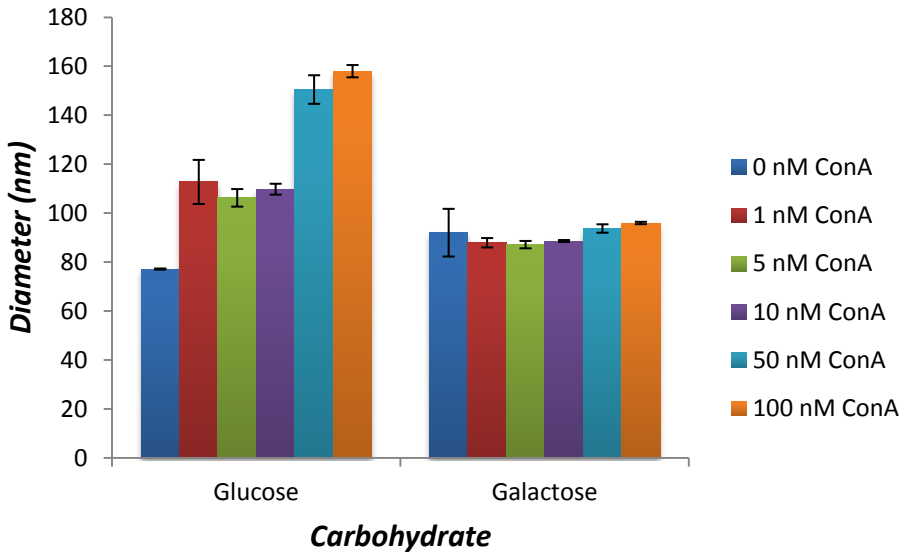

Figure 40. Glyconanoparticle size 30 minutes after addition of 0 (blue), 1 (red), 5 (green), 10 (purple), 50 (orange) and 100 nM (yellow) of ConA.

Figures 37 and 38 illustrate the selectivity of the prepared glyconanoparticles when incubated with ConA. Upon addition of the lectin, the gluconanoparticles aggregated as demonstrated by the considerable red-shift in λmax. and increase in the extinction ratio which remained constant after 2 hours. Within that same time, there were minimal changes to the extinction ratio of the galactonanoparticles as a result of the minimal interaction between these particles and ConA. The results demonstrated both the reactivity of the gluconanoparticles towards ConA and the selectivity of the galactonanoparticle system generated. This is reinforced in figure 40 which demonstrates the changes in size in the presence of ConA when compared with the galactonanoparticles. The galactonanoparticles reacted with Jacalin lectin as shown by the increase in extinction ratio in figure 39, demonstrating the activity of these particles towards the galactose specific lectin.

The SERS response of the glyconanoparticles upon aggregation with ConA was evaluated to compare with the lack of response observed when using the citrate reduced silver nanoparticles. The normalised SERS increase was evaluated at different concentrations of $CTPEG_{12}$, from 10 to 50 μM.

Table 10. Normalised SERS increase 5 minutes after addition of 100 nM ConA to either gluco- or galactonanoparticles coated with increasing concentrations of $CTPEG_{12}$ linker.

	Normalised SERS Increase @ 1364 cm^{-1}	
$CTPEG_{12}$ (μM)	GLU	GAL
20	1.49	1.34
30	4.83	0.92
40	5.88	0.91
50	5.80	1.19

The data in table 10 demonstrates the normalised SERS increase measured for both gluco- and galactonanoparticles in the presence of 100 nM ConA. Different concentrations of PEG were used to prepare the particles. As shown in figure 41, with 40 μM $CTPEG_{12}$, there was significant SERS enhancement measured when compared with the other concentrations of $CTPEG_{12}$. Also shown in table 10 and figure 42 is the minimal enhancement measured for the galactonanoparticles in the presence of ConA. The results also demonstrated the selectivity achieved when using 40 μM $CTPEG_{12}$. At 20 μM $CTPEG_{12}$ the selectivity was compromised, where the SERS enhancement measured for both gluco- and galactonanoparticles was similar. At 30 and 50 μM there was selectivity, however the enhancement measured for the gluconanoparticles was lower than for the 40 μM coverage.

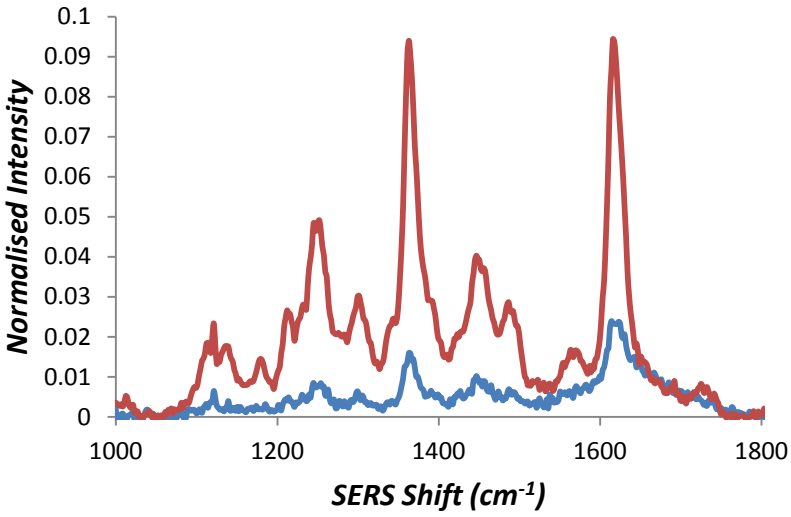

Figure 41. SERS of RB1-coated gluconanoparticles (40 μM $CTPEG_{12}$) before (blue) and 5 minutes after incubation with 100 nM ConA (red).

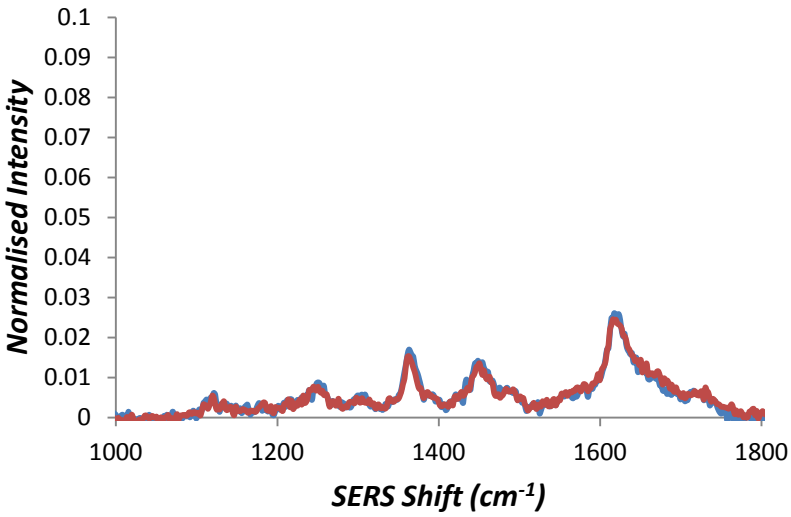

Figure 42. SERS of RB1-coated galactonanoparticles (40 µM $CTPEG_{12}$) before (blue) and 5 minutes after incubation with 100 nM ConA (red).

While the overall SERS signal intensity was lower (by a factor of 10) for the EDTA particles compared with the citrate reduced particles, this was explained by the lower concentration of the EDTA colloid (7.55 x 10^{-11} M) when compared with citrate colloid (4.04 x 10^{-10} M).

A SERS limit of detection was determined for ConA using silver-EDTA glyconanoparticles using equation 5.

Equation 5.

$$Limit\ of\ Detection\ (M) = \frac{3 \times blank\ (0\ M) standard\ deviation}{m\ (gradient\ from\ graph)}$$

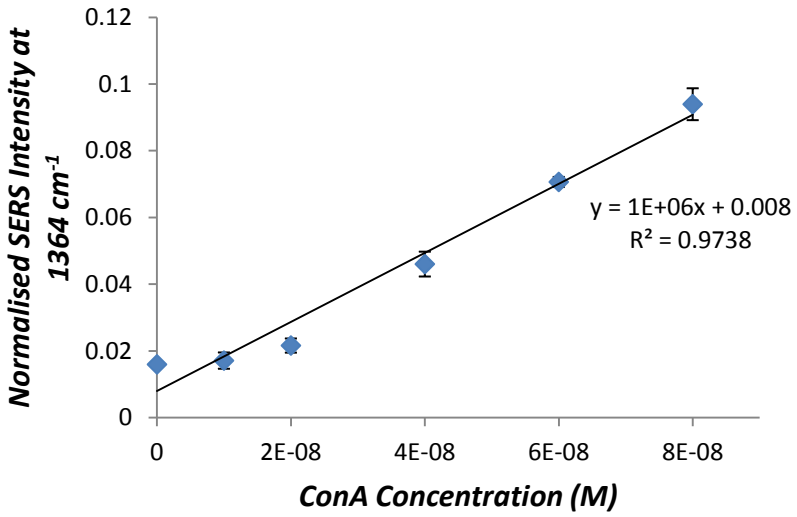

Figure 43. Normalised SERS intensity of the surface-bound RB1 signal at 1364 cm^{-1} measured 5 minutes after addition of 0, 10, 20, 40, 60 and 80 nM Con.

Using equation 5 together with figure 43, the limit of detection was calculated as 3 nM. This was, however increased compared with previous work (40 pM).[14] This was caused by the use of PEG on the nanoparticles surface which increased the interparticle distance upon aggregation. Weaker hot-spots were subsequently generated and a reduced increase in SERS was measured. While the use of PEG appeared to decrease the sensitivity of the sensor when compared with shorter, alkanethiol-based sensors, the stability improvement would allow the developed sensor to be used in synthetic freshwater (containing a large variety of metal ions and interferents which could cause non-specific aggregation of the particles). This would enable measurement to be made on samples as taken from the environment of interest, without the need for sample preparation to avoid non-specific aggregation.

5. Improvements to SERS Response of Lectin-Mediated Aggregation

5.1 Phenyl-Derivatised Galactose Testing

To test the effect of carbohydrate derivatives on lectin binding activity and SERS response of the glyconanoparticles, galactosamine was replaced with the phenyl-conjugated carbohydrate 4-aminophenyl-β-D-galactopyranoside (APGAP), shown in figure 44.

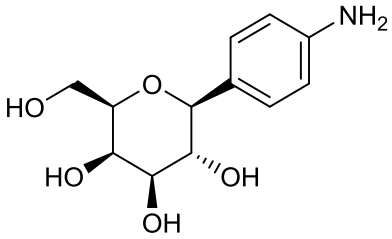

Figure 44. Structure of 4-aminophenyl-β-D-galactopyranoside (APGAP).

This carbohydrate has previously been used to target the galactose binding toxin, Ricin. [173] The APGAP concentration used in preparing the particles was equivalent to the galactosamine used in amide coupling. The prepared particles were evaluated by UV-vis. extinction spectroscopy, DLS and gel electrophoresis.

Table 11. Summary of extinction and size measurements taken for EDTA nanoparticles conjugates (functionalised with CTPEG12 and subsequently coupled to APGAP).

Nanoparticle Coating	λ maximum (nm)	Size (nm)
EDTA	404	57.89 (± 0.51)
RB1/CTPEG$_{12}$	408	62.21 (±0.61)
RB1/CTPEG$_{12}$-APGAP	411	73.48 (± 0.01)

A B C

Figure 45. Agarose gel electrophoresis image showing transit of silver nanoparticles with various coatings; A) EDTA, B) PEG$_{12}$, C) PEG$_{12}$-APGAP

As shown in table 11 and figure 45 there was a red-shift in λ max. and corresponding increase in size measured together with a change of behaviour in the agarose gel respectively which indicated the successful functionalisation of the particles with CTPEG$_{12}$ and subsequent coupling of APGAP to the surface.

Generating Stable, Lectin-Reactive Glyconanoparticles

The activity of the APGAP-nanoparticles towards the Jacalin lectin was compared with galactonanoparticles using the normalised SERS intensity measured before and after addition of the lectin to cause aggregation.

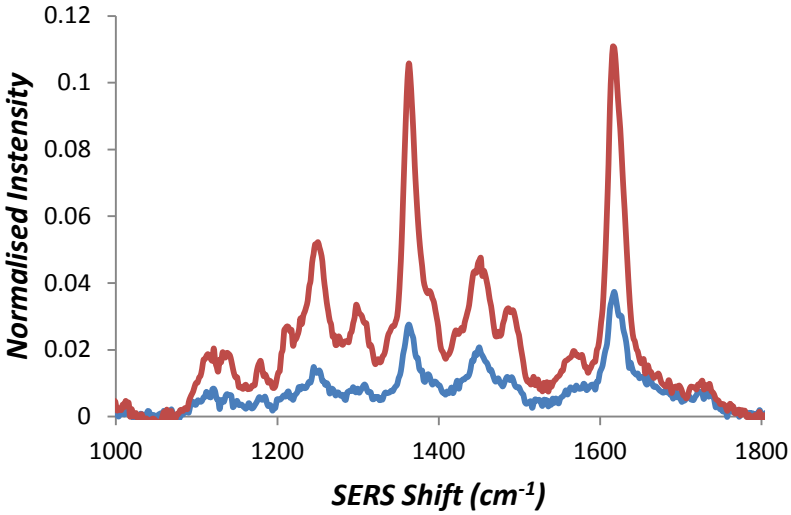

Figure 46. SERS of RB1-coated APGAP-nanoparticles (40 µM $CTPEG_{12}$) before (blue) and 5 minutes after incubation with 40 nM Jacalin lectin (red).

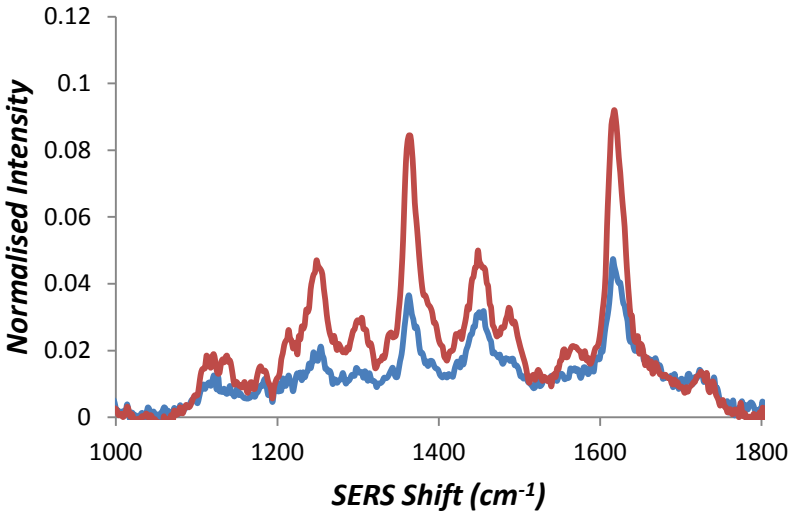

Figure 47. SERS of RB1-coated galactonanoparticles (40 µM $CTPEG_{12}$) before (blue) and 5 minutes after incubation with 40 nM Jacalin lectin (red).

Table 12. Normalised SERS increase in spectra measured 5 minutes after addition of 100 nM ConA or 40 nM jacalin to galactonanoparticles or APGAP-nanoparticles.

	Normalised SERS Increase@ 1364 cm^{-1}	
Carbohydrate	ConA	Jacalin Lectin
Galactose	1.01 (± 0.09)	2.47 (± 0.29)
APGAP	0.84 (± 0.07)	3.85 (± 0.34)

Figures 46 and 47 demonstrate the respective responses measured by the galactose and APGAP coated particles in the presence of 40 nM Jacalin lectin. In addition to this, the response of the nanoparticles in the presence of 100 nM ConA is shown in table 12. There was minimal change in SERS intensity measured upon addition of ConA (the signal ratio before and after addition of the lectin is 1) demonstrating that the galactose functionality present on the surface of either nanoparticle type had no affinity for ConA. In the presence of Jacalin lectin the normalised SERS increase measured for the APGAP particles was significantly greater than that measured for the galactonanoparticles (from 2.47 to 3.85). This indicated that the particles aggregated to a greater degree as a result of the different surface moiety. The greater affinity for Jacalin lectin towards APGAP compared with galactose has previously been demonstrated by inhibition assay.[174] Possible reasons for this greater affinity include the phenyl group which both extends the galactose from the nanoparticle-PEG layer, reducing the interaction between adjacent galactose molecules. A second proposed reason was the interaction between the phenyl group and the hydrophobic moiety of the lectin binding pocket. Hydrophobic groups on carbohydrates (for example phenyl and methyl groups) have been previously noted in strengthening the interaction between these and lectins, for example, glucose and Concanavalin A.[175-178]

The greater sensitivity of the APGAP system is also demonstrated with the lower limit of detection achieved for Jacalin lectin when compared with the galactonanoparticles.

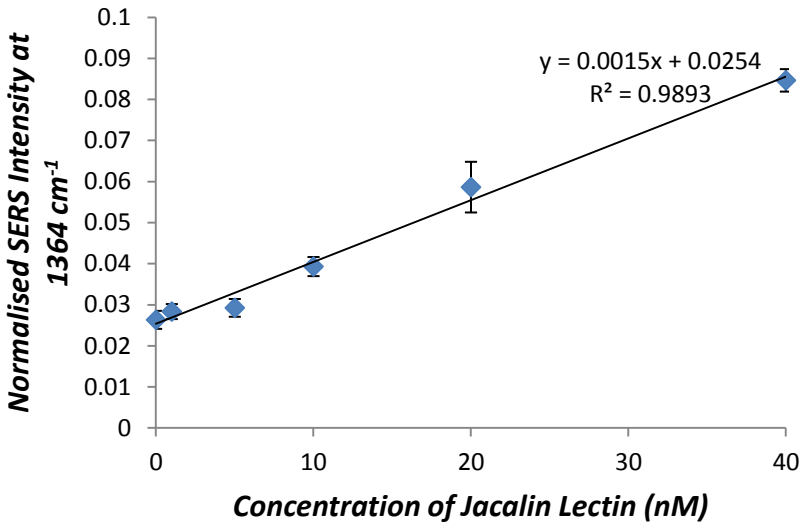

Figure 48. Normalised SERS intensity of the surface-bound RB1 signal at 1364 cm^{-1} taken 1 minute after addition of 0, 1, 5, 10, 20, 40 nM Jacalin to APGAP-nanoparticles.

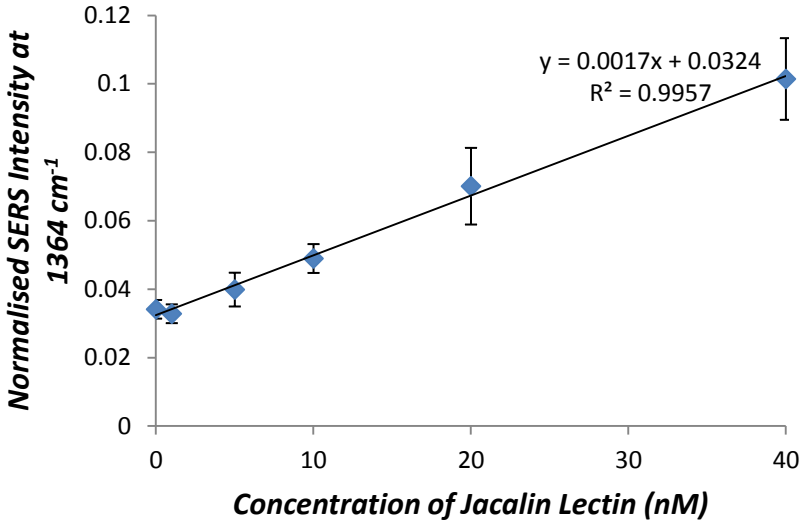

Figure 49. Normalised SERS intensity of the surface-bound RB1 signal @ 1364 cm^{-1} taken 1 minute after addition of 0, 1, 5, 10, 20, 40 nM Jacalin lectin to galactonanoparticles.

Using figures 48 and 49 and equation 5, the SERS limits of detection for Jacalin lectin using the galactose or APGAP-nanoparticles were calculated as 4.8 and 0.2 nM respectively. This reiterates the results shown in Table 12 and supports the suggestion that APGAP is able to better stabilise the lectin binding pocket than galactose because of the presence of the hydrophobic, phenyl, substituent. This has important implications in the development of

lectin and toxin detecting glyconanoparticles, particularly when considering which carbohydrates to functionalise nanoparticles with to ensure maximum sensitivity.

5.2 Raman Reporter Evaluation

Following the successful preparation of glyconanoparticles for the detection of lectins by SERS, the effect of different Raman reporter molecules on the sensitivity and performance of the system was evaluated. The SERS response from glyconanoparticles labelled with the isothiocyanate molecule, malachite green (MGITC), was compared with the benzotriazole (RB1) coated particles. Particles were labelled with MGITC in an analogous way to those tagged with RB1 with a 10 times lower concentration of MGITC compared with RB1 (1 μM MGITC compared with 10 μM RB1), as above this, non-specific aggregation was observed. The particles were subsequently functionalised with carbohydrates as previously described. The particles were incubated with 100 nM of either ConA or Jacalin lectin and SERS measurements made 5 minutes after addition of the lectin.

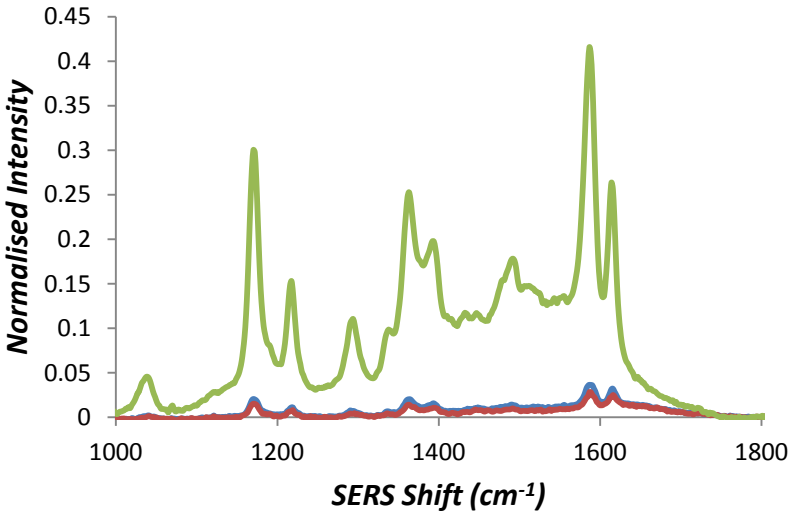

Figure 50. SERS of MGITC-coated galactonanoparticles (40 μM $CTPEG_{12}$) before (blue) and 5 minutes after incubation with 100 nM ConA (red) or Jacalin lectin (green).

Table 13. Normalised SERS increase in the 1587 cm^{-1} signal of MGITC or the 1364 cm^{-1} signal of RB1 measured 5 minutes after addition of 100 nM ConA or Jacalin lectin to MGITC or RB1-coated galactonanoparticles.

	Normalised SERS Increase	
Raman Reporter	ConA	Jacalin Lectin
MGITC	0.92 (± 0.09)	11.75 (± 4.13)
RB1	1.03 (± 0.12)	4.21 (± 0.42)

As shown in figure 50 and table 13 there was a considerable increase in the measured SERS response of the MGITC-coated galactonanoparticles in the presence of the aggregation-inducing, Jacalin-lectin, when compared with the RB1-coated galactonanoparticles. This enhanced increase can be explained by the greater proportion of aggregates formed with an excitation frequency corresponding to that of MGITC (630 nm).[179] This occurred because of the increase in the ratio of 600 nm to plasmon extinction and greatly raised the SERS increase as the enhancing substrate was in resonance with the scattering molecule's excitation.[73] There was however, far greater variability in the measured response (± 35%) indicating a less reliable aggregation system than with the use of RB1. This experiment demonstrated that while the MGITC may provide a greater enhancement and hence sensitivity, the reproducibility was hampered, demonstrating the use of the RB1 coated conjugates in the development of a sensor for lectins and, subsequently, toxins.

6. Sensor Reversibility

Lectin-carbohydrate interactions are known to be reversible.[23] It was therefore thought that by incubating pre-aggregated glyconanoparticles with a carbohydrate for which the aggregating lectin would have greater affinity, it would be possible to disturb the aggregation. The reversibility of the sensor was therefore tested. ConA binds the carbohydrates methyl α-D-mannose > mannose > glucose.[176] For this reason, methyl α-D-mannose was used as an inhibitor for ConA, to establish whether it would be possible to reverse the binding of the nanoparticles to the lectin.

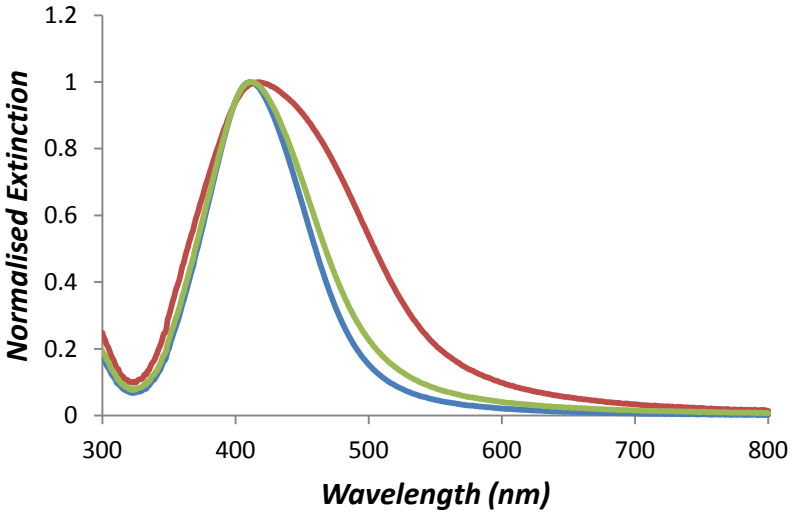

Figure 51. Normalised extinction spectra of gluconanoparticles (blue), gluconanoparticles aggregated with 100 nM ConA (red) and ConA aggregated gluconanoparticles with 25 mM methyl α-D-mannose added and measured 30 minutes after addition of the lectin (green).

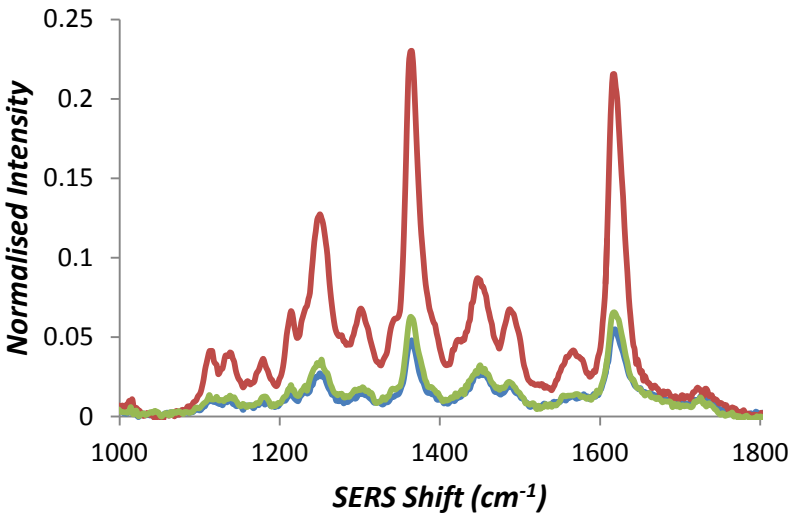

Figure 52. Normalised SERS spectra of RB1-coated gluconanoparticles (blue), RB1-coated gluconanoparticles aggregated with 100 nM ConA (red) and ConA aggregated RB1-coated gluconanoparticles with 25 mM methyl α-D-mannose taken 30 minutes after addition of the lectin (green).

Figures 51 and 52 illustrate the initial red shift of the extinction and corresponding SERS increase measured respectively. This was caused by the aggregation of the gluconanoparticles with ConA, as previously shown. The addition of 25 mM methyl α-D-mannose resulted in a near recovery of the initial extinction profile. It was proposed that the methyl α-D-mannose occupied the sites previously bound by the glucose on the nanoparticle surface thereby releasing the gluconanoparticles. There was a corresponding decrease in SERS intensity of the RB1 signal measured; the signal intensity returned to the level measured prior to the ConA-mediated aggregation. The recovery of biosensors, particularly those made with a precious metal core, is essential to improving the sustainability of nanotechnology. By allowing the recovery of these sensors following displacement from the target, they could potentially be recycled or reused. Additionally, the competitive binding of different carbohydrates with a target lectin can be exploited for bioanalysis, for example in glucose sensing.[127, 180, 181] Related research was pursued and the results obtained are discussed further in the chapter, "Developing a SERS-based Glyconanoparticle Glucose Sensor".

7. Conclusions

Glyconanoparticles have been generated and used for the detection of lectins by both UV-visible extinction spectroscopy and SERS. The research builds on previous work, however with the novel use of PEGylated linkers, both stability and selectivity are greatly improved.

Glyconanoparticles generated using alkanethiols demonstrated reactivity towards the lectins tested, however non-specific binding became problematic. Conversely the use of large PEG linkers (5000 g mol^{-1}) generated stable particles, which did not measurably aggregate upon addition of the target lectins (glucose-binding ConA and galactose-binding Jacalin lectin). While interaction between the particles and lectin may have occurred, the distance between the lectin-bound particles resulted in little changes in the extinction or Raman scattering properties of the nanoparticles or nanoparticle-bound RB1 respectively. Smaller PEG molecules (635 g mol^{-1}) were subsequently used in the generation of the glyconanoparticle providing a balance between reactivity and selectivity. While changes in extinction were measured for the glyconanoparticles generated from citrate-reduced nanoparticles, changes in SERS intensity were minimal. This was unexpected as aggregation was visibly observed and measured. By changing the colloid type used in preparing the glyconanoparticles to EDTA-reduced silver nanoparticles, this enabled the measurement of aggregation by both extinction spectroscopy and SERS. It was proposed that the greater monodispersity of this colloid encouraged a more measurable increase in SERS as a result of a greater number of individual particles being present prior to addition of the lectin. EDTA colloid was subsequently used in the preparation of glyconanoparticles to obtain a limit of detection for ConA and evaluate the activity of glyconanoparticles against Jacalin lectin, which were prepared using phenyl-derived galactose instead of the aminated galactose previously used. An alternative Raman reporter molecule (malachite green isothiocyanate) was used to coat the glyconanoparticles to assess any change of performance in comparison to RB1. While there was a significant improvement in the sensitivity achieved when using this RRM, the variability of the response discouraged further use of this molecule for coding the glyconanoparticles. Finally, the reversibility of carbohydrate-lectin interactions was also demonstrated for the gluconanoparticles with ConA, using methyl α-D-mannose as the displacing carbohydrate. It may be possible to prepare an analogous magnetic glyconanoparticle which could be recovered following reversal of aggregation.

Developing a SERS-Based Glyconanoparticle Glucose Sensor

High performance and reliable glucose sensing is currently of great interest because of the sharp rise in cases of metabolic disease such as diabetes. The World Health Organization have reported that approximately 350 million people are currently diabetic with the disease expecting to become the 7th leading cause of death by 2030.[182, 183] Diagnosis is achieved with the measurement of blood glucose levels. Commonly, treatment of diabetes has relied on monitoring blood glucose levels using electrochemical enzymatic techniques involving glucose oxidase, dehydrogenase and hexokinase.[184] These techniques are common-place and relatively easy to use, allowing for deployment in home-use; impossible for HPLC or mass spectrometric methods of detection. Issues of reliability do exist however, with the response based on the rate of reaction between glucose and the enzyme which is often affected by changes in blood oxygen content, temperature and humidity.[127, 184, 185] Mass transport into the measurement device also affects the oxygen-glucose ratio, influencing sensor response and hampering accuracy.[127, 186] While three generations of enzymatic glucose sensors have sought to mitigate the influence of external factors, temperature, humidity and interferent dependence still impact on reliability. There is therefore a need for alternative methods to electrochemical enzymatic detection of glucose in the form of non-enzymatic glucose (NEG) sensors.[187]

Recent developments in electrochemical, non-enzymatic glucose sensing have included the use of metals, metal oxides and metal composites. Disadvantages of these include a lack of stability of the metal substrate, low sensitivity and selectivity for glucose.[188] Carbon-based nanomaterials including nanotubes and graphene have also been exploited in glucose sensing due to their high electronic conductivity and ability to remain electrochemically inert, providing a stable platform for developing glucose sensors. While these are being developed for use in-vivo, questions remain about their biocompatibility.[187]

Metallic nanomaterial-based glucose sensors have been developed to utilise both non-enzymatic and enzymatic systems.[188, 189] Luo *et al.* have produced electrodes of copper nanoparticle-modified graphene sheets which oxidize glucose.[188] Cyclic voltammetry and chronamperometry measurements vary at different glucose concentrations. Advantages of this system include the wide linear range achievable (0.5 μM - 4.5 mM or 0.09 - 810 μg/mL)

together with the stability of the electrode and its selectivity towards glucose with minimal chloride poisoning caused by interfering species.[188]

Zhai *et al.* developed an enzymatic glucose sensor using platinum nanoparticles within hydrogels.[189] Platinum nanoparticles catalyse the decomposition of hydrogen peroxide and the porous nature of the hydrogel allows for effective immobilization of glucose oxidase and transport of glucose. The advantages of this system include rapidity (3 second response time) and the wide linear range (0.01 - 8 mM or 1.8 - 1441 μg/mL).[189]

Optical measurement provides an alternative to electrochemical methods of glucose sensing. This includes the use of fluorescent proteins or metallic nanoparticles.[127, 190, 191] In each case the use of the glucose-binding protein ConA has proved successful. This protein has previously been used by Cote *et al.* in glucose sensing by fluorescence.[190, 191] Fluorescently-tagged ConA was incubated with a glycodendrimer together with different glucose concentrations. ConA-glycodendrimer aggregation decreased at increasing glucose concentrations (caused by replacement of the glycodendrimer with glucose within the ConA binding pocket). Increasing fluorescence intensity was found to correlate with increasing glucose concentrations throughout the physiological range (0-5000 μg/mL).[190] The use of glycodendrimers alleviates the issues of irreversible aggregate formation in similar systems using dextran, allowing the sensor to perform more effectively. A second example of the use of ConA by Cote *et al.* was in a FRET assay.[191] Fluorescently (ADOTA) tagged ovalbumin, expressing a tri-mannose residue (to which ConA has affinity for), was added to fluorescently (Alexa Fluor 647) tagged ConA which, upon binding, generated FRET. Addition of glucose was shown to reduce this interaction between the proteins, lowering the measured FRET intensity. Changes were measured over the physiological range (0 - 5000 μg/mL) and the research demonstrates an important step towards developing non-invasive glucose sensors.[191]

The reversibility of aggregation allows for inhibition assays to be performed with nanoparticles. This has previously been demonstrated by Lim *et al.* using mannose-coated gold nanoparticles.[127] The particles were aggregated with ConA solutions, each containing a different concentration of glucose. The aggregation was monitored by measuring changes in the extinction spectrum of the gold nanoparticles. The development of this system is an important step in the development of glucose sensors without the need for enzymes.

Developing a SERS-Based Glyconanoparticle Glucose Sensor

Building on this, a SERS-based glucose sensor was proposed, based on the displacement of gluconanoparticles from the ConA binding pocket with free glucose, with the aim of eventually testing this in simulated biological fluid samples.

1. Sensor Design

As previously demonstrated in the chapter "Generating Stable, Lectin-Reactive Glyconanoparticles", adding the lectin ConA to gluconanoparticles causes aggregation and subsequently a change in the extinction profile of the particles, together with a corresponding increase in the SERS intensity of the RB1 RRM on the glyconanoparticle surface. By mixing a binding carbohydrate, for example glucose, with ConA prior to addition to the gluconanoparticles, it was proposed that the binding of gluconanoparticles to ConA would be inhibited resulting in a lessened SERS intensity increase. Additionally, it was hoped that concentration dependent inhibition would be measured *via* a decrease in the SERS intensity change. Figure 53 summarises the proposed experiment.

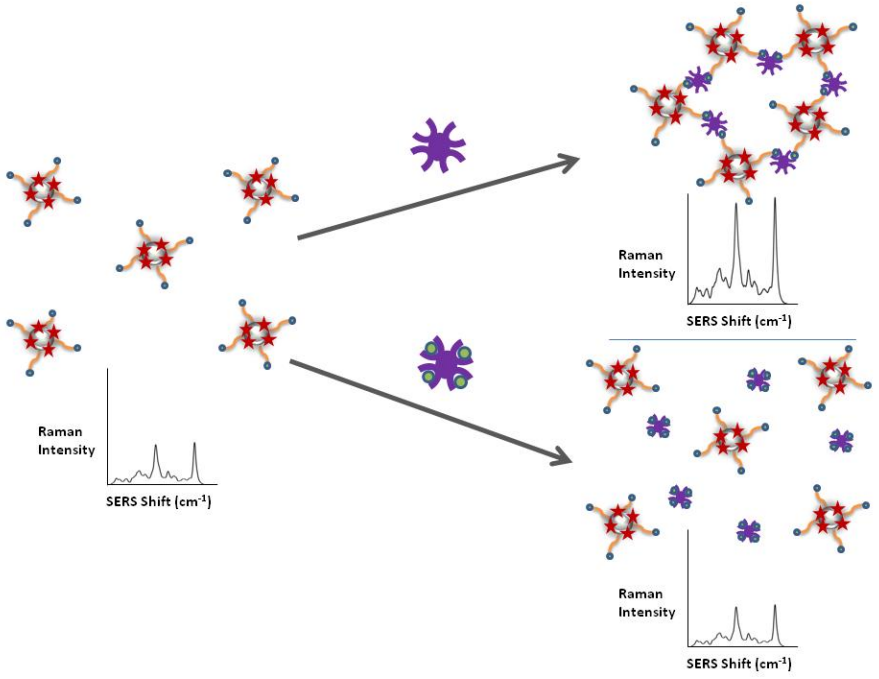

Figure 53. Schematic of the proposed glucose-sensing experiment. ConA (with or without bound glucose) (shown in purple with and without green circles respectively) is added to the glyconanoparticles. A) ConA (without bound glucose) aggregates the particles resulting in an increase in the surface-bound RB1 SERS signal. B) ConA (with bound glucose) does not aggregate the particles, causing minimal change in the SERS signals measured for surface-bound RB1.

2. Glyconanoparticle Choice

The same silver (EDTA-reduced) gluconanoparticles previously used for the detection of Concanavalin A (see "Generating Stable, Lectin-reactive Glyconanoparticles") were prepared and employed for glucose sensing. Initial testing was carried out in 10 mM HEPES buffer, pH 7.4, with 0.2 mM $Ca(NO_3)_2$ and $Mn(NO_3)_2$. The interaction between these particles and ConA had previously been shown to be reversible in the presence of methyl α-D-mannose (figures 51 and 52).

3. Free Glucose Incubation Testing.

It was necessary to establish the optimal time for the incubation of a glucose-containing sample with ConA, prior to addition to the glyconanoparticles. 10, 20 and 30 minute incubation times were used and the resulting SERS response measured. The normal human blood glucose concentration is 800 - 1400 µg/mL. It was therefore decided to test 1000 µg/mL of glucose for incubation testing as, if successful, the sensor would respond to the inhibition of ConA at a physiologically relevant glucose concentration. The concentration of ConA tested was 40 µg/mL, to ensure glucose was in excess, thereby resulting in a measurable reduction in change to the SERS intensity.

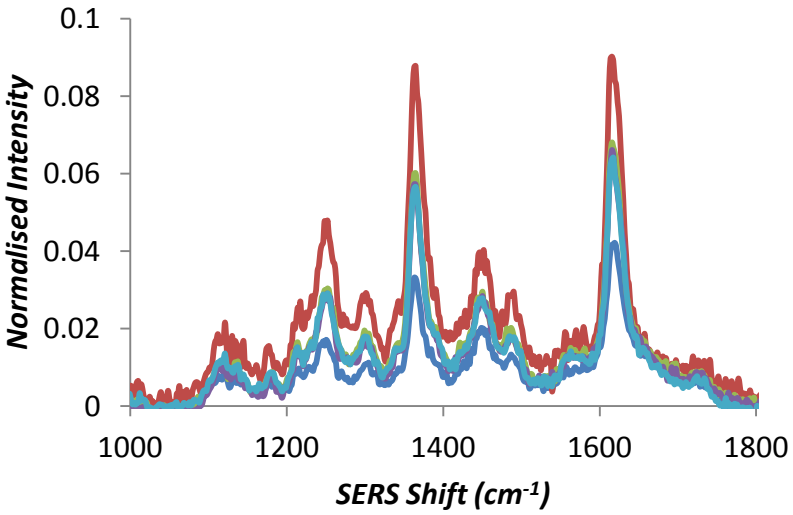

Figure 54. Normalised SERS spectra of RB1-coated gluconanoparticles (blue), RB1-coated gluconanoparticles aggregated with 40 µg/mL ConA (red) or 40 µg/mL ConA incubated with 1000 µg/mL glucose for 10 minutes (green), 20 minutes (purple) or 30 minutes (light blue) 5 minutes after addition of ConA to the particles.

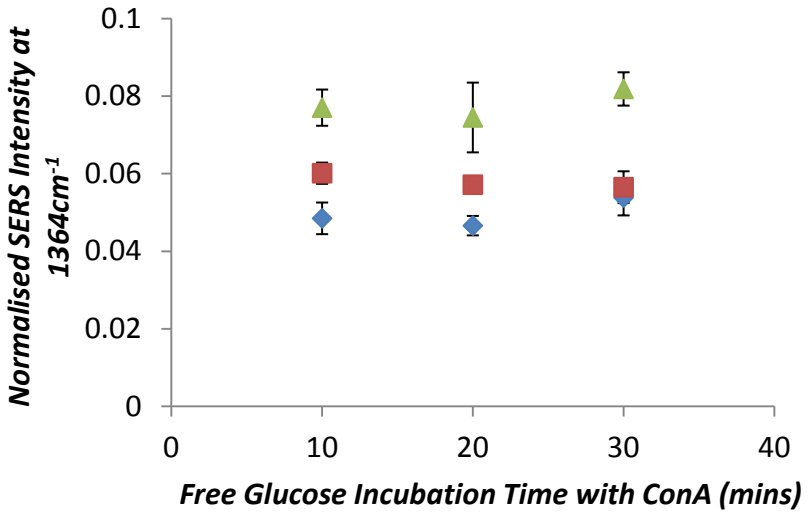

Figure 55. Normalised SERS intensity of RB1-coated gluconanoparticles (measured at 1364 cm^{-1}) following addition of 40 µg/mL ConA, incubated with 1000 µg/mL glucose for varying amounts of time (10, 20 and 30 minutes). The glucose-ConA samples were incubated with the glyconanoparticles prior to SERS measurement for 1 (blue), 5 (red) or 30 minutes (green).

Figures 54 and 55 demonstrate the changes with the incubation of 40 µg/mL ConA with 1000 µg/mL glucose. The changes to the intensity were minimal after 20 minutes of incubating the glucose with the ConA. As shown in figure 55, the most reproducible results were obtained for the 20 minute incubation samples by measuring the SERS signals of the gluconanoparticles 1 to 5 minutes after addition of the glucose-ConA sample to the gluconanoparticles. Subsequently, the concentration of ConA used was evaluated to determine the most appropriate amount to use in developing the glucose sensor.

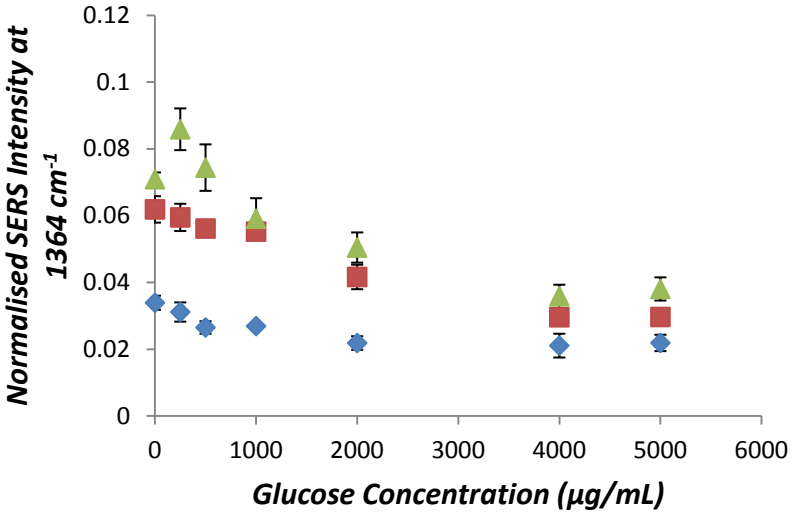

Figure 56. Normalised SERS intensity of RB1-coated gluconanoparticles (measured at 1364 cm^{-1}) following addition of 20 (blue), 40 (red) and 80 µg/mL (green) ConA. Free glucose was pre-incubated with ConA at the indicated concentration for 20 minutes. SERS measurements were made 1 minute after addition of ConA samples to the gluconanoparticles.

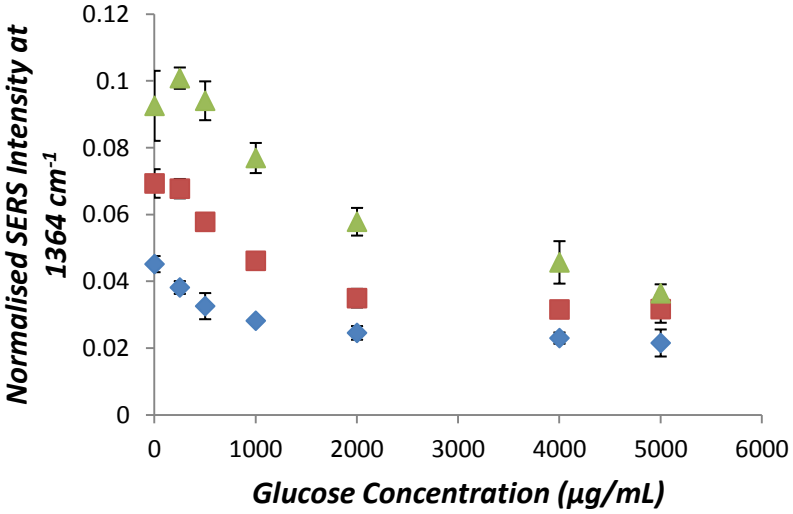

Figure 57. Normalised SERS intensity of RB1-coated gluconanoparticles (measured at 1364 cm^{-1}) following addition of 20 (blue), 40 (red) and 80 µg/mL (green) ConA. Free glucose was pre-incubated with ConA at the indicated concentration for 20 minutes. SERS measurements were made 5 minutes after addition of ConA samples to the gluconanoparticles.

Figures 56 and 57 demonstrate that at the lower concentration of ConA (20 µg/mL) , there was a lower concentration of glucose required to prevent aggregation of the gluconanoparticles. The most measurable changes occurred below 1000 µg/mL. This is desirable for the determination of hypoglycaemic states, however as stated, normal glucose levels in human blood range from 800-1400 µg/mL, hence using this concentration of ConA

would not allow the system to respond across the physiological range. At 80 µg/mL the opposite was observed; the gluconanoparticles aggregation plateaued at 1000 µg/mL and below. This was as a result of an insufficient amount of glucose present to inhibit the higher concentration of ConA. This system is therefore more suited to levels of glucose > 1000 µg/mL. The drawback of this is that the lower limit of the physiological range is excluded. At 40 µg/mL the linear range was from 250 µg/mL to 4000 µg/mL. This covers the physiological range and much of the hyper and hypoglycaemic levels of glucose. This led to the conclusion that 40 µg/mL was the most appropriate concentration of ConA to use in the development of the sensor.

As shown in figure 58, linearity of the sensor was achieved using 40 µg/mL ConA with SERS measurement made 1 minute after addition of the ConA-glucose sample to the glucoconjugates, highlighting the rapidity of the sensor. While 80 µg/mL ConA could be used to detect 5000 µg/mL of glucose, this concentration of ConA could not be used to accurately detect lower concentrations of glucose and there was increased variability in the response measured.

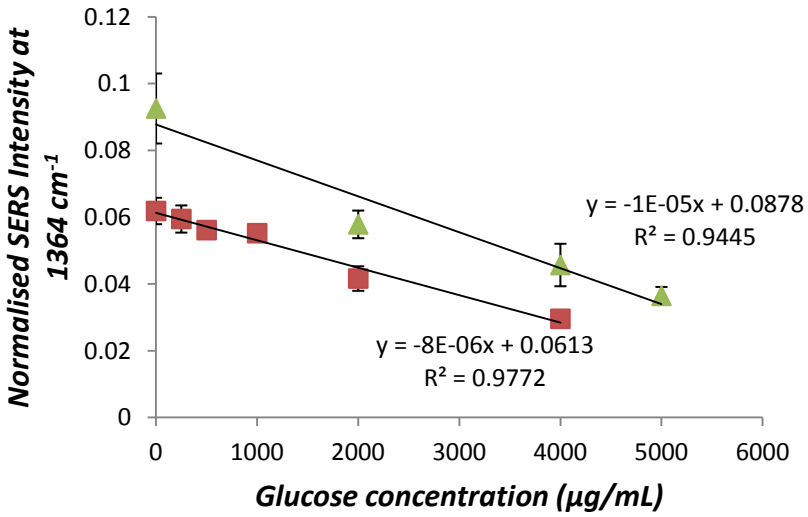

Figure 58. Normalised SERS intensity of RB1-coated gluconanoparticles (measured at 1364 cm^{-1}) following addition of 40 (red) and 80 µg/mL (green) ConA. Free glucose was pre-incubated with ConA at the indicated concentration for 20 minutes. SERS measurements were made 1 minute after addition of ConA samples to the gluconanoparticles.

As shown in figure 58 the sensor was found to perform best when using 40 µg/mL ConA with a 20 minute glucose incubation time and SERS measurement made 1 minute after addition of the ConA-glucose samples to the gluconanoparticles.

Following demonstration in buffered environments, the next stage was to test in plasma as this would best simulate the type of sample which would be measured using the sensor.

4. Non-Buffer Testing

4.1 Fetal Bovine Serum (FBS) Testing

Fetal bovine serum (FBS) was used as a non-buffer medium for testing the gluconanoparticle-ConA based glucose sensor. This was to assess the sensor performance in biological samples that would partially simulate blood media. Prior to testing with any glucose, 40 μg/mL ConA was mixed in FBS and subsequently added to the gluconanoparticles to evaluate the presence of any interferents. Interestingly, and as shown in table 14, there was minimising of the SERS signal increase to a similar level previously observed at ~4000 μg/mL glucose. This implied the presence of carbohydrate-based interferents which were thought to inhibit the interaction between the gluconanoparticles and ConA.

To prove this, FBS was passed through 30,000 g mol^{-1} spin columns to remove any larger proteins and establish whether the interferents were protein or free carbohydrate-based. The filtered FBS was mixed with 40 μg/mL ConA for 20 minutes and subsequently added to the gluconanoparticles. An increase in SERS response was measured 1 minute after addition of the lectin-FBS mixture, corresponding to 0 μg/mL glucose, namely 0.06, (see table 14 and figure 57). This indicated that the protein, removed in the spin column filter, was glycated, binding to the ConA and inhibiting any interaction with gluconanoparticles.

Table 14. Summary of normalised SERS intensity for gluconanoparticles when using FBS or filtered FBS as the testing medium.

Medium Used	Normalised SERS Intensity @ 1364 cm^{-1}
FBS	0.025 ± 0.003
Filtered FBS	0.060 ± 0.005

A suggestion for the interfering protein is fetuin, which has a carbohydrate content of ~25% (composed of hexose, hexosamines and sialic acid).[192] It was therefore decided that FBS would not be an appropriate medium to test in because of the presence of the protein-based interferents.

4.2 Simulated Biological Fluid (SBF) Testing

Simulated biological fluid (SBF) was used as an alternative testing medium for the glucose assay. The ionic content of SBF is compared with blood plasma in table 15. It was hoped that the similarity between these media would mean SBF would provide an adequate model for testing the performance of the glucose sensor in a plasma-mimicking liquid.

Table 15. Ionic content of SBF and blood plasma

Ion	Simulated Biological Fluid Concentration (mM)	Blood Plasma Concentration (mM)
Na^+	142	142
K^+	5	5
Mg^{2+}	1.5	1.5
Ca^{2+}	2.5	2.5
Cl^-	148.8	103
HCO^{3-}	4.2	27
HPO_4^{2-}	1	1
SO_4^{2-}	0.5	0.5

40 µg/mL ConA was mixed with glucose solutions in SBF (at increasing glucose concentrations) and subsequently added to the RB1-coated gluconanoparticles. Figure 59 demonstrates the SERS results obtained from this testing.

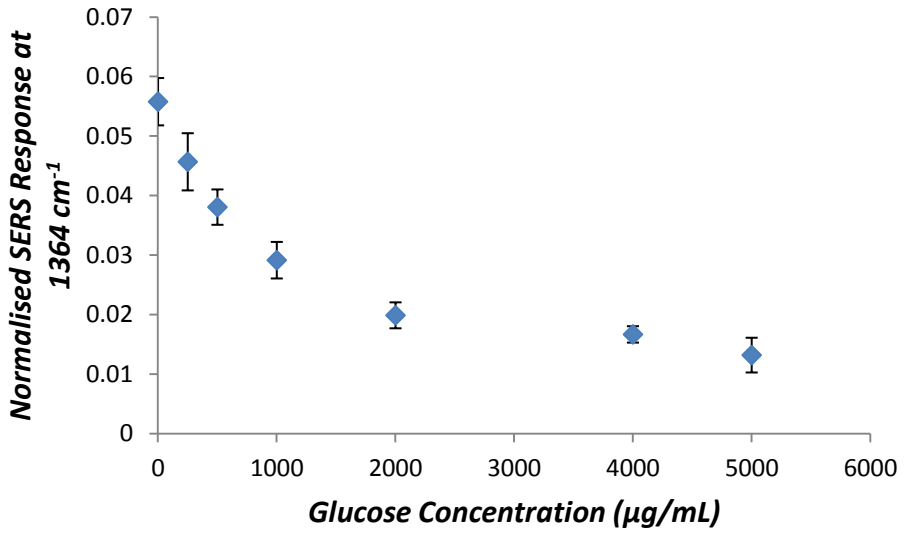

Figure 59. Normalised SERS of RB1-coated gluconanoparticles (measured at 1364 cm^{-1}) following addition of 40 µg/mL Free glucose was pre-incubated with ConA at the indicated concentration for 20 minutes. SERS measurements were made 1 minute after addition of ConA samples to the gluconanoparticles.

The assay responded effectively across the normal blood glucose range (800-1400 μg/mL) and above and below these values (250-2000 μg/mL), demonstrating the use of this SERS-based glyconanoparticle system in simulated biological media. The assay did not perform as effectively as in buffer conditions however and did not respond to the 4000 μg/mL glucose levels as previously observed.

This could have been caused by the salt content of SBF, subsequently impacting on the solution behaviour of ConA and its binding to free glucose. This could also have been caused by the increased Ca^{2+} concentration which could have been inhibiting the binding of the nanoparticles to the ConA (since glucose, bound to the surface, interacts with this metal ion at high concentrations).[26]

4. Conclusions

By inhibiting the binding of the gluconanoparticles to ConA with free carbohydrate, a SERS-based glyconanoparticle glucose sensor was developed. The promising results obtained from initial experiments demonstrated the sensor's ability to measure hypo and hyperglycaemic glucose levels (250-4000 μg/mL) in buffered conditions. The most appropriate concentration of ConA to use was determined as 40 μg/mL. This is validated by research carried out by Lee *et al.* using gold mannonanoparticles in the development of a glucose sensor based on the inhibition of ConA with free glucose and detection by extinction spectroscopy. The researchers determined an optimal ConA concentration of 40 μg/mL where the greatest range of glucose concentrations was able to be measured.[127] Further research needs to be performed to improve the response of the RB1-coated glyconanoparticles across a wide range of glucose concentrations in biological fluids with a view to eventual testing in plasma. This could include changing the concentrations of PEG on the surface of the particles which would subsequently have an effect on the carbohydrate coverage. Mannose could also be tested as an alternative surface sugar to bind more strongly to ConA. This would result in a higher concentration of glucose required to displace the particles from ConA, moving the linear portion of the response curve towards 4000 μg/mL glucose. A mixed monolayer of glucose and mannose could also be tested to evaluate the impact this has on the detectable range.

SERS Detection of Cholera Toxin

Toxins and lectins can be targeted for detection to confirm the presence or absence of a pathogen or toxic biological agent. Kataoka *et al.* have previously reported on the detection of the lectin, Ricin (*Ricinus communis* agglutinin - RCA_{120}) using gold nanoparticles coated in lacotsyl- residues. Detection was performed by colorimetric analysis and a 8.3 nM (1 μg/mL) limit of detection achieved.[193] The reversibility of the Ricin-lactonanoparticle interaction was demonstrated by adding 1mg/mL galactose; potentially allowing the sensor to be recovered and reused.

A potentially important use of metallic nanoparticles is in the analysis of environmental samples such as water, air and soil. The applications of nanotechnology in this field are far reaching and have included metal-ion sensing to monitoring and treatment of pathogens detected in either water or air.[21, 194] With the world population and density increasing, the strain on resources including water, rises. In 2009, the economic cost of illness attributed to waterborne disease in the U.S.A was estimated to be $20 billion[21]. It is therefore, of great importance to develop strategies in water treatment which couple affordability with efficacy and it is believed that nanotechnology can offer a solution with respect to these requirements[21].

Many waterborne pathogens, including Clostridium botulinum *(C. botulinum)* and *E. coli* express lectins which can interact with host glycans[38, 195]. By developing materials that simulate the moiety with which the bacteria or virus interacts, it may be possible to utilise these in detection of that species. With regards to nanoparticles, a major challenge lies in developing materials that will remain colloidal in the presence of other interferents, while also interacting strongly with a target of interest. The suspension of nanoparticles in liquid relies heavily on the conditions into which they are introduced. It is therefore challenging to create a nanoparticle system which remains robust under conditions frequently encountered in natural water samples which contain a variety of ion types at different concentrations.

The benefits of developing a system capable of analysing field samples would be far-reaching. The reliability, coupled with the rapidity and cost-effective benefits of utilising nanoparticles in analyte detection, would warrant the development of assays based on this system. While ensuring nanoparticle stability is one challenge, the other is to develop a SERS/SERRS-based method of analyte detection using these stable nanoparticles.

SERS Detection of Cholera Toxin

Research by Russell *et al.* has previously demonstrated the colorimetric detection of pathogens and associated biomolecules.[30, 126] Gold nanoparticles, coated in a surface of N-acetyl neuraminic acid, were prepared and used to target the hemagglutinin protein present on the surface of the influenza virus (H3N2 strain).[126] The detection was achieved by measuring plasmonic changes upon incubation of the glyconanoparticles with the virus. The virus was detected at a concentration of 0 - 3 μg/mL.[126]

As previously described, the *vibreo cholerae* cellular attachment protein, cholera toxin B (CTB), was detected by colorimetric measurement using gold glyconanoparticles coated with lactose, providing a rapid way of measuring CTB in solution.[30] The limit of detection achieved using this technique was 54 nM (3 μg/mL).[30] CTB has previously been detected by assay involving antibodies (for example ELISA) or DNA (for example PCR).[196-198] However, antibody-based assays rely on reproducible creation of antibodies which are expensive and not always guaranteed. PCR reagents and equipment can also be expensive and the assays are time-consuming.[197, 199] The native CTB binding molecule, GM1, has been exploited in generating CTB-specific assays.[197] While these make use of the carbohydrates of GM1 for CTB capture, detection relies on a secondary development antibody.[197] Using exclusively carbohydrates based on GM1, combined with metallic nanoparticles, provides a relatively low cost and rapid method of CTB detection without the need for analyte amplification or the use of a secondary detection species. The speed of CTB detection is a great advantage at the early stages of a cholera outbreak where rapid detection is of high importance. Combining this assay with SERS as the detection technique, improves the sensitivity capability.

1. Galactonanoparticle Testing

A similar strategy to that employed for the preparation of glyconanoparticles for the detection of ConA was used for CTB detection. Initial experiments focussed on the preparation of galactonanoparticles for the detection of CTB. Galactose is a major binding component in the interaction between CTB and exists as a part of the cellular host molecule to which CTB attaches to, namely the GM1 ganglioside.[30] It was hoped that in coating nanoparticles in both galactose residues and RRM, it would be possible to generate a SERS-active sensor for the rapid and sensitive detection of CTB. Particles were initially coated in 40 μM $CTPEG_{12}$, followed by coupling of galactosamine to the surface of the particles. The galactonanoparticles were subsequently tested with 100 nM of CTB and changes in extinction measured over 30 minutes.

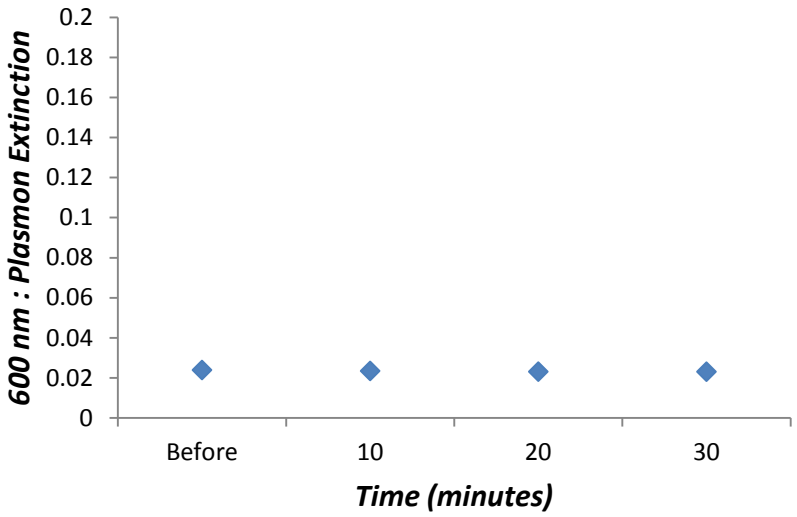

Figure 60. Ratio of 600 nm to plasmon extinction measured for galactonanoparticles before and after incubation with 100 nM CTB.

As indicated by figure 60, minimal changes in extinction ratio were observed for the galactonanoparticles in the presence of CTB. This was unexpected as it was thought the particles would interact and measurably aggregate in the presence of the toxin. To determine if the concentration of CTB (100 nM) was insufficient for aggregation, the galactonanoparticles were incubated with 1 μM CTB and extinction spectra measured for 2 hours. Additionally, gluco- and mannonanoparticles were prepared (each with a 40 μM $CTPEG_{12}$ coating), incubated with CTB and extinction measurements made. As these carbohydrates are not involved in the binding between GM1 and CTB, aggregation of the associated particles was not expected.[53]

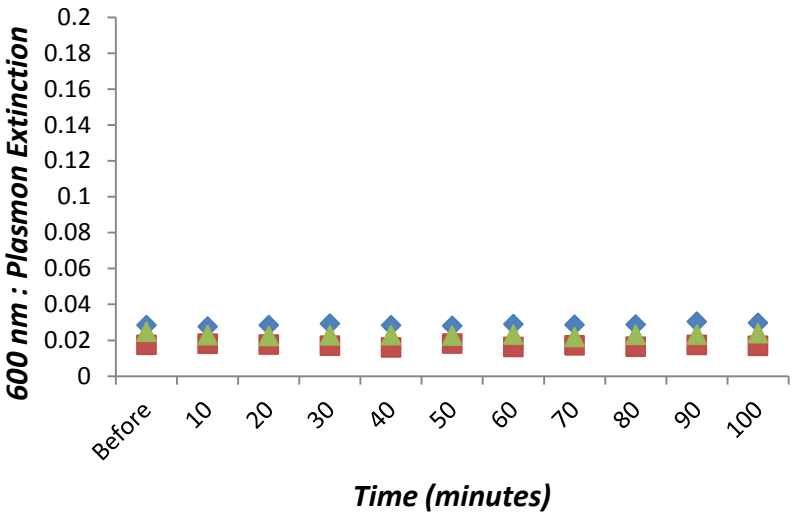

Figure 61. Ratio of 600 nm to plasmon extinction measured for galacto- (blue), gluco- (red) and mannonanoparticles (green) before and after incubation with 1 μM CTB.

Figure 61 illustrates that 1 μM CTB did not appreciably aggregate the galactonanoparticles. As expected, minimal changes to the extinction ratio of the gluco- or mannonanoparticles were measured with addition of CTB

The galactonanoparticles were incubated with 1 μM CTB and changes in SERS intensity monitored. This was to determine if more subtle changes in aggregation could be measured by SERS which may otherwise go unnoticed by extinction spectroscopy. Gluconanoparticles were used as a negative control.

SERS Detection of Cholera Toxin

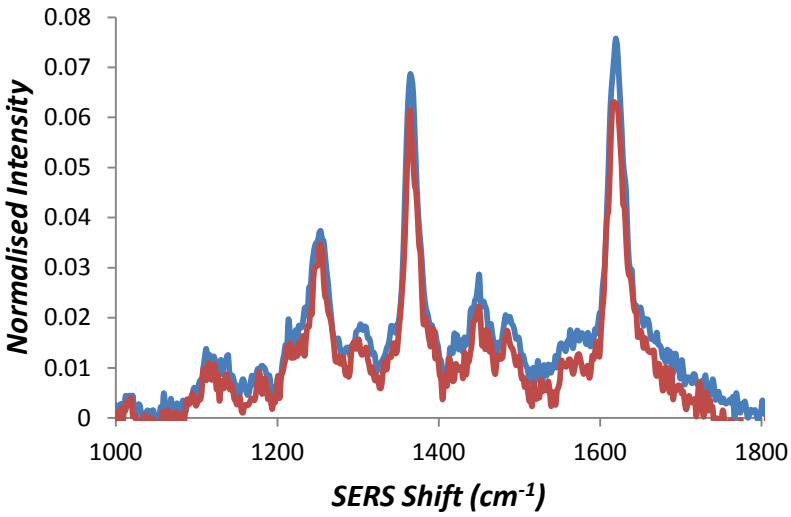

Figure 62. Normalised SERS spectra of RB1-coated galactonanoparticles before (blue) and 5 minutes after incubation with 1 µM CTB (red).

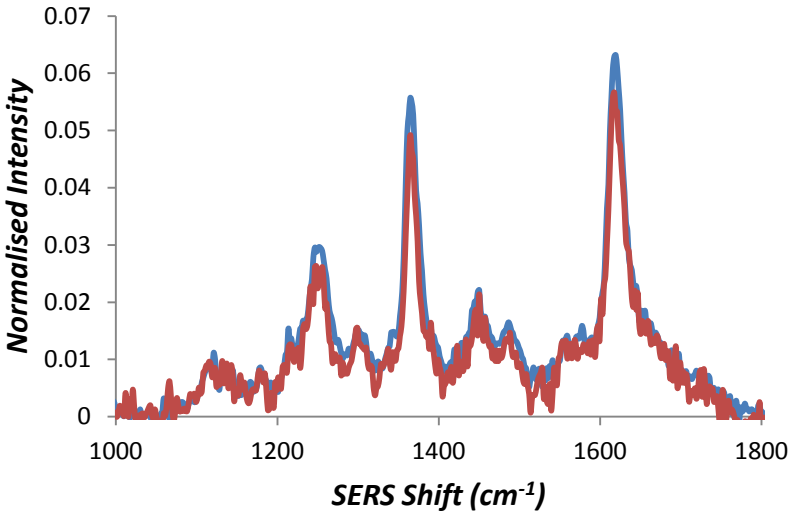

Figure 63. Normalised SERS spectra of RB1-coated gluconanoparticles before (blue) and 5 minutes after incubation with 1 µM CTB (red).

As shown in figures 62 and 63, there were minimal changes measured in the intensity of the RB1 Raman peaks indicating a lack of interaction between both the galactonanoparticles and CTB (1 µM final concentration). This same observation was also noted for the gluconanoparticles, as expected.

2. Galacto-Sialonanoparticle (GSNP) Testing

Note. The following, up to and including page 103, refers to research published as a paper titled "Mixed-Monolayer Glyconanoparticles for the Detection of Cholera Toxin by SERS" first available on 20/11/2015 in Nanoscale Horizons.[200]

The GM1 ganglioside contains a pentameric carbohydrate component composed of galactose, N-acetylgalactosamine, glucose and N-acetyl neuraminic acid (a type of sialic acid). Of these carbohydrates, galactose and N-acetyl neuraminic acid are of greatest importance to the stabilisation of the CTB binding pocket as shown in figure 64.[201]

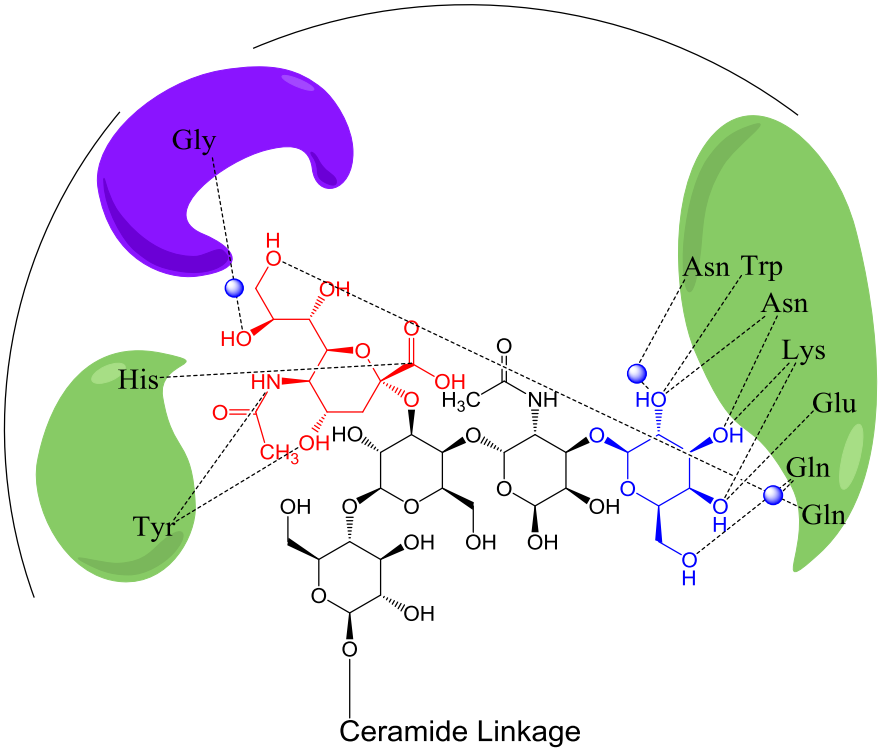

Figure 64. GM1-CTB stabilisation structure (H-bonding) with sialic acid (red) and galactose (blue) residues shown. Water is shown as blue spheres.

The interaction between CTB and the GM1 ganglioside is strengthened when compared with that between galactose alone and CTB (Kd Gal-CTB = 52 mM compared with Kd GM1-CTB = 0.3 nM).[53, 201, 202] The glyconanoparticle preparation strategy was modified so as to incorporate both sialic acid and galactose residues on the nanoparticle surface. To achieve this, separate PEG linkers of galactose (PEGGal) and N-acetylneuraminic acid (PEGSia) were prepared *via* amide coupling chemistry as shown in figure 65.

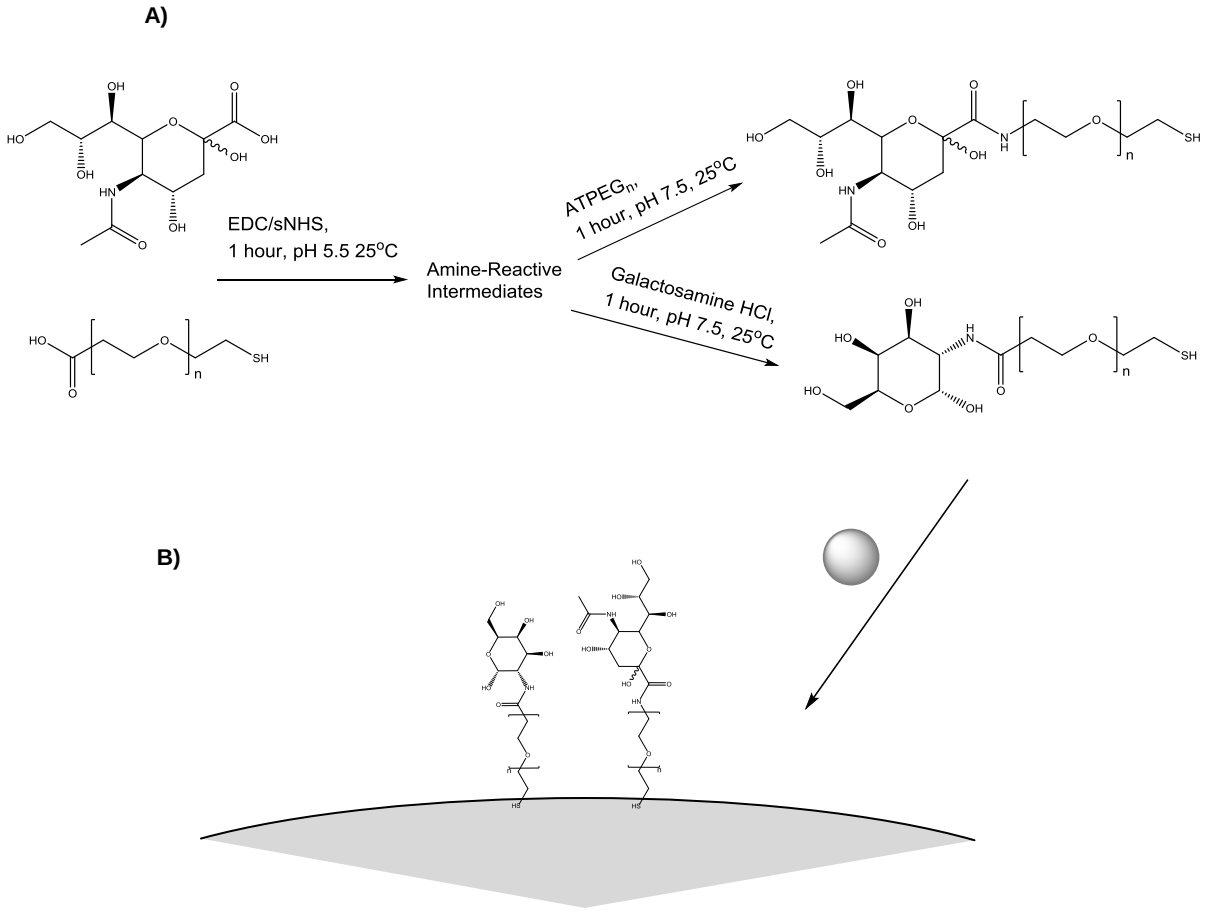

Figure 65. A) Reaction schematic of PEG_nGal and PEG_nSia linkers. B) Subsequent addition of the linkers to the nanoparticles (pre-coated in RB1 - not shown).

The amine functionality of Amine-thiol PEG (ATPEG) linkers was used to couple to the carboxyl of the sialic acid, while the carboxyl functionality of carboxyl/thiol PEG linkers was used, as before, to couple to the amine of galactosamine. PEG linkers of different sizes were tested including PEG_8 (400 g mol^{-1}), PEG_{12} (635 g mol^{-1}) and PEG_{18} (1000 g mol^{-1}).

The linkers were prepared separately in aqueous solution prior to addition to the nanoparticles (see figure 65) to avoid any side amide coupling reactions for example between the CTPEG and ATPEG or galactosamine and sialic acid. A large excess of EDC, sNHS and carbohydrate of interest was used to ensure maximal conversion of the PEG molecules to corresponding glycated linkers. The galacto-sialonanoparticles (GSNPs) produced with these linkers were characterised and subsequently tested with CTB.

SERS Detection of Cholera Toxin

2.1 Characterisation of GSNPs

Size and extinction measurements were taken for the GSNPs (table 16). Gel electrophoresis was also performed on the conjugates together with PEG coated and uncoated (EDTA-capped) particles (figure 66).

To demonstrate the success of amide coupling, the PEG_{12} and PEG_{18} linkers were characterised by attenuated total reflectance infra-red (ATR-IR) spectroscopy (see tables 17 to 20). The linkers were isolated from any excess carbohydrate, 1-(3-(dimethylamino)propyl-3-ethylurea or sNHS using C18 spin columns (Thermo Scientific™, Pierce™). The standardised procedure for using the spin columns is given in section 7 of the Experimental chapter.

Table 16. Extinction and size data for bare and functionalised GSNPs. Gal = galactose and Sia = sialic acid.

NP Capping	λ maximum (nm)	Size (nm)
EDTA	407	55.05 ± 0.30
RB1/PEG_{12}/$_{18}$ Mixture	414	61.19 ± 0.56
RB1/PEG_{12}Gal PEG_{12}Sia	409	65.39 ± 3.58
RB1/PEG_{12}Gal PEG_{18}Sia	410	66.27 ± 1.19
RB1/PEG_{18}Gal PEG_{12}Sia	411	72.08 ± 0.62
RB1/PEG_{18}Gal PEG_{18}Sia	411	82.43 ± 4.97

Figure 66. Agarose gel electrophoresis of AgNPs with various coatings; 1) EDTA, 2)PEG_{12}/$_{18}$, 3) PEG_{12}Gal PEG_{12}Sia, 4) PEG_{12}Gal PEG_{18}Sia, 5) PEG_{18}Gal PEG_{12}Sia and 6) PEG_{18}Gal PEG_{18}Sia.

The changes in λmax. and size (given in table 16) indicated successful functionalisation of the nanoparticles as with the gluco- and galactonanoparticles. While the λmax. blue-shifted,

with functionalisation using the carbohydrate-derivatised linkers (in comparison with the $PEG_{12/18}$ coated nanoparticles), the changes in size indicated modification of the nanoparticle surface chemistry with increasing length of the PEG chains used. The changes to the nanoparticle surface were confirmed by gel electrophoresis (figure 66). Those nanoparticles coated in EDTA alone aggregated, possibly caused by the lack of surface protection in the presence of the highly concentrated testing buffer. Coating with PEG protected these particles and these were seen to travel the length of the gel following application of the potential. The carbohydrate functionalisation caused the nanoparticles to interact strongly with the agarose gel which resulted in minimal movement in the gel as shown for the various GSNP samples tested in figure 66.

Table 17. Infra-red spectrum data for the PEG_{12}-galactose linker.

Wavenumber (cm^{-1})	Functionality/Comment
3362	Secondary amine stretch (masked)
2500-3500	Carbohydrate-OH (strong, broad)
2912	C-H stretch (moderate)
2559	SH stretch (weak)
1674	Amide C=O stretch (strong)
1184	C-N stretch (strong)
1044	C-O stretch (ether, moderate)
726	N-H wag (secondary amine, moderate)
674	C-S stretch (moderate)

Table 18. Infra-red spectrum data for the PEG_{18}-galactose linker.

Wavenumber (cm^{-1})	Functionality/Comment
3219	Secondary amine stretch (masked)
2500-3500	Carbohydrate-OH (strong, broad)
2975	C-H stretch (strong)
2500	C-S stretch (weak)
1676	Amide C=O stretch (strong)
1180	C-N stretch (strong)
1038	C-O stretch (ether, strong)
724	N-H wag (secondary amine, moderate)
696	C-S stretch (moderate)

Table 19. Infra-red spectrum data for the PEG_{12}-sialic acid linker.

Wavenumber (cm^{-1})	Functionality/Comment
3407	Secondary amine stretch (masked)
2650-3500	Carbohydrate-OH (strong, broad)
2981	C-H stretch (strong)
2700	SH stretch (weak, masked)
1683	Amide C=O stretch (strong)
1186	C-N stretch (strong)
1040	C-O stretch (ether, strong)
725	N-H wag (secondary amine, moderate)
699	C-S stretch (moderate)

Table 20. Infra-red spectrum data for the PEG_{18}-sialic acid linker.

Wavenumber (cm^{-1})	Functionality/Comment
3368	Secondary amine stretch (masked)
2500-3500	Carbohydrate-OH (strong, broad)
2973	C-H stretch (strong)
2700	SH stretch (weak, masked)
1673	Amide C=O stretch (strong)
1182	C-N stretch (strong)
1039	C-O stretch (ether, strong)
724	N-H wag (secondary amine, moderate)
696	C-S stretch (moderate)

As shown in tables 17 to 20, there were common peaks measured which correspond to the functionalities of the successfully coupled PEG linkers. This together with the extinction, size and gel electrophoresis results obtained from the characterisation of the GSNPs confirmed the successful preparation of the linkers of interest.

2.2 CTB Aggregation Testing

The results shown in this section are for GSNPs prepared using PEG_{12}Gal and PEG_{18}Sia (in a 15:1 ratio) following optimisation of the appropriate linker length and ratio of galactose to sialic acid linker to give the greatest, selective aggregation response to CTB. Results from optimisation are given in section 2.3 Optimisation of Nanoparticle Surface Coverage.

Following preparation, the GSNPs were tested with CTB and changes in extinction monitored to determine aggregation. The results obtained are shown in figure 67 and table 21.

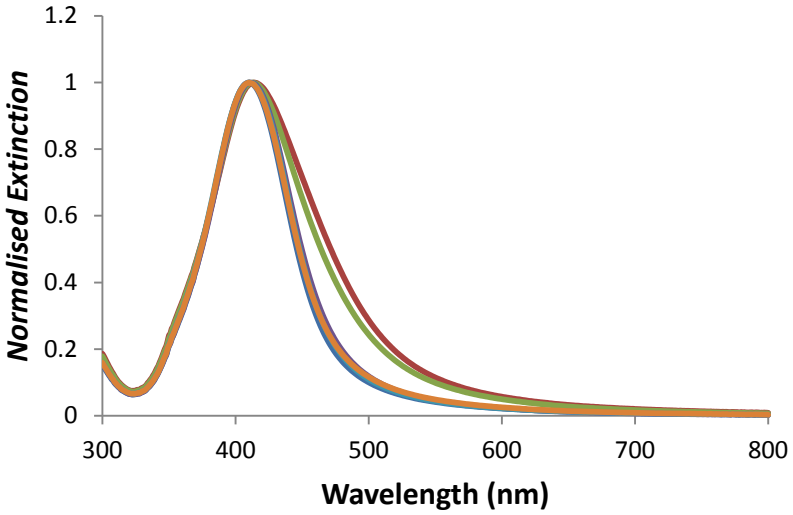

Figure 67. Normalised extinction of GSNPs (blue) with 100 (red), 50 (green), 10 (purple) and 5 nM (cyan) CTB and 100 nM ConA (orange).

Table 21. Summary of extinction data (λmax. and ratio of 600 nm to plasmon extinction) for GSNPs incubated with different concentrations of CTB or ConA.

GSNP Sample	λmax.	600 nm : Plasmon Extinction
0 nM CTB/ConA	410	0.022
5 nM CTB	410	0.022
10nM CTB	411	0.023
50nM CTB	413	0.050
100nM CTB	414	0.057
100nM ConA	410	0.026

The concentration dependent changes in extinction measured are shown in figure 67 and table 21. The red-shift in extinction maximum (from 410 to 414 nm) and corresponding increase in the ratio of 600 nm to plasmon extinction demonstrated the interaction between the GSNPs and CTB. The lack of aggregation and hence minimal change in extinction measured upon addition of ConA to the particles, reinforced the selectivity of the GSNPs prepared.

To further demonstrate aggregation, size measurements of the GSNPs in the presence of either ConA or CTB were taken 5 minutes after addition of each protein.

Table 22. Size data for GSNPs (with a 15:1 gal:sia coating ratio) before and 5 minutes addition of 100 nM CTB of ConA.

Sample	Size (nm)
GSNPs	53.68 ± 0.71
GSNPs with 100 nM CTB	95.29 ± 2.76
GSNPs with 100 nM ConA	54.37 ± 0.18

The results in table 22 reinforce the selectivity of the system; there was no significant increase in size measured for the GSNPs in the presence of ConA when compared with CTB. These results reinforce the findings presented in figure 67 and table 21.

Following the demonstration of reactivity and selectivity of the GSNPs when compared with the galactonanoparticles, the SERS response of the particles towards both CTB and ConA was evaluated.

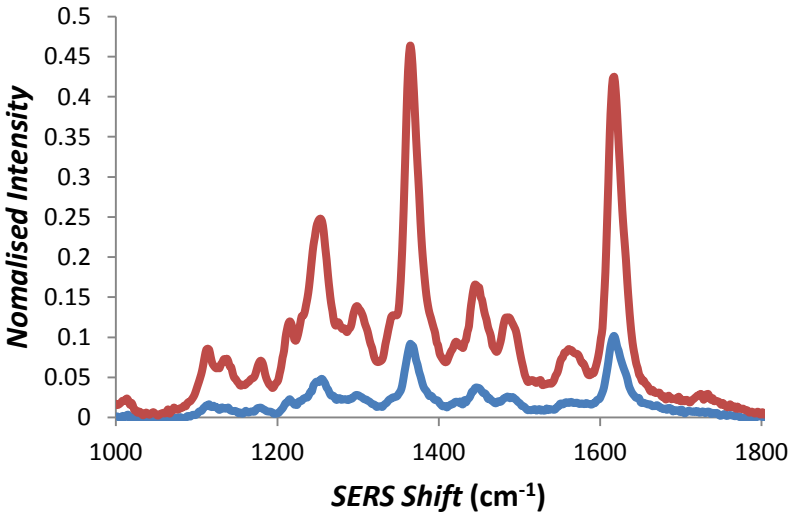

Figure 68. Normalised SERS spectra of RB1-coated GSNPs before (blue) and 5 minutes after incubation with 80 nM CTB (red).

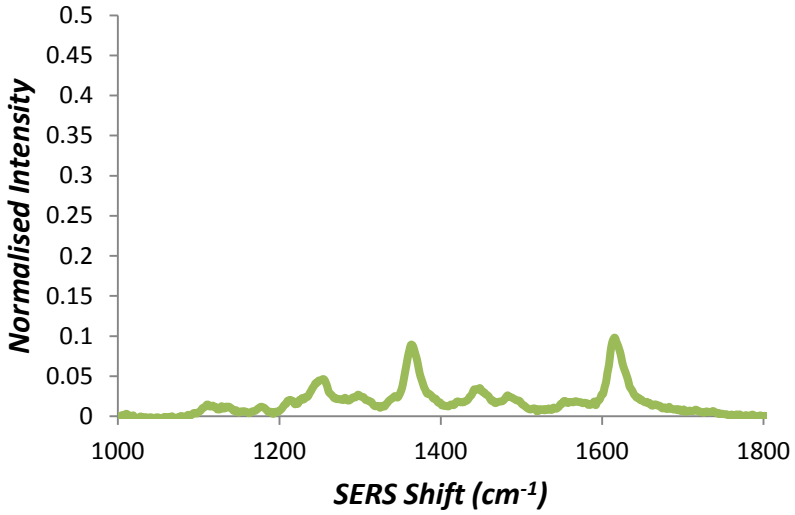

Figure 69. Normalised SERS spectra of RB1-coated GSNPs 5 minutes after incubation with 100 nM Con A (green).

Figure 68 demonstrates the increase in SERS intensity measured 5 minutes after incubation of the particles with 80 nM CTB. The same measurement was made for the particles 5 minutes after incubation with 100 nM ConA and, as shown in figure 69, there was no significant increase in the SERS intensity measured. This reinforced the selectivity of the GSNPs towards CTB, as previously demonstrated by UV-vis. extinction spectroscopy and DLS.

2.3 Optimisation of Nanoparticle Surface Coverage

PEG linkers of different lengths were tested together with different ratios of galactose to sialic acid to establish the combination giving the greatest, selective aggregation response by SERS. The peak at 1364 cm^{-1} was monitored before and after addition of 80 nM CTB.

Table 23. CTB-mediated SERS enhancement with different galacto-sialo surface ratios and PEG chain lengths. The normalised SERS enhancement values are listed below the corresponding galactose to sialic acid ratio[a]. The enhancement is a ratio of the RB1 signal at 1364cm^{-1} prior to aggregation with 80 nM CTB to the same signal measured five minutes after CTB addition.[200]

Coverage Type	Relative SERS Increase at 1364 cm^{-1}			
	1:1[a]	3:1[a]	15:1[a]	30:1[a]
$PEG_{12}Gal/PEG_{12}Sia$	1.2 ± 0.16	2.0 ± 0.20	3.5 ± 0.19	3.0 ± 0.21
$PEG_{12}Gal/PEG_{18}Sia$	0.9 ± 0.10	1.7 ± 0.22	5.2 ± 0.49	3.3 ± 0.51
$PEG_{18}Gal/PEG_{12}Sia$	0.9 ± 0.06	0.9 ± 0.09	0.9 ± 0.06	1.0 ± 0.07
$PEG_{18}Gal/PEG_{18}Sia$	0.9 ± 0.20	1.7 ± 0.15	1.8 ± 0.07	2.3 ± 0.14

SERS Detection of Cholera Toxin

The data in table 23 reveals a maximum relative SERS increase of 5.2 indicating an optimal ratio of PEG12Gal to PEG18Sia of 15:1. Ratios above and below this yielded a lower increase. Extending the sialic acid further from the surface of the nanoparticle than the galactose encouraged maximal binding and the subsequent aggregation of the glyconanoparticles. It was proposed that the steric hinderance of the sialic acid by surrounding galactose was minimised by the extension. This is supported by the drop in relative SERS increase when galactose and sialic acid linkers are at equivalent distance from the nanoparticle surface. The multivalency provided by nanoparticles, which can strengthen individually weak carbohydrate-lectin/toxin interactions, can also hinder toxin binding with crowding of the surface. The interaction between glyconanoparticle and CTB could be discouraged if the spacing between repeating galactose and sialic acid pairs does not match the toxin shape or the spacing between toxin binding units. Carbohydrates which are packed close together on the nanoparticle surface may hydrogen bond which may also reduce protein-binding. This could explain the measured reduction in relative SERS increase in the case of $PEG_{12}Gal/PEG_{12}Sia$ and $PEG_{18}Gal/PEG_{18}Sia$. The length of the PEG_{18} will increase the distance between bound particles, decreasing the magnitude of the distance dependent SERS enhancement as a result of the weaker interparticle hot-spots generated. In the case of the $PEG_{18}Gal/PEG_{12}Sia$ coated particles, it was proposed that the sialic acid could have been blocked by the relatively extended galactose linkers, effectively giving galactonanoparticles and explaining the lack of interaction with CTB.

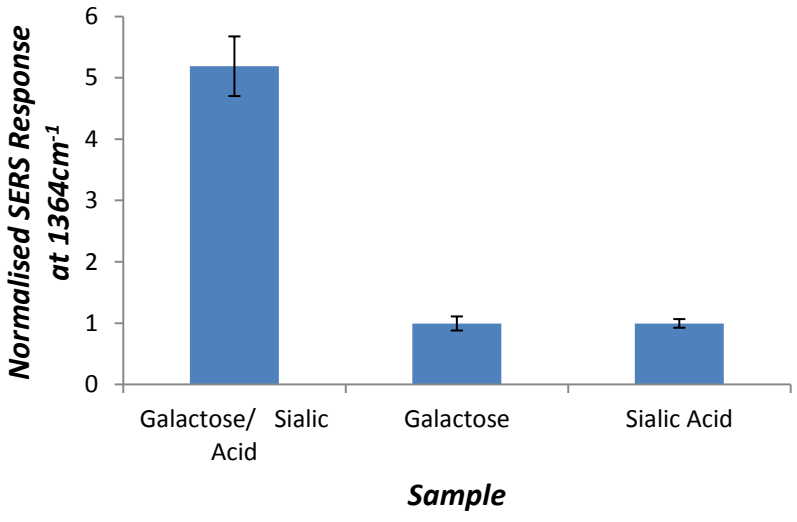

Figure 70. Normalised SERS response for mixed or unique carbohydrate-coated nanoparticles 5 minutes after addition of 80 nM CTB. Those particles coated uniquely in either sugar are incubated with 30 µM of the appropriate PEGylated sugar prior to testing with CTB.[200]

SERS Detection of Cholera Toxin

Figure 70 compares the relative SERS increase of the galacto-sialonanoparticles (15:1 ratio of $PEG_{12}Gal/PEG_{18}Sia$ linkers) with those particles coated in either galactose or sialic acid linkers (30 μM final concentration). The results obtained demonstrated the significance of both carbohydrates in binding CTB as a significant increase in SERS response was only measured in the case of GSNPs and not for the particles coated uniquely in one carbohydrate.

In addition to the linkers noted in table 16, galactose and sialic acid derivatives of PEG_8 were also prepared, however the selectivity demonstrated by these linkers was insufficient to justify their use. Unlike the longer linker combinations, and as shown in figure 71 the PEG_8 linkers aggregated in the presence of ConA making them unsuitable for use in preparing a CTB sensor.

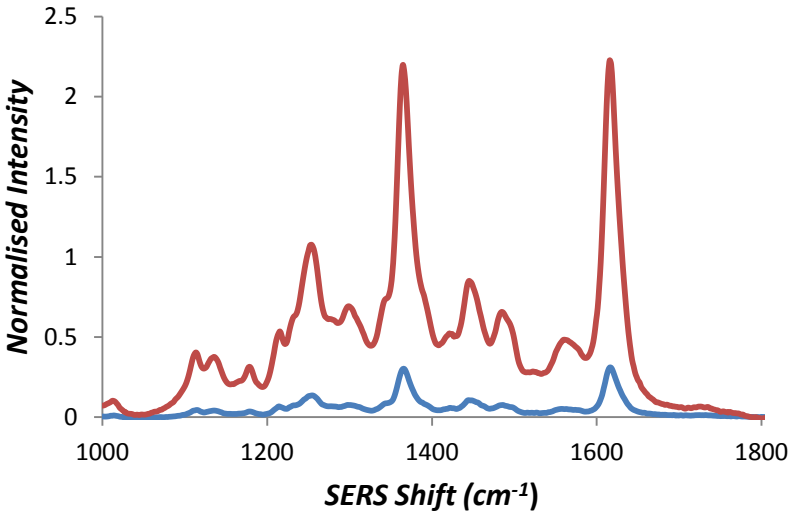

Figure 71. Normalised SERS spectra of RB1-coated galacto-sialonanoparticles before (blue) and 5 minutes after incubation with 100 nM Con A (red).

Table 24. Summary of non-specific ConA-mediated SERS enhancement with increasing galacto-sialo concentration added. The enhancement is a ratio of the RB1 signal at 1364cm^{-1} prior to aggregation with 100 nM ConA to the same signal measured five minutes after ConA addition.

Coverage Concentration of PEG_8Gal/Sia (μM)	Relative SERS Increase @ 1364 cm^{-1}
15/1	7.4
30/2	7.3
60/4	6.7
90/6	3.1

SERS Detection of Cholera Toxin

Table 24 summarises the SERS increase observed for conjugates coated in increasing amounts of the PEG_8 carbohydrate linkers. There was a concentration dependent rise in the normalised SERS increase measured, indicating that a higher concentration of linker on the surface discourages the non-specific aggregation of the glyconanoparticles by ConA (see figure 71 as an example of the increase measured for the 30/2 μM PEG_8Gal/Sia conjugate). However, even at the highest linker concentration (90/6 μM) there was a 3 times increase in the SERS signal measured. The lack of selectivity observed, discouraged further use of this linker system.

2.4 Limit of Detection

The SERS response following addition of different concentrations of CTB to the GSNPs was evaluated as shown in figure 72. The limit of detection of this system for CTB was calculated in the same way as for the detection of the ConA using the gluconanoparticles.

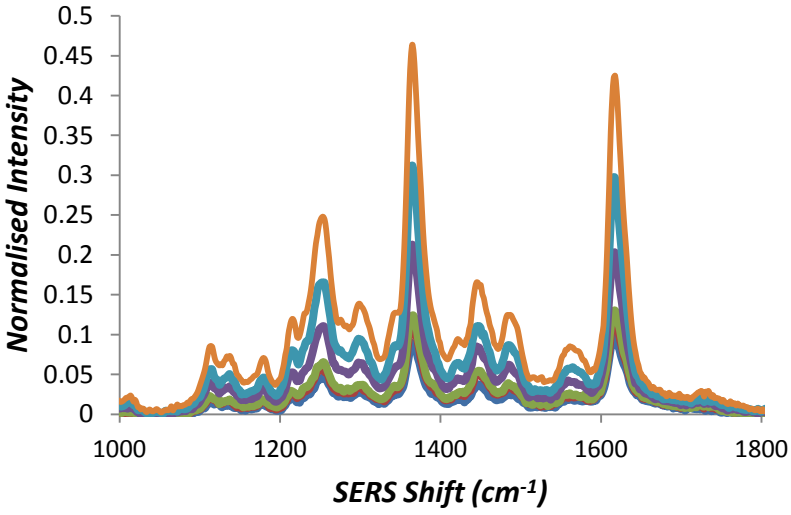

Figure 72. Normalised SERS spectra of RB1-coated galacto-sialonanoparticles before (blue) and 5 minutes after incubation with 5 (red), 10 (green), 20 (purple), 40 (cyan) and 80 nM (orange) CTB.

SERS Detection of Cholera Toxin

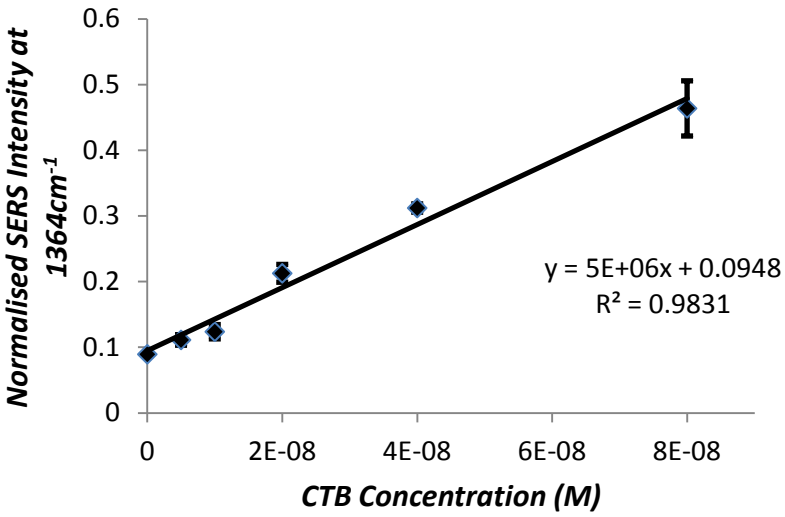

Figure 73. Normalised SERS of RB1-coated gluconanoparticles at 1364 cm^{-1}, measured 5 minutes after addition of 0, 5, 10, 20, 40 and 80 nM CTB.

The limit of detection calculated using figure 73 and equation 5 was determined as 1 nM (56 ng/mL). This limit is ~50 times greater than that previously achievable by UV-vis. extinction spectroscopy and falls within the recommended detection range of 100 ng/mL - 10 pg/mL.[198] This matches the detection limit achieved by WHO approved tests including the infant rabbit and coaggulation assays demonstrating the relevance of the detection limit and hence the assay.[197]

3. Synthetic Freshwater Limit of Detection

The relevance of the SERS CTB assay was assessed by preparing synthetic freshwater (Esthwaite water). Synthetic freshwater simulates the ion compositions of natural waters and was used as the medium for storing CTB samples prior to addition to glyconanoparticles for detection. Diluting CTB into this would provide a simulated environment in which the toxin could be found. It was hoped the assay would behave in a similar way as in buffer conditions. Table 25 lists the ions and associated concentrations contained within the prepared synthetic freshwater (Esthwaite water) (SF) used in testing.

Table 25. Ionic content of synthetic freshwater (Esthwaite water)

Ion	Concentration (μM)
Na^+	250
Ca^{2+}	264
Mg^{2+}	60
K^+	25
Cl^-	280
NO_3^-	30
SO_4^{2-}	114.5
HCO_3^-	385

3.1 Particle Stability in Synthetic Freshwater

GSNPs were resuspended in either the lectin testing buffer previously used (HEPES buffer, pH 7.4 with 0.2 nM $Ca(NO_3)_2$ and $Mn(NO_3)_2$ (HB3)) or synthetic freshwater and the particles stability assessed the following day (24 hours later) by UV-vis. extinction spectroscopy. This was to ensure that any aggregation observed would only be as a result of the interaction between the GSNPs and CTB and not caused by the synthetic freshwater.

Table 26. Extinction data for GSNPs 24 hours after resuspension in HB3 or synthetic freshwater (SF)

Sample	λmax. (nm)	600 nm : Plasmon extinction
GSNP (HB3)	413	0.166
GSNP (SF)	413	0.166

The data in table 26 demonstrates the minimal difference in the extinction profile of the GSNPs resuspended in the lectin testing buffer or synthetic freshwater (SF).

3.2 CTB Limit of Detection in Synthetic Freshwater

CTB was diluted into synthetic freshwater prior to addition to the GSNPs. Following mixing for 5 minutes, SERS measurements were made in an equivalent way as was performed in buffer conditions. The SERS response following addition of different concentrations of CTB to the GSNPs was evaluated as shown in figure 74 and the limit of detection in synthetic freshwater was calculated using figure 75.

SERS Detection of Cholera Toxin

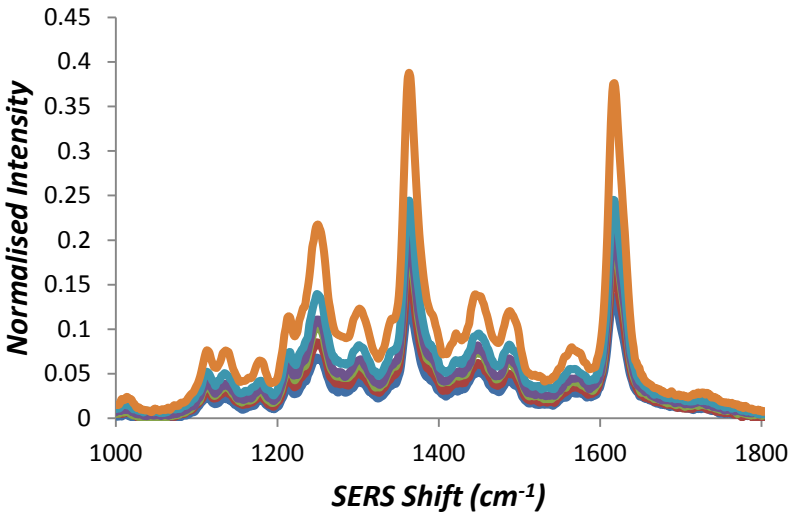

Figure 74. Normalised SERS spectra of RB1-coated galacto-sialonanoparticles before (blue) and 5 minutes after incubation with 5 (red), 10 (green), 20 (purple), 40 (cyan) and 80 nM (orange) CTB in synthetic freshwater.

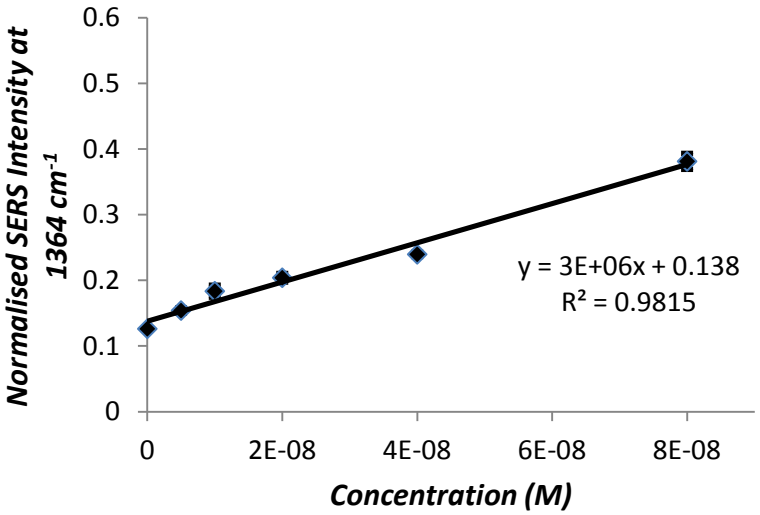

Figure 75. Normalised SERS of RB1-coated gluconanoparticles at 1364 cm^{-1}, measured 5 minutes after addition of 0, 5, 10, 20, 40 and 80 nM CTB in synthetic freshwater.

As shown in figures 74 and 75, a linear, concentration dependent change in SERS intensity was measured for CTB in synthetic freshwater. The limit of detection was again determined as 1 nM (54 ng/mL), demonstrating the response of the sensor in this medium. The capability of the rapid and sensitive nanoparticle sensor developed is reinforced by the successful detection of CTB in synthetic freshwater samples.

4. Conclusions

The research described builds on the work carried out in the previous chapter titled " Generating Stable, Lectin-Reactive Glyconanoparticles" in order to produce a novel bacterial biomarker detection assay. Cholera toxin B-subunit (CTB) was chosen as the bacterial marker of interest due to its availability and relevance as a waterborne disease target. Galactose, known to interact with the CTB, was used to functionalise silver nanoparticles, prepared using a EDTA-reduction method and pre-coated with the Raman reporter molecule RB1. The galactonanoparticles prepared originally were found not to react with CTB. There was no measurable aggregation either by extinction spectroscopy and no increase in the RB1 SERS signals measured. Literature on the binding site of CTB was reviewed and it was found that both galactose and sialic acid are key components of the GM1 ganglioside-CTB interaction. In order to partially mimic the GM1 interaction, PEG-based linkers of both galactose and sialic acid were used in functionalising the surface of Raman reporter molecule-coated silver nanoparticles. The use of both sialic acid and galactose on the nanoparticle surface significantly increased the reactivity of the galacto-sialonanoparticles (GSNPs) towards CTB when compared with the galactose-functionalised nanoparticles. The effect of the lengths of the PEG-based carbohydrate linkers together with the ratio of galactose to sialic acid was evaluated extensively to determine the most reactive combination of the component carbohydrates. Following this evaluation, the appropriate sizes of PEG linkers together with the ratio of carbohydrates were determined (15:1 $PEG_{12}Gal$ to $PEG_{18}Sia$) a limit of detection for CTB was determined as 1nM (54 ng/mL) using the GSNPs in buffer and synthetic freshwater conditions. This level is within the detection range (10 pg/mL to 100 ng/mL) of WHO approved tests which include infant rabbit and coagglutination assays.[197, 198] A low volume was required to aggregate the nanoparticles (10 μL of CTB sample in 200 μL of GSNP colloid) and detection was achieved in 5 minutes. Comparable techniques used in the detection of CTB include PCR or antibody-based methods (for example ELISAs).[203, 204] These techniques require multiple assay steps for eventual measurement, increasing detection time. The selectivity of the GSNPs was assessed by adding ConA to the particles and measuring aggregation by UV-vis. extinction spectroscopy, DLS and SERS. The lack of aggregation caused by the glucose/mannose-specific ConA demonstrated the selectivity of the CTB-reactive GSNPs.

Developing Carbohydrate Microarrays

Carbohydrate-based microarrays have been developed for a variety of applications including profiling the glycan binding behaviour of lectins and antibodies and the detection of disease-related glycan-binding antibodies and whole cells including pathogenic species.[205-208] The arrays are produced on solid substrates using variety of chemical immobilisation techniques involving covalent and non-covalent methods. For covalent attachment, substrates are functionalised with a variety of species including epoxide, amine and N-hydroxysuccinimide esters.[209-211] This subsequently allows for attachment of carbohydrates and/or glycoproteins to generate arrays. The generation of effective arrays relies on appropriate spacing between the surface glycans as shown in figure 76.[147] Carbohydrate-based interactions are typically weak and therefore rely on multivalency for strength.[28] This can be aided by ensuring the printed glycans are close together and in the correct orientation so as to allow effective binding of the analyte.[147] As well as density, the type of printed species also affects the binding of the analyte. The use of oligosaccharide derivatives such as glycodendrimers, glycoclusters and neoglycoproteins, each affect binding of the analyte differently.[212-214]

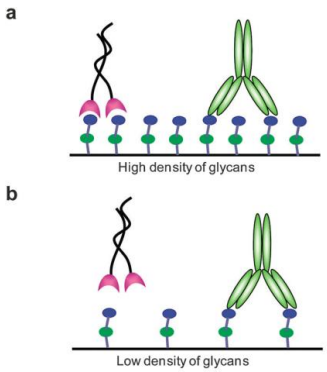

Figure 76. a) Lectins with short spacing between binding sites may bind strongly to the high density of glycans on the surface. (b) Lectin with short spacing between binding sites are unable to bind strongly to the low density of glycans on the surface while an antibody with greater spacing between binding sites can bind well to glycans at either high or low density.[147]

Lectin microarrays have been key to the understanding of glycan-protein interactions. Mammalian lectins, for example DC-SIGN and DC-SIGNR, have been investigated using microarrays to better understand their function and binding capabilities to both endogenous and foreign (pathogenic) species.[215] Galectins, the presence of which has been linked with

tumour progression, have also been investigated using carbohydrate microarrays whereby the arrays could be used to differentiate between galectin types.[216, 217] Viral and bacterial lectins have previously been detected using microarrays.[218-220] CTB and tetanus toxin (TT) were selectively detected using GM1 and GT1b coated substrates, respectively, by Fang *et al.*.[220] CTB and TT selectively bound only those areas of the substrate coated in GM1 or GT1b as shown in figure 77. Each lectin was detected sensitively (30 and 60 pM limits of detection for CTB and TT respectively).[220]

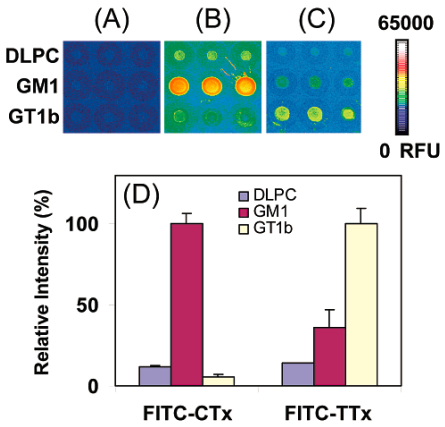

Figure 77. Fluorescence images of microarrays consisting of 1,2-Dilauroyl-sn-glycero-3-phosphocholine (DLPC), DLPC doped with 4 mol % GM1, and DLPC doped with 4 mol%GT1b. The images correspond to microarrays treated with (A) buffer, (B) 1nMfluorescein-labeled cholera toxin B-subunit, (FITC-CTx), and (C) 2 nM fluorescein-labeled tetanus toxin (C fragment,FITC-TTx). (D) Normalised histograms showing the relative amounts of binding of the labelled cholera and tetanus toxins to the ganglioside microarrays.[220]

An issue with this assay is the requirement for each lectin to be tagged. While this is feasible with an isolated lectin, it may not be possible to selectively tag the toxins alone over other non-target proteins present in complex samples.

A solution proposed to this was to use SERS-active glyconanoparticles that would have a particular binding affinity for the target lectin and be coded with a specific RRM, to indirectly detect that lectin. This would remove the requirement for tagging of the analyte, allowing the lectin to be detected in its native state.

1. Proposed Array Design

A sandwich-assay was proposed for the detection of lectins by SERS as shown in figure 78. Following functionalisation of a suitable surface, with an appropriate carbohydrate and blocking agent, a lectin-containing solution would be added with the hope that the lectin of

interest interacted with the carbohydrate surface. Following several wash steps to remove any unbound lectin, nanoparticles coated with either the same or different carbohydrate as those on the solid surface would be added and either interact or remain unbound respectively. This would demonstrate the selectivity of the surface created.

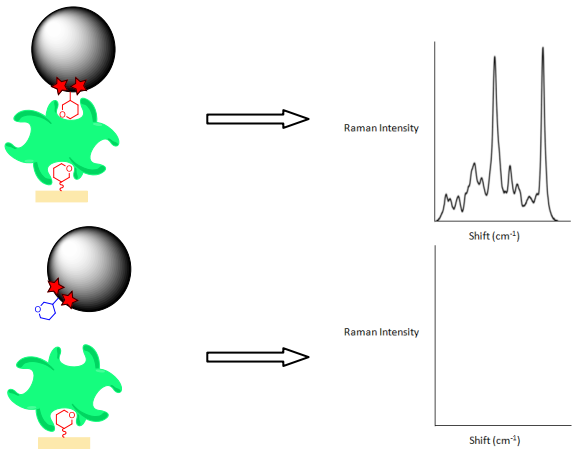

Figure 78. Proposed interaction of Raman reporter molecule (red star)/carbohydrate-(red or blue hexose) coated nanoparticles and microarray surface-bound lectin ConA (via surface carbohydrate). Glucose (red) is bound to the surface. Nanoparticles coated with either glucose (red) or galactose (blue) will either interact or not respectively. SERS is measured only if the nanoparticles bind, thereby indicating the presence of the lectin of interest.

Functionalised glass slides were chosen for the assay platform. A number of different functional groups, designed to react with various carbohydrates and their associated derivatives can be used. These include epoxide, biotin, boronic acid and sNHS groups. As the carbohydrate derivatives used were mainly aminated, for example glucosamine and galactosamine, it was decided that the most appropriate coating used would be epoxide-coated slides.

2. Functionalisation Method and Plant Lectin Testing

The surface was prepared for lectin binding by initially coating the surface with PEG molecules. This was to discourage non-specific binding of lectin to the glass surface. The heterobifunctional PEG added was either carboxy-amine PEG_8 ($CAPEG_8$) or a 50:50 mixture of $CAPEG_8$ and methoxy-amine PEG_4 ($MAPEG_4$). This was to assess if the density of carbohydrates on the surface had any effect in ConA binding and subsequent nanoparticle attachment.

Developing Carbohydrate Microarrays

Note. In the following discussion galactose = Gal, glucose = Glu, glucose glass surface-ConA-glucose nanoparticle sandwich = GluConAGluNP. The preparation of glass slides, subsequent addition of lectin and nanoparticles is described in detail in section 9 of the experimental chapter.

Surfaces of 50:50 $CAPEG_8$:$MAPEG_4$ or solely $CAPEG_8$ were prepared on epoxy-coated glass slides. Amide coupling (between the carboxylic acid of the heterobifunctional $CAPEG_8$ and the amine of the aminated carbohydrate) was performed on the glass slides to present a carbohydrate coated surface. Subsequently the surfaces were incubated with the lectin ConA at 200 nM (or 14 pmoles on the surface) and, subsequently, glyconanoparticles. The silver nanoparticles used were those prepared via citrate reduction as described in the chapter "Generating Stable, Lectin-Reactive Glyconanoparticles". The use of the Raman reporter molecule RB1 allowed measurement of attachment to the surface by SERS. This resulted in areas of GluConAGluNP, GluConAGalNP, GalConAGluNP and GalConAGalNP. The white light images for each of these areas are shown in figures 79 and 80.

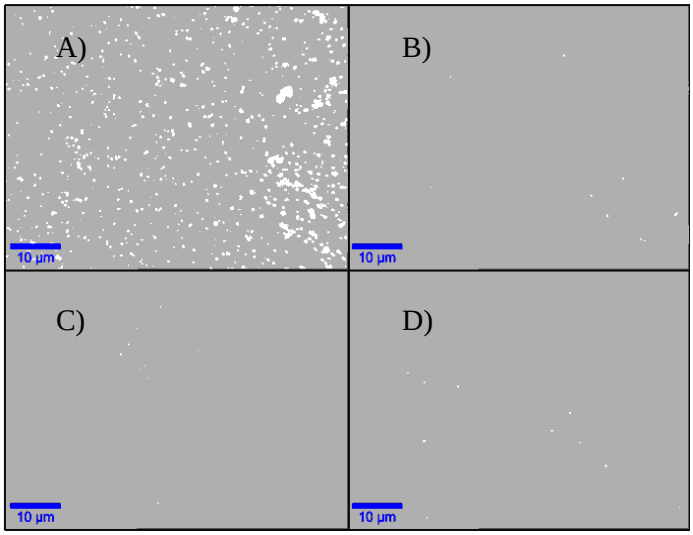

Figure 79. White light images (taken with a 100x objective) of 50:50 $CAPEG_8$:$MAPEG_4$ surface coated glass slides. A) GluConAGluNP, B) GluConAGalNP, C) GalConAGluNP, D) GalConAGalNP

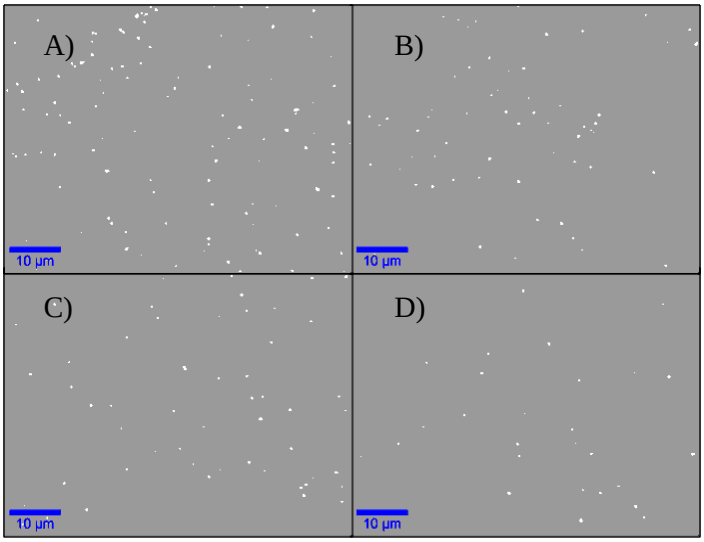

Figure 80. White light images (taken with a 100x objective) of $CAPEG_8$ surface coated glass slides. A) GluConAGluNP, B) GluConAGalNP, C) GalConAGluNP, D) GalConAGalNP

The surfaces with 50:50 $CAPEG_8$:$MAPEG_4$ were shown to encourage greater binding of the ConA and subsequently the nanoparticles. This is shown by the more numerous aggregates in figure 79A compared with 80A. As the 50:50 $CAPEG_8$:$MAPEG_4$ surfaces proved to encourage attachment of the greatest number of aggregates, this surface coverage chemistry was employed for subsequent testing. To prove that the "white specs" observed in the white light image were indeed nanoparticle aggregates, a Raman map was taken for a section of the GluConAGluNP area. This and all subsequent SERS spectra measured were normalised against the SERS intensity of the 520 cm^{-1} peak of the spectrum of silicon, measured prior to each experiment. The white light image and corresponding Raman map and spectra are shown in figure 81.

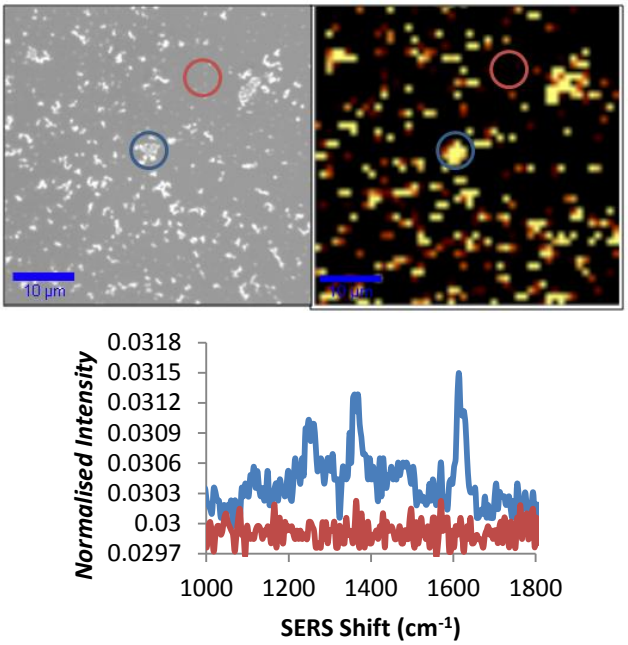

Figure 81. White light to Raman map (x100 objective) comparison. The map was measured at 1616 cm^{-1} with one measurement taken per µm. SERS spectra are measured for RB1 at the area defined over the aggregate in the white light image (blue spectrum and circle) and at the blank area (red spectrum and circle).

Figure 81 demonstrates that the light areas in the white light image do correspond to nanoparticle aggregates as there are Raman signals measured for RB1 in these areas; RB1 signals would only have been measured if the RRM were bound to the particle surface or non-specifically bound to the glass surface. As there was no signal measured for RB1 on the area of glass, it was proposed that there were indeed particle aggregates on the surface.

It was expected that nanoparticles would only be visible on the areas of GluConAGluNP, however as shown by figures 79 and 80 B, C, D, there was some non-specific binding observed. This could have been caused by an interaction between the BSA and the nanoparticles (BSA interacts strongly with nanoparticles as a result of the high cysteine content of the protein). To evaluate this, a non-protein, PEG-based blocking agent was used prior to the addition of ConA to the glass slide and compared with BSA.

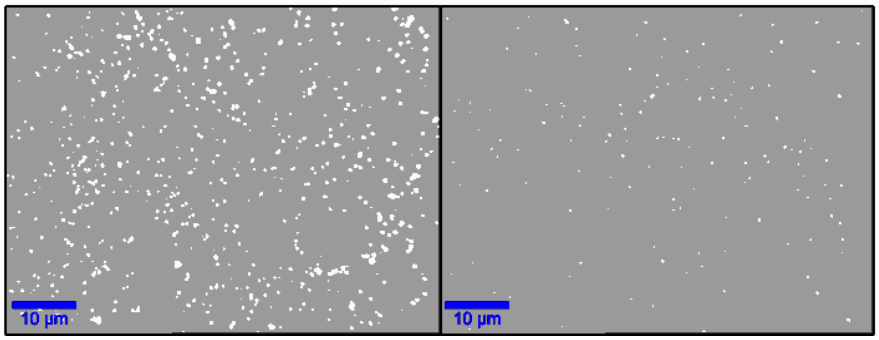

Figure 82. White light images (taken with a 100x objective) of left: GluConAGluNP (PEG blocking), right: GluConAGluNP (BSA blocking)

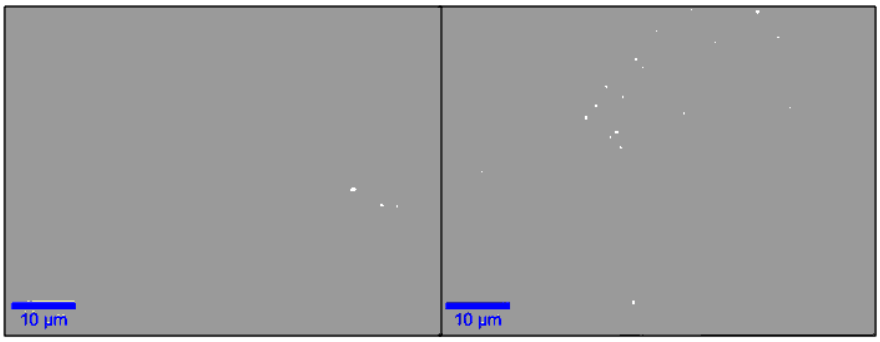

Figure 83. White light images (taken with a 100x objective) of left: GluConAGalNP (PEG blocking), right: GluConAGalNP (BSA blocking)

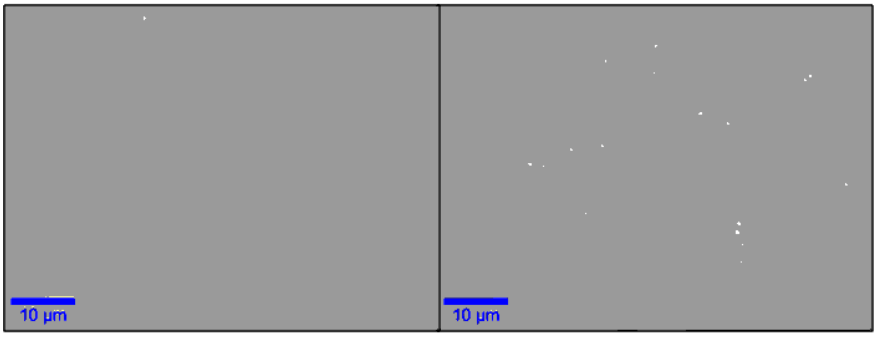

Figure 84. White light images (taken with a 100x objective) of left: GalConAGluNP (PEG blocking), right: GalConAGluNP (BSA blocking)

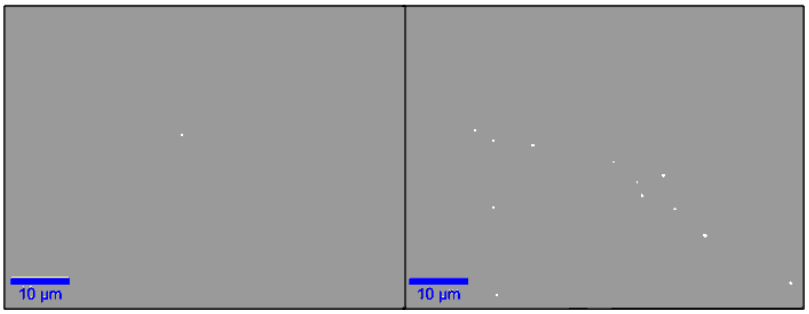

Figure 85. White light images (taken with a 100x objective) of left: GalConAGalNP (PEG blocking), right: GalConAGalNP (BSA blocking)

The images presented in figures 82, 83, 84 and 85 indicate that the PEG blocker discouraged non-specific binding of the nanoparticle more effectively than the previously used BSA blocker. Subsequently Raman spectra were taken in triplicate of each area (PEG blocked and measured with a 10x objective) as shown in figure 86, averaged and presented in figure 87.

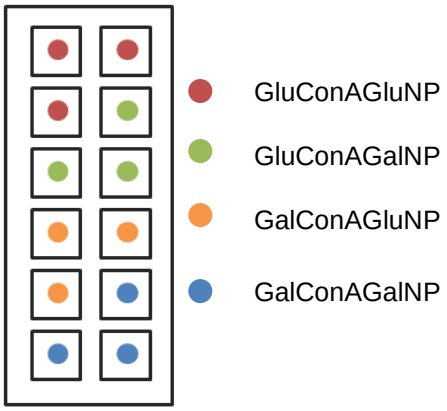

Figure 86. Layout of each carbohydrate-lectin-glyconanoparticle area where Raman measurements were made in triplicate.

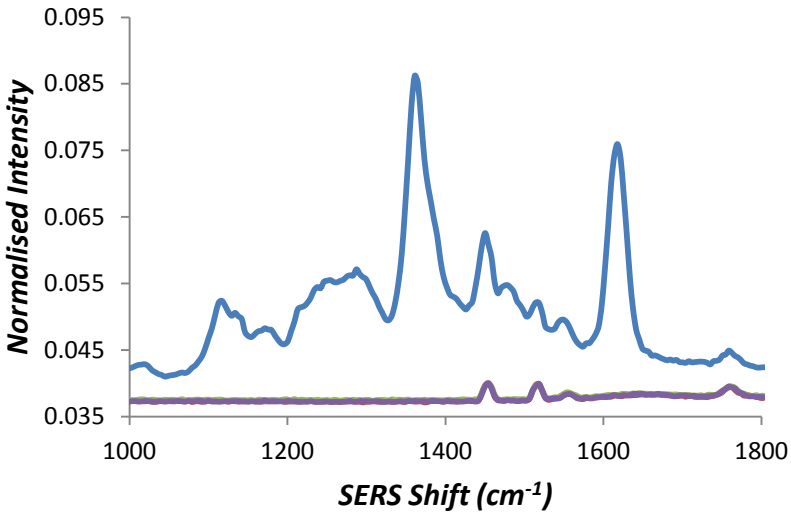

Figure 87. Raman spectra of GluConAGluNP area (blue), GluConAGalNP (red), GalConAGluNP (green), GalConAGalNP (purple). Green and Red are masked by Purple.

The results shown in figure 87 demonstrate the selectivity of the system generated. Negligible response in SERS was measured for all areas except GluConAGluNP. This was expected since ConA interacts with glucose hence only the gluconanoparticles should have attached to the surface and only if the surface was coated with glucose.

While the system proved selective, the reproducibility of the SERS response was found to be low as demonstrated by the results in table 27.

Table 27. Average Normalised SERS response (ANSR) @ 1616 cm^{-1} for different glycoconjugate areas with standard deviation (SD) (%) given.

	Glycoconjugate Areas			
	GluConAGluNP	GluConAGalNP	GalConAGluNP	GalConAGalNP
ANSR @ 1616 cm^{-1}	0.076	0.038	0.038	0.038
SD (%)	33.9	0.420	0.305	0.131

While the standard deviation was negligible where there was a low SERS response measured, the GluConAGluNP area gave a highly variable SERS response (34 %). Improvements are required to enable the system to be eventually developed into an working assay. This is discussed in greater detail in the further work section.

3. Bacterial Lectin Testing

As described in the chapter "SERS Detection of Cholera Toxin", bacteria can express lectins which are used in surface or host adhesion. *Pseudomonas aeruginosa (P. aeruginosa)* are gram negative bacteria found in a variety of different environments including natural and artificial surfaces such as medical equipment and on board the international space station.[221] Infection is characterised by inflammation and sepsis and if untreated while present in critical organs, including the liver or kidneys, can be fatal.[222] Additionally, the bacteria has developed antibiotic resistance and infection can only be treated by intravenously administered antibiotics. There is however great risk of further resistance being developed to the current treatments.[223] There is therefore a need to detect the bacterium sensitively and rapidly to prevent infection. *P. aeruginosa* express the lectins PA-I and PA-II. These bind galactose or fucose-bearing glycans respectively. For this reason it was decided to carry out preliminary testing of the activity of the previously tested galactonanoparticles in the presence of the PA-I lectin. Both the activity of the galactonanoparticles towards PA-I and the ability of the surfaces to attach PA-I would be evaluated. As with the ConA testing previously described, 200 nM (14 pmoles) of PA-I lectin was tested.

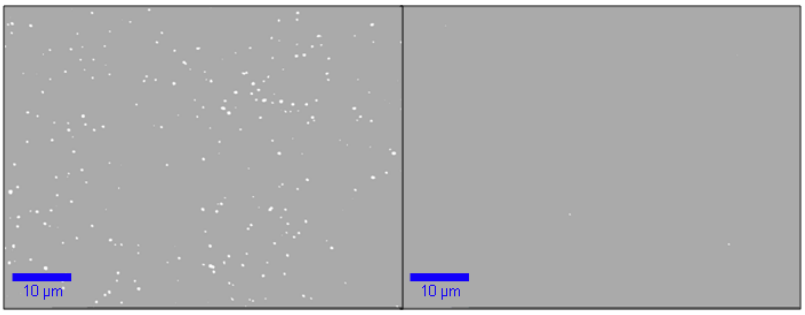

Figure 88. White light images (taken with a 100x objective) of left: GluConAGluNp and right: GluConAGalNP.

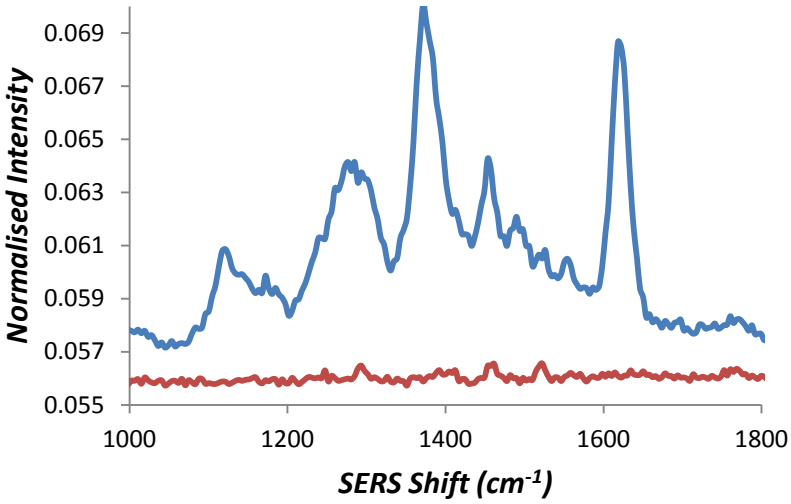

Figure 89. SERS spectra of the GluConAGluNP area (blue) and GluConAGalNP area (red).

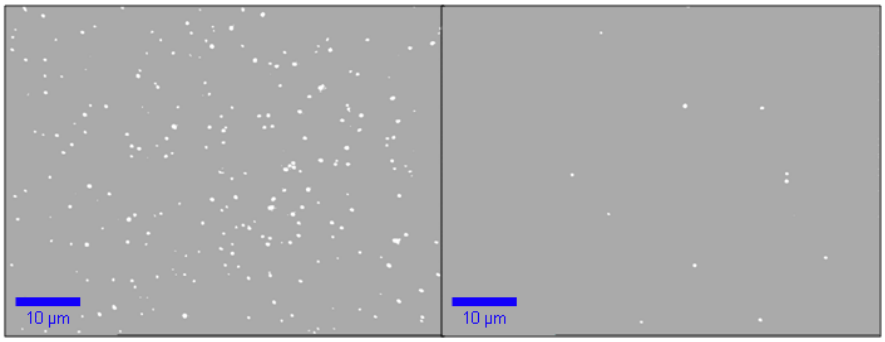

Figure 90. White light images (taken with a 100x objective) of left: GalPA-IGalNP and right: GalPA-IGluNP.

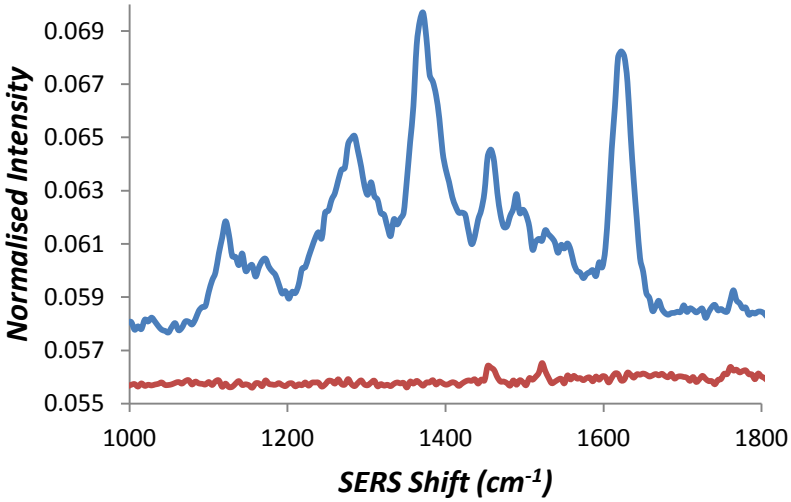

Figure 91. SERS spectra of the GalPA-IGalNP area (blue) and GalPA-IGluNP area (red).

Figure 88 and 89 reinforce previous observations where attachment of the gluconanoparticles to the surface-bound ConA was measured both in the white light image, and SERS spectrum (measured with a 10x objective). Conversely, the galactonanoparticles do not attach, resulting in lack of aggregates observed in the white light images or SERS signals in the associated spectra.

Figures 90 and 91 illustrate that when ConA is replaced with PA-I, galactonanoparticles are seen to attach to the surface via the surface-bound PA-I lectin and form aggregates as indicated both in the white light image and SERS spectrum. The gluconanoparticles demonstrated a lack of affinity for the surface with few aggregates seen in the white light image and measured by SERS. This was as expected, given that there is no affinity for glucose towards PA-I.

This preliminary piece of work demonstrates the potential of surface-based methods of detecting bacterial lectins and encourages pursuit of further research in this area. At the time of commencement of mapping experiments the instrument used became unavailable, preventing further results from being obtained and hindering miniaturisation of the format to give carbohydrate microarrays.

4. Conclusions

Carbohydrate microarrays have previously been developed for glycan analysis and results obtained with a variety of measurement techniques including fluorescence microscopy, surface plasmon resonance and mass spectrometry. There are currently no examples of the use of glyconanoparticles or SERS-based detection with carbohydrate arrays. This project aimed to couple these to generate a glyconanoparticle-based carbohydrate microarray assay with detection by SERS. RB1-coated silver glyconanoparticles, produced *via* a citrate reduction method, were used. Epoxide-functionalised glass slides were employed to allow functionalisation of the surface with heterobifunctional PEG linkers ($CAPEG_8$ and $MAPEG_4$) for subsequent coupling to aminated carbohydrates and functionalising the nanoparticle surface with the sugars of interest (in this case glucose or galactose). The reactivity of the carbohydrate-coated glass surfaces was initially tested with the plant lectin ConA. It was proposed that the lectin attached itself to the glucose-coated surface, allowing subsequent attachment of gluconanoparticles. This was initially observed with the appearance of aggregates in the white light images taken of the glass slides coated with glucose, incubated with ConA and subsequently with gluconanoparticles. To prove that the objects observed were indeed nanoparticle aggregates, Raman maps were made of the surface with Raman signals measured at aggregate areas. 200 nM (14 picomoles) of ConA were added to the surface to enable attachment of the gluconanoparticles, demonstrating the low level of lectin detected by the glyconanoparticles. In the case of a galactose-coated surface, or with incubation of galactonanoparticles, minimal aggregate formation was observed on the glass surface, resulting from a lack of interaction between the carbohydrates and glucose-specific ConA. The surfaces prepared with a mixture of methoxy and carboxy-terminated PEG were found to cause the greatest deposition of particles when compared with those coated exclusively with carboxyl groups. PEG and BSA were compared as blocking agents for the surface, prior to addition of the lectin and subsequently, glyconanoparticles. It was found that the PEG block encouraged greater selectivity and discouraged non-specific binding to a greater extent than BSA. ConA was replaced with the galactose-specific, bacterial lectin PA-I. Galactonanoparticles bound to the surface in the presence of PA-I, having been added to the galactose-coated glass surface. 200 nM (14 picomoles) of PA-I were added to the glass surfaces, again demonstrating the low level of bacterial lectin which could be detected. Early efforts in turning the bulk-spotting approach into a microarray format were attempted. These were however, unsuccessful as the printing technique (conditions and method) could not be determined within the span of the project due to timing

and availability of the instrument being used This is an aspect of the project which could be pursued further in the future.

Concluding Remarks and Future Outlooks

Glyconanoparticles have previously been shown to be applicable in a number of sensor platforms. Detection of targets of interest with these particles have made use of extinction and fluorescence spectroscopy and dynamic light scattering.[49, 110, 224] There is little previous research on the use of SERS-active glyconanoparticles in biodetection. Previous examples have included the detection of plant lectins with lactose-coated nanoparticles. and differentiation between cancerous and non-cancerous cells using lectin-coated nanoparticles.[10, 14] In each instance, these have proven to be the first examples of their kind. The research described herein builds on previous efforts to apply glyconanoparticles to a wide variety of detection platforms including bacterial protein detection, glucose sensing and the development of surface-based detection techniques. The common approach taken in developing the particles for the experiments described herein involved the use of heterobifunctional linkers to both protect the nanoparticle surface and provide functional groups which could subsequently be coupled to a variety of aminated or carboxy-functionalised carbohydrates.

Initial research involved using the short, alkanethiol-based linker, 6-mercaptohexanoic acid. While using this led to the production of lectin-reactive glyconanoparticles, the selectivity and stability of these particles was found to be limited. This encouraged the use of heterobifunctional carboxyl/thiol PEG linkers instead. The glyconanoparticles generated proved to be stable while remaining selective and allowing for the sensitive detection of the plant lectins ConA and Jacalin. Particles produced using an EDTA-reduction method were found to give a measurable change in the SERS intensity of the surface-bound RRM following aggregation.

The reversibility of carbohydrate interactions was exploited to develop a glucose sensor using the developed gluconanoparticles. The sensor relied on the inhibition of gluconanoparticle-ConA binding as a result of the presence of free glucose. This decreased the aggregation measured as observed with the drop in the SERS intensity increase compared with the signal intensity measured for the reference situation (addition of ConA to the gluconanoparticles in the absence of free glucose). Comparison of the SERS signal measured with that of the reference situation gave an indication of the level of free glucose present and accommodating the ConA binding sites. The sensor was found to be effective across the

physiological range and the hyper/hypoglycaemic range. The sensor performance was limited to the physiological range alone in simulated biological fluid as shown by the results obtained. Future work in this area could focus on improving the performance of the sensor in plasma samples and extending the range of glucose concentrations detectable by modifying the surface chemistry or type of carbohydrates used in preparing the glyconanoparticles

The successful detection of plant lectins led to the development of glyconanoparticles for the rapid and sensitive detection of the cholera toxin B subunit (CTB) in synthetic freshwater by SERS. This was achieved by evaluating particles coated with a single or multiple carbohydrates. The mixed monolayer (multiple carbohydrate) approach was found to be more effective as this more closely mimicked the natural CTB binding motif. A mixture of both galactose and sialic acid linkers at a specific ratio and of different lengths was found to produce galacto-sialonanoparticles (GSNPs) which reacted sensitively, yet selectively with CTB in buffer conditions. The sensor was also found to perform equally well in synthetic freshwater, demonstrating the application of the sensor to a variety of samples. Future research with these particles could be carried out to evaluate their use in remote detection. Developments in portable Raman spectrometers have produced hand-held, battery-powered devices, capable of sensitive and rapid detection. These could be used to assess the performance of GSNPs for the detection of CTB and related species in the field, for example at the site of contaminated bodies of water. Sensitivity of detection could be improved with the use of magnetic nanoparticles, which have previously been shown to significantly increase the sensitivity of SERS-based DNA assays.[162] Attempts could be made to mimic other gangliosides which are implicated in the establishment of bacteria. These could include the G1b class of gangliosides (GT1b, GD1b and GQ1b) which bind to several toxins including the tetanus and botulinum toxins.

The glyconanoparticles developed for the detection of plant lectins in solution were also used in early-stage developments of surface-based detection of lectins (plant and bacterial). The glass substrates were functionalised with carbohydrates *via* heterobifunctional PEG linkers. The lectin ConA was detected sensitively and selectively on carbohydrate-functionalised epoxy-glass substrates following addition of gluconanoparticle. Different blocking species were tested to assess the mitigation of non-specific binding. Using an analogous strategy, the galactose binding PA-I lectin (expressed by *Pseudomonas aeruginosa*) was also detected, however the selectivity of detection was reduced as some non-specific binding of gluconanoparticles to the surface was observed. The focus could now turn to improve the selectivity of the surface-based detection technique further by expanding on the blocking

agents tested and the carbohydrate coating method used to functionalise the surface. Following this, carbohydrate microarrays could be developed to allow for the low volume, microarray detection of various lectins using SERS-coated glyconanoparticles. A host of glycans could subsequently be analysed, some of which are useful biomarkers (for example bacterial toxins, or host glycans).

Experimental

1. Reagents Used

Silver nitrate, sodium citrate tribasic, ethylenediaminetetraacetic acid disodium salt dihydrate (EDTA), sodium hydroxide (anhydrous), calcium nitrate tetrahydrate, manganese nitrate tetrahydrate, magnesium chloride dihydrate, calcium chloride hexahydrate, calcium carbonate, sodium sulfate, potassium bicarbonate, sodium bicarbonate, potassium phosphate dibasic trihydrate, β-D-glucose, β-D-galactose, D-(+)-glucosamine hydrochloride, N-acetylneuraminic acid (sialic acid), concanavalin A (ConA), cholera toxin B-subunit (CTB), 1-Ethyl-3-(3-dimethylaminopropyl) carbodiimide hydrochloride (EDC), N-hydroxysulfosuccinimide sodium salt (sNHS), DL-dithiothreitol (DTT), 4-(2-hydroxyethyl)-1-piperazineethanesulfonic acid (HEPES) powder and 2-(N-morpholino)ethanesulfonic acid (MES) powder were purchased from Sigma-Aldrich Co Ltd. (Gillingham, UK). Methyl-α-D-mannopyranoside and D-mannosamine hydrochloride were purchased from Carbosynth Limited (Compton, UK). C18 Spin Columns, D(+)-galactosamine hydrochloride and heterobifunctional carboxyl/thiol, carboxyl/amine and methoxy/amine polyethylene glycol ($CTPEG_{12}$, $CAPEG_8$, $MAPEG_4$) were all purchased from Thermo Fisher Scientific Inc. (Waltham, USA). Heterobifunctional amine/thiol polyethylene glycol (AT PEG_8, $ATPEG_{12}$ and $ATPEG_{18}$) and carboxyl/thiol polyethylene glycol ($CTPEG_8$ and $CTPEG_{18}$) were purchased from Nanocs Inc. (New York, USA). $CTPEG_{90}$ was purchased from Laysan Bio Inc. (Arab, USA) triply distilled and deionised water (dH_2O) was prepared in-house. All solvents were of laboratory grade and chemicals were obtained from commercial sources.

2. Instrumentation

2.1 Raman Instrumentation

514.5 nm Excitation:

An argon ion laser radiation source with a 514.5 nm excitation wavelength coupled with a Renishaw InVia Raman microscope, was used for analysis of benzotriazole- and MGITC-containing samples. A 20x long working distance objective lens was used for laser focusing. A charge coupled device (CCD) detector was used for detection. Static collection of spectra was made at 1360 cm^{-1} recorded with an accumulation time of 1 second per sample and 3

accumulations at 100% laser power. For all Raman spectra, data handling was carried out using GRAMS/AI software for spectra baseline correction.

All SERS spectra measured using this instrument were normalised against the SERS intensity of the 800 cm^{-1} peak of the spectrum of cyclohexane, measured prior to each experiment.

532 nm Excitation:

A WITec Alpha 300R confocal microscope was coupled to an argon ion laser with excitation wavelength of 532 nm. Mapping of the glass substrates was carried out for a 50 μm x 50 μm area using 50 lines per image and 50 points per line. An integration time of 0.04 seconds was used at 10 % laser power. For all Raman spectra, data handling was carried out using WITec data processing software.

All SERS spectra measured using this instrument were normalised against the SERS intensity of the 520 cm^{-1} peak of the spectrum of silicon, measured prior to each experiment.

2.2 Centrifuges

Heraeus Biofuge Pico:

24 place microlitre (0.2-2 mL)

Maximum Speed: 13000 rpm/ 16060 xg

Thermo Scientific Sorvall Biofuge Primo:

6 place millilitre (6 x 50 mL)

Maximum Speed: 15000 rpm/ 21890 xg

2.3 UV-Visible Extinction Spectrometer

Varian, Cary Win-UV 300:

Dual Beam Scanning UV-vis. spectrophotometer

Range: 190 – 900 nm

Lamps: Deuterium (UV), Tungsten-Halogen (Visible)

2.4 Dynamic Light Scattering Instrument

Malvern Zetasizer Nano Zs:

Measurement Range (Particle Sizing): 0.3 nm – 10.0 μm

Experimental

3. Nanoparticle Preparation

3.1 Silver Citrate Colloid

The glassware (3-necked flask and stirrer bar) was cleaned with aqua regia overnight, rinsed four times with dH_2O with washings neutralised using sodium bicarbonate. The 3-necked flask was then filled with 500 mL of dH_2O. 90 mg of silver nitrate was dissolved in 1 mL of dH_2O and added to the 3-necked flask. The contents of the flask were heated to boiling with a Bunsen burner and boiled for 30 minutes. 111 mg of sodium citrate, dissolved in 1 mL of dH_2O, was added and the resulting mixture stirred for 15 minutes with boiling. The heat was removed and the colloid left to cool to room temperature and for 16 hours thereafter. Silver nanoparticle concentration was calculated as 4.04×10^{-10} M (using $A = \varepsilon.c.l$, where A is absorbance, ε is molar absorptivity, c is concentration and l is path length).

3.2 Silver EDTA Colloid

All glassware was cleaned with aqua regia before use and rinsed thoroughly with dH_2O. 23 mg of EDTA was added to 500mL of dH_2O. This was heated and prior to boiling, 80 mg of sodium hydroxide, dissolved in 1 mL dH_2O was added. Once boiled, 22 mg of silver nitrate in 5 mL of dH_2O was added slowly in 1 mL aliquots with stirring. The water was boiled further with stirring for 15 minutes before the heat was removed and stirring continued until the silver EDTA colloid reached room temperature and for 16 hours thereafter. Silver nanoparticle concentration was calculated as 7.55×10^{-11} M (using $A = \varepsilon.c.l$, where A is absorbance, ε is molar absorptivity, c is concentration and l is path length).

4. Buffer Preparations

4.1 Amide Coupling Buffers

MES buffer (MB):

A 100 mM stock solution of MES buffer was prepared by dissolving 2.13 g of MES powder in 50 mL of dH_2O. This was adjusted to pH 5.5 with 1 M NaOH before adding enough volume of dH_2O to give 100 mL of 100 mM MES buffer. 10 mM MES buffer was prepared by taking 10 mL of the 100 mM stock MES buffer and diluting this in 90 mL (giving a total volume of 100 mL).

HEPES Buffers (HB1 and HB2):

A 100 mM stock solution of HEPES buffer (HB1) was prepared by dissolving 2.38 g of HEPES powder in 50 mL of dH_2O. This was adjusted to pH 7.4 with 1 M NaOH before

adding enough volume of dH_2O to give 100 mL of 100 mM HEPES buffer. 10 mM HEPES buffer (HB2) was prepared by taking 10 mL of the 100 mM stock HEPES buffer and diluting this in 90 mL (giving a total volume of 100 mL).

4.2 Lectin Testing Buffers

HEPES Buffer With $Ca(NO_3)_2$ and $Mn(NO_3)_2$ (HB3):

To 100 mL of 10 mM HEPES buffer at pH 7.4, 3.5 mg of $Mn(NO_3)_2.4H_2O$ was added and dissolved. Following this, 3.4 mg of $Ca(NO_3)_2.4H_2O$ was added and dissolved giving a 10 mM HEPES buffer at pH 7.4 with 0.2 mM $Ca(NO_3)_2$ and $Mn(NO_3)_2$ (HB3).

4.3 Synthetic Freshwater

Three solutions containing a variety of ions at varying concentrations were prepared using the volumes indicated in table E1. After combining the components (S1, S2 and S3), the solution was mixed for 6 hours to ensure sufficient dissolution and mixing of all components. The pH was measured as 7.4.

Table E1. Ionic content of the constituent solutions (S1, S2 and S3) of synthetic freshwater (Esthwaite water) including the volumes of each component solution required.

Stock solution	Concentration (g L^{-1})	Volume of Stock Solution Required (µL)
S1		50
$MgCl_2 \cdot 6H_2O$	12.2	
$CaCl_2 \cdot 6H_2O$	17.5	
$Ca(NO_3)_2 \cdot 4H_2O$	3.5	
S2		45450
$CaCO_3$	0.02	
S3		50
Na_2SO_4	16.3	
$KHCO_3$	2.5	
$NaHCO_3$	1.68	
dH_2O		4450

4.4 Simulated Biological Fluid

The concentration (mass/volume) of each component required for the preparation of simulated biological fluid, pH 7.4 (SBF), is given in table E2.

Table E2. Reagent concentration of SBF in order of dissolution.

Reagent	Final required concentration or volume (g L^{-1} or *mL*)
NaCl	8.0
$NaHCO_3$	0.35
KCl	0.22
$K_2HPO_4.3H_2O$	0.23
$MgCl_2.6H_2O$	0.31
HCl (1M)	*40*
$CaCl_2$	0.28
Na_2SO_4	0.07
Tris.HCl	6.1

5. Solution Preparation

5.1 Lectins and Toxin

Lectin and toxin solutions were prepared at a stock concentration of 2 mg/mL in 10 mM HEPES with 0.2 mM $Ca(NO_3)_2$ and $Mn(NO_3)_2$, pH 7.4 buffer (HB3), synthetic freshwater (SF) of simulated biological fluid (SBF). These were aliquoted and stored at 2 °C. Subsequent dilutions of the lectin stocks were made in HB3 or SF or SBF.

5.2 Free Carbohydrate

β-D-glucose and methyl α-D-mannose were dissolved in HB3 or SBF for reversibility testing with gluconanoparticles and ConA depending on whether the sensor were being tested in buffer or SBF conditions.

6. Preparation of SERS-active glyconanoparticles

6.1 Raman Reporter Molecule

4-((1H-benzo[d][1,2,3]triazol-6-yl)diazenyl)-3,5 dimethoxyphenol (RB1) and N-[4-[[4-(dimethylamino)phenyl](4-isothiocyanatophenyl)methylene]-2,5-cyclohexadien-1-ylidene]-N-methyl-, chloride (Malachite Green isothiocyanate (MGITC)) were used as the Raman reporter molecules for SERS detection involving both lectins and toxins. These were each dissolved in methanol to give 1 mM and 0.1 mM stock solutions of RB1 and MGITC respectively and subsequently diluted in dH_2O to give 0.1 mM and 0.01 mM of RB1 and

MGITC respectively, to add to silver nanoparticles. The associated structures and spectra of RB1 and MGITC are shown in figures E1 and E2 respectively.

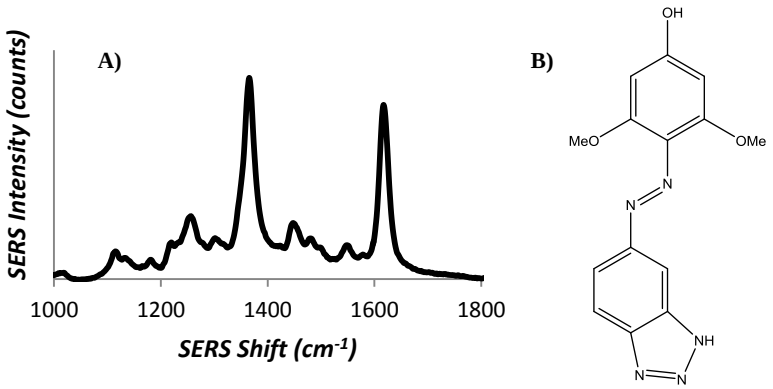

Figure E1 A) SERS spectrum of RB1 obtained at an excitation wavelength of 514.5 nm, 1 second acquisition, 3 accumulations. B) Structure of RB1.

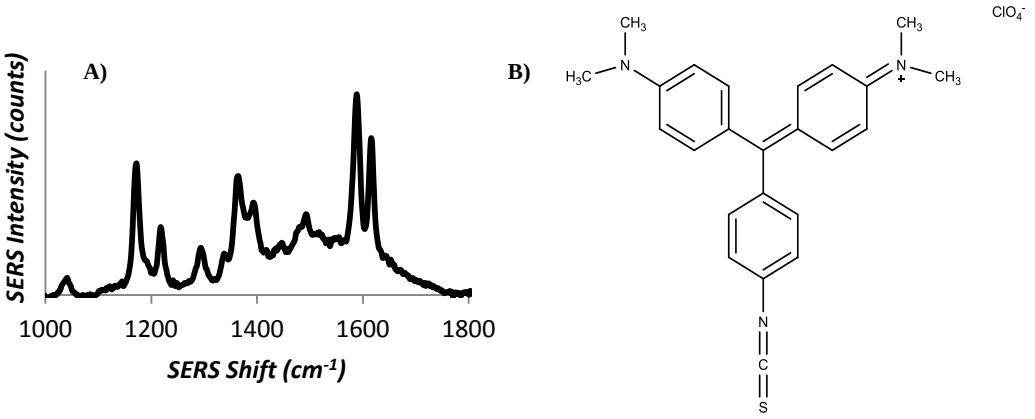

Figure E2 A) SERS spectrum of MGITC obtained at an excitation wavelength of 514.5 nm, 1 second acquisition, 3 accumulations. B) Structure of MGITC.

6.2 PEG-Carbohydrate Linker Preparation and Nanoparticle Functionalisation

The PEG-carbohydrate linkers were prepared using two methods; on and off nanoparticle coupling. Both methods were used depending on the type of carbohydrate used in nanoparticle functionalisation. All concentrations stated are final.

On-Nanoparticle Coupling - *used for the preparation of glucose-, galactose- and APGAP-coated nanoparticles:*

10 μM RB1 or 1 μM MGITC (dissolved in 10% methanol/water) and the appropriate concentration of CTPEG or MHA (each dissolved in dimethyl sulfoxide, DMSO) were added to the appropriate volume of silver nanoparticles. For example 100 μL of 0.1 mM RB1 and 40 μL of 1 mM $CTPEG_{12}$ were added to 860 μL of silver nanoparticles (this procedure was scaled up as required) to give 10 μM RB1 and 40 μM $CTPEG_{12}$. A 10 mM aminated

carbohydrate (glucosamine, galactosamine, mannosamine or APGAP) solution was prepared in 100 mM HEPES buffer @ pH 7.4 (HB1). The conjugates were centrifuged at 4000 rpm for 10 minutes. The pellets from this were kept and the supernatants removed and centrifuged at 7000 rpm for 15 minutes. The supernatants from the second centrifugation step were subsequently removed and discarded and the pellets from each centrifugation step combined. 5.4 mM EDC and 4.6 mM sNHS solutions were prepared in 10 mM MES buffer, pH 6.0 (MB). The separate 100 μL EDC and 240 μL sNHS solutions were mixed (340 μL total) and added to each pellet and mixed for 15 minutes at room temperature.

After 15 minutes 1.1 mM of carbohydrate solution in HB1 was added to the coupling mixture (for 1mL of particles this was 100 μL of the 10 mM solution), with sufficient HB1 added to ensure a pH of 7-7.4 (400 μL for 1 mL of particles), and shaken for 16 hours at room temperature. Following mixing, the previous centrifugation steps were employed. The collected pellets were then resuspended in HB3 for lectin/toxin testing and glucose sensing in buffer conditions or simulated biological fluid (for simulated plasma testing experiments).

Off-Nanoparticle Coupling (aminated carbohydrates) - *used for the preparation of the galactose-based linkers:*

This procedure refers to a 1.7 mL scale batch. A 10 mM solution of carboxyl/thiol $CTPEG_n$ (in DMSO) was prepared in 100 μL MB. A 156 mM aqueous solution of aminated carbohydrate was prepared in 500 μL 10 mM HEPES buffer @ pH 7.4 (HB2). 200 mM EDC and 225 mM sNHS (in MB) solutions (200 μL each) were combined. This mixture was added to the 10 mM $CTPEG_n$ solution and mixed for 1 hour. The solution of aminated carbohydrate was then added to this and mixed for 1 hour. Following this, 700 μL of 0.01M NaOH solution was added to raise the pH to 7.5-8 and mixed for 16 hours. This same procedure can apply to any aminated carbohydrates such as galactosamine, glucosamine and mannosamine.

Off-Nanoparticle Coupling (carboxylated carbohydrates) - *used for the preparation of the sialic acid-based linkers:*

This procedure refers to a 1.7 mL scale batch. A 19 mM aqueous solution of carboxylated carbohydrate was prepared in 100 μL MB. 200 mM EDC and 225 mM sNHS MB solutions (200 μL each) were combined. The 400 μL EDC and sNHS mixture was added to the 19 mM carboxylated carbohydrate solution and mixed for 1 hour. A 1.25 mM $ATPEG_n$ solution was prepared in 500 μL HB2. This was added to the coupling mixture and shaken for 1 hour at room temperature. Following this, 700 μL of 0.01 M NaOH solution was added and mixed for 16 hours. This same procedure can apply to any carboxyl-functionalised carbohydrate.

Experimental

6.3 GSNP Preparation

The off-nanoparticle coupled products were added to the nanoparticles and mixed for 16 hours. To generate 15:1 galactose:sialic acid coverage, 30μM of galactosyl-PEG_n and 2 μM sialyl-PEG_n was added to RB1 (10 μM) coated silver nanoparticles by premixing the carbohydrate linkers together for 10 seconds before adding to the nanoparticles. Following 16 hours mixing, the galacto-sialonanoparticles (GSNPs) were centrifuged at 4000 rpm for 15 minutes and the supernatant centrifuged at 7000 rpm for 15 minutes. The supernatant from the second centrifugation was discarded and the pellets from each centrifugation step combined and resuspended in HB3 or SF depending on the testing to be carried out. The overall reaction scheme and preparation of GSNPs is illustrated in figure E3.

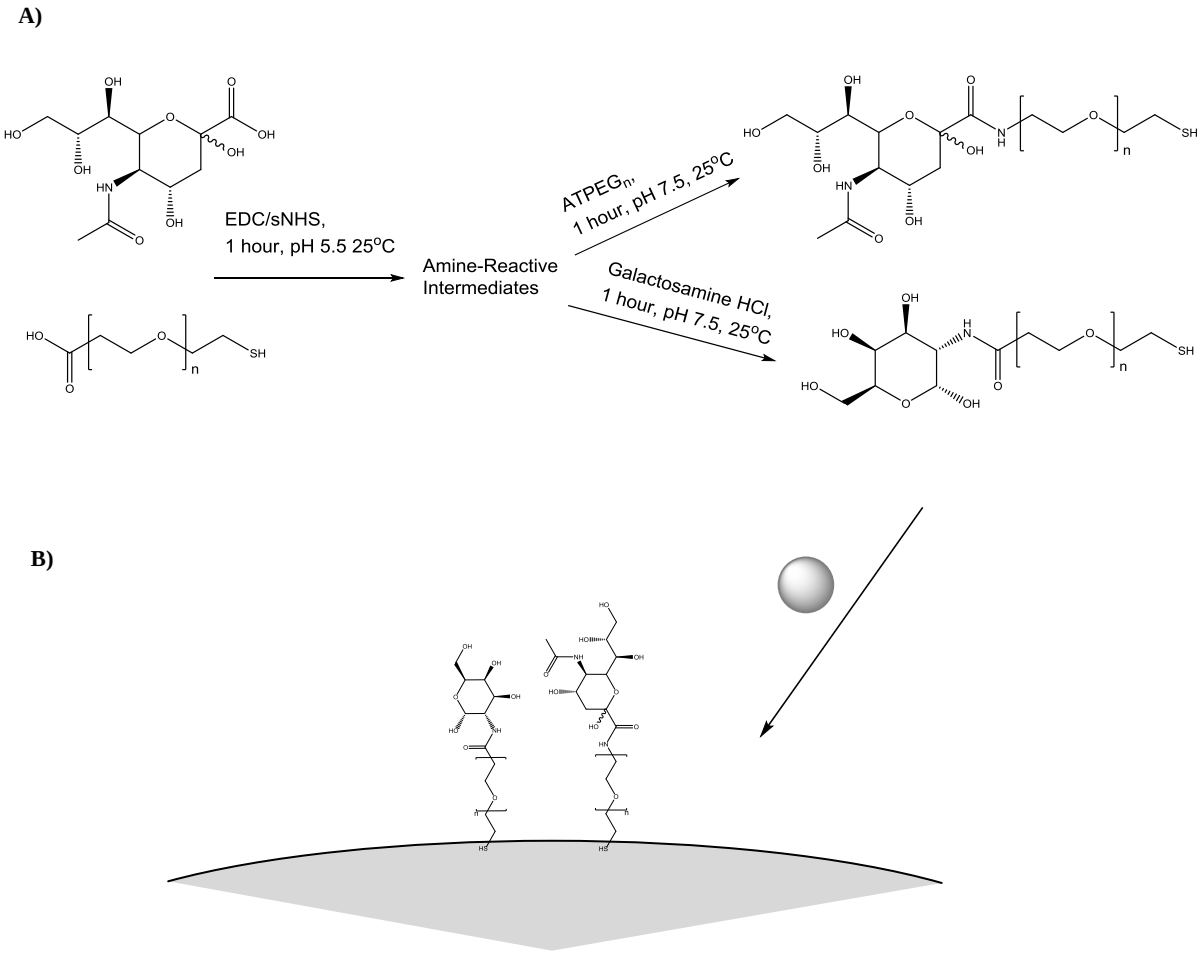

Figure E3. A) Reaction schematic of PEG_nGal and PEG_nSia linkers. B) Subsequent addition of the linkers to the nanoparticles (pre-coated in RB1 - not shown).

7. Characterisation of Linker

The linkers, prepared off-nanoparticle, were characterised by attenuated total reflectance infra-red (ATR-IR) spectroscopy to demonstrate the success of the amide coupling reaction. The linkers were isolated from any excess carbohydrate, EDC or sNHS using C18 spin columns (Thermo Scientific™, Pierce™). Following preparation, the eluted samples (80 μL each) were heated to remove the solvent (70% acetonitrile in dH_2O). Following evaporation, the linkers were re-dissolved in 20 μL dry ethanol to run on the ATR-IR instrument. Each sample was added to the ATR probe so as to allow the ethanol to evaporate, leaving behind the linker residue. The entire sample was added and analysed.

Prior to using the spin columns, 10 mL of glyconanoparticles (either galactose or sialic acid-coated nanoparticles with a 40 μM final linker concentration) were prepared as previously described. These were centrifuged at 4000 rpm for 15 minutes and the supernatant centrifuged at 7000 rpm for 15 minutes. The supernatant from the second centrifugation was discarded and the pellets from each centrifugation step combined and resuspended in HB2. The centrifugation steps were repeated and the pellets from the spin steps combined to give 150 μL of pellets. 152 mM of DTT was added to the pellets and heated at 50 °C for 6 hours then at 40 °C for 16 hours. After this time the resulting red-brown mixture was centrifuged at 13000 rpm for 25 minutes. The supernatant was removed and the pellet was resuspended in 100 μL of dH_2O and centrifuged a second time (with the previous conditions). The second supernatant was combined with the first and this solution was purified using the aforementioned C18 spin columns.

8. Lectin Testing with Nanoparticle Conjugates

Glyconanoparticle test samples (200 μL total volume, comprising a minimum of 190 μL of glyconanoparticle colloid and a maximum of 10 μL lectin/toxin solution to give the desired final concentration of lectin) were analysed by UV-visible extinction spectroscopy, DLS or SERS after mixing with the lectin for at least 30 seconds with gentle mixing.

9. Carbohydrate-Coated Glass Surface Preparation and Testing with Lectins/Glyconanoparticles

The procedure to functionalise epoxy-coated glass slides with carbohydrates is described below.

Experimental

Day 1.

100 mg of $CAPEG_8$ (Mw = 441.51) and $MAPEG_4$ (Mw = 207.27) were dissolved in 1.13 mL and 2.41 mL of DMSO respectively to give 200 mM solutions of each PEG derivative. These were subsequently diluted in DMSO to give 20 mM solution. 1 µL of $CAPEG_8$ or $MAPEG_4$ was diluted in 400 µL of epoxide activation buffer (20mM HEPES buffer, pH 8.9) to a 50 µM solution of PEG derivative. The epoxy-coated glass slide was placed in a 16 well chamber to give distinct sample areas as shown in results figure 86. 10 µL of surface coating PEG (50 µM, CA only or a 25µM/25µM CA/MAPEG mix) was added to each well and the whole glass slide heated at 60 °C for 4 hours. This included a second application of the heterobifunctional PEG solution to each well and then 10 µL addition of 20 mM HEPES buffer, pH 8.9 to keep the slide wet. This was repeated 4 times over 4 hours. Following the 5th application the slide was incubated for 16 hours in a sealed chamber at 50% humidity.

Day 2.

A 2.6 mM glucosamine/galactosamine aqueous solution was prepared by dissolving 1.1 mg of each sugar in 2 mL of 10 mM HEPES buffer, pH 7.4. Any residual PEG was removed from the glass slide by washing each well with 100 µL of 10 mM HEPES buffer, pH 7.4 with 0.05% TWEEN three times and finally with 10 mM MES buffer, pH 6.0 twice more. 2 mg EDC and 2 mg sNHS were each dissolved in 1 mL 10 mM MES buffer, pH 6.0. 20 µL of EDC and sNHS solutions were then rapidly premixed (giving 40 µL) and added to each well and mixed for 1 hour. The EDC/sNHS mixture was removed from each well and 40 µL of the aqueous carbohydrate solution (glucosamine or galactosamine) was added to each well and heated at 60°C for 30 minutes. Additional 10 mM HEPES buffer, pH 7.4 was added to each well, ensuring effective mixing and coverage of the glass with liquid. The slide was shaken for 2 hours and incubated overnight (16 hours) at room temperature in a sealed chamber at 50% humidity.

Day 3.

Each well was washed with 100 µL of 10 mM HEPES buffer, pH 7.4 with 0.05% TWEEN three times and 100 µL of ethanolamine buffer (100 mM HEPES buffer, pH 9.0 with 50 mM ethanolamine and 0.1% SDS) was added to each well. The slide was heated at 60°C for 2 hours. The ethanolamine buffer was removed and each well washed with 100 µL of 10 mM HEPES buffer, pH 7.4 with 0.05% TWEEN, twice. 100 µL of either PEG block solution or 1% BSA blocker was added to the wells and mixed for 2 hours. The blocker was removed and the wells washed twice with 10 mM HEPES buffer, pH 7.4 with 0.2 mM Ca/Mn $(NO_3)_2$,

once with 10 mM HEPES buffer, pH 7.4 with 0.05% TWEEN and twice with 10 mM HEPES buffer, pH 7.4 with 0.2 mM Ca/Mn $(NO_3)_2$. 70 μL of 200 nM lectin solution (ConA or PA-I) was added to the wells and mixed for 1 hour. Each well was rinsed twice with 10 mM HEPES buffer, pH 7.4 with 0.2 mM Ca/Mn$(NO_3)_2$, once with 10 mM HEPES buffer, pH 7.4 with 0.05% TWEEN and twice with 10 mM HEPES buffer, pH 7.4 with 0.2 mM Ca/Mn $(NO_3)_2$. 50 μL of silver citrate glyconanoparticles were added to each well and mixed for 10-15 minutes. Each well was washed with the previous 5 step rinsing and dried under nitrogen.

References

1. E. Smith and G. Dent, *Modern Raman Spectroscopy: A Practical Approach*, John Wiley & Sons Ltd., Chichester, West Sussex., 1st edn., 2005.

2. Y. Li, H. Schluesener and S. Xu, *Gold Bulletin*, 2010, **43**, 29-41.

3. C. R. Steven, G. A. Busby, C. Mather, B. Tariq, M. L. Briuglia, D. A. Lamprou, A. J. Urquhart, M. H. Grant and S. V. Patwardhan, *Journal of Materials Chemistry B*, 2014, **2**, 5028-5042.

4. B. Roldan Cuenya, *Accounts of Chemical Research*, 2012, **46**, 1682-1691.

5. P. E. G. Casillas, C. A. R. Gonzalez and C. A. M. Pérez, *Infrared Spectroscopy of Functionalized Magnetic Nanoparticles*, 2012.

6. C. Buzea, I. Pacheco and K. Robbie, *Biointerphases*, 2007, **2**, MR17-MR71.

7. V. Labhasetwar and D. L. Leslie-Pelecky, in *Biomedical Applications of Nanotechnology*, John Wiley & Sons, Inc., New Jersey, 2007, pp. 1-5.

8. R. Kannan and K. V. Katti, in *Biomedical Applications of Nanotechnology*, John Wiley & Sons, Inc., 2007, pp. 173-189.

9. S. McAughtrie, K. Lau, K. Faulds and D. Graham, *Chemical Science*, 2013, **4**, 3566-3572.

10. D. Craig, S. McAughtrie, J. Simpson, C. McCraw, K. Faulds and D. Graham, *Analytical Chemistry*, 2014, **86**, 4775-4782.

11. S. Zeng, K.-T. Yong, I. Roy, X.-Q. Dinh, X. Yu and F. Luan, *Plasmonics*, 2011, **6**, 491-506.

12. C. A. M. C. F. Niemeyer, *Nanobiotechnology: Concepts, Applications and Perspectives*, Wiley-VCH Verlag GmbH & Co. KGaA, Weinheim, 1st edn edn., 2004.

13. C. A. Mirkin, R. L. Letsinger, R. C. Mucic and J. J. Storhoff, *Nature*, 1996, **382**, 607-609.

References

14. D. Craig, J. Simpson, K. Faulds and D. Graham, *Chemical Communications*, 2013, **49**, 30-32.

15. D. Graham, R. Stevenson, D. G. Thompson, L. Barrett, C. Dalton and K. Faulds, *Faraday Discussions*, 2011, **149**, 291-299.

16. H. J. Chung, C. M. Castro, H. Im, H. Lee and R. Weissleder, *Nat Nano*, 2013, **8**, 369-375.

17. M. A. Syed and S. H. Bokhari, *J Biomed Nanotechnol*, 2011, **7**, 229-237.

18. C. Zhang, Z. Zhang, B. Yu, J. Shi and X. Zhang, *Analytical Chemistry*, 2001, **74**, 96-99.

19. A. G. Barrientos, J. M. de la Fuente, T. C. Rojas, A. Fernandez and S. Penades, *Chemistry*, 2003, **9**, 1909-1921.

20. M. Marradi, M. Martín-Lomas and S. Penadés, in *Advances in Carbohydrate Chemistry and Biochemistry*, ed. H. Derek, Academic Press, 2010, vol. Volume 64, pp. 211-290.

21. P. J. Vikesland and K. R. Wigginton, *Environmental Science & Technology*, 2010, **44**, 3656-3669.

22. D. B. B. Alberts, J. Lewis, M. Raff, K. Roberts, J. D. Watson, *Molecular Biology of the Cell*, Garland Publishing, Taylor and Francis Group, New York, NY, 3rd edn. edn., 1994.

23. T. K. Lindhorst, *Essentials of Carbohydrate Chemistry and Biochemistry*, Wiley-VCH Verlag GmbH & Co. KGaA, Weinheim, 3 edn., 2007.

24. E. Juaristi and G. Cuevas, *The Anomeric Effect*, CRC Press, Boca Raton, 1995.

25. R. Challa, A. Ahuja, J. Ali and R. K. Khar, *AAPS PharmSciTech*, 2005, **6**, E329-357.

26. A. J. Reynolds, A. H. Haines and D. A. Russell, *Langmuir*, 2006, **22**, 1156-1163.

27. I. Bucior and M. M. Burger, *Current Opinion in Structural Biology*, 2004, **14**, 631-637.

References

28. N. C. Reichardt, M. Martin-Lomas and S. Penadés, *Chem. Soc. Rev.*, 2013, **42**.

29. K. J. Mengerink and V. D. Vacquier, *Glycobiology*, 2001, **11**, 37R-43R.

30. C. L. Schofield, R. A. Field and D. A. Russell, *Analytical Chemistry*, 2007, **79**, 1356-1361.

31. C. W. Frevert and P. L. Sannes, *European Respiratory Review*, 2005, **14**, 137-144.

32. S. Reitsma, D. Slaaf, H. Vink, M. M. J. van Zandvoort and M. A. oude Egbrink, *Pflügers Archiv - European Journal of Physiology*, 2007, **454**, 345-359.

33. K. S. Saladin, *Anatomy & physiology : the unity of form and function*, McGraw-Hill, New York, NY, 2012.

34. Q. Yang, C. Kaul and M. Ulbricht, *Langmuir*, 2010, **26**, 5746-5752.

35. J. D. Esko, T. L. Doering and H. Raetz Cr, *Essentials of Glycobiology, 2nd edition*, Cold Spring Harbor Laboratory Press, New York, 2009.

36. N. Sharon and H. Lis, *Glycobiology*, 2004, **14**, 53R-62R.

37. D. C. Kilpatrick, *Biochimica et Biophysica Acta (BBA) - General Subjects*, 2002, **1572**, 187-197.

38. Y.-T. Tseng, H.-T. Chang, C.-T. Chen, C.-H. Chen and C.-C. Huang, *Biosensors and Bioelectronics*, 2011, **27**, 95-100.

39. R. Hamid and A. Masood, *Pakistan Journal of Nutrition*, 2009, **3**, 293-303.

40. L. J. Schep, W. A. Temple, G. A. Butt and M. D. Beasley, *Environment International*, 2009, **35**, 1267-1271.

41. P. Sehgal, M. Khan, O. Kumar and R. Vijayaraghavan, *Food and Chemical Toxicology*, 2010, **48**, 3171-3176.

42. W. J. Judd, *Crit Rev Clin Lab Sci*, 1980, **12**, 171-214.

43. F. Khan, R. H. Khan, A. Sherwani, S. Mohmood and M. A. Azfer, in *Med Sci Monit*, Poland, 2002, vol. 8, pp. RA293-300.

References

44. T. W. Hamelryck, J. G. Moore, M. J. Chrispeels, R. Loris and L. Wyns, *Journal of Molecular Biology*, 2000, **299**, 875-883.

45. V. Sharma and A. Surolia, *Journal of Molecular Biology*, 1997, **267**, 432-445.

46. R. Banerjee, K. Das, R. Ravishankar, K. Suguna, A. Surolia and M. Vijayan, *J Mol Biol*, 1996, **259**, 281-296.

47. S. Kaushik, D. Mohanty and A. Surolia, *Biophys J*, 2009, **96**, 21-34.

48. J. B. Sumner and S. F. Howell, *Journal of Biological Chemistry*, 1936, **115**, 583-588.

49. C. L. Schofield, A. H. Haines, R. A. Field and D. A. Russell, *Langmuir*, 2006, **22**, 6707-6711.

50. H. Jans, X. Liu, L. Austin, G. Maes and Q. Huo, *Analytical Chemistry*, 2009, **81**, 9425-9432.

51. M. M. Ngundi, C. R. Taitt, S. A. McMurry, D. Kahne and F. S. Ligler, *Biosensors and Bioelectronics*, 2006, **21**, 1195-1201.

52. L. Chen and F. Li, *Journal of Virology*, 2013, **87**, 4118-4120.

53. E. A. Merritt, S. Sarfaty, F. V. D. Akker, C. L'Hoir, J. A. Martial and W. G. J. Hol, *Protein Science*, 1994, **3**, 166-175.

54. G. W. G. Sharp, *Annual Review of Medicine*, 1973, **24**, 19-28.

55. B. Isin, P. Doruker and I. Bahar, *Biophys J*, 2002, **82**, 569-581.

56. J. P. Upham, D. Pickett, T. Irimura, E. M. Anders and P. C. Reading, *Journal of Virology*, 2010, **84**, 3730-3737.

57. C. Pacheco-Soares, L. C. Gaziri, W. Loyola and I. Felipe, *Braz J Med Biol Res*, 1992, **25**, 1015-1024.

58. D. G. Nguyen and J. E. K. Hildreth, *European Journal of Immunology*, 2003, **33**, 483-493.

References

59. X. Ji, G. G. Olinger, S. Aris, Y. Chen, H. Gewurz and G. T. Spear, *Journal of General Virology*, 2005, **86**, 2535-2542.

60. I. C. Michelow, C. Lear, C. Scully, L. I. Prugar, C. B. Longley, L. M. Yantosca, X. Ji, M. Karpel, M. Brudner, K. Takahashi, G. T. Spear, R. A. B. Ezekowitz, E. V. Schmidt and G. G. Olinger, *Journal of Infectious Diseases*, 2011, **203**, 175-179.

61. P. Atkins and J. De Paula, *Atkins' Physical Chemistry*, Oxford University Press, Great Clarendon Street, Oxford, OX2 6DP, 8th edn., 2006.

62. M. J. Pelletier, *Ananlytical Applications of Raman Spectroscopy*, Blackwell Science Ltd., Oxford, UK, 2 edn., 1999.

63. Jasco, *Carbon Nanotube Analysis by Raman Spectroscopy*, 2012.

64. J. R. Ferraro and K. Nakamoto, *Introductory Raman Spectroscopy*, Elsevier Science, San Diego, CA, 2 edn., 2003.

65. U. S. Raikar, V. B. Tangod, B. M. Mastiholi and V. J. Fulari, *Optics Communications*, 2011, **284**, 4761-4765.

66. M. Fleischmann, P. J. Hendra and A. J. McQuillan, *Chemical Physics Letters*, 1974, **26**, 163-166.

67. D. L. Jeanmaire and R. P. Van Duyne, *Journal of Electroanalytical Chemistry and Interfacial Electrochemistry*, 1977, **84**, 1-20.

68. M. G. Albrecht and J. A. Creighton, *Journal of the American Chemical Society*, 1977, **99**, 5215-5217.

69. G. McNay, D. Eustace, W. E. Smith, K. Faulds and D. Graham, *Appl. Spectrosc.*, 2011, **65**, 825-837.

70. S. Zeng, D. Baillargeat, H.-P. Ho and K.-T. Yong, *Chemical Society Reviews*, 2014, **43**, 3426-3452.

71. K. L. Kelly, E. Coronado, L. L. Zhao and G. C. Schatz, *The Journal of Physical Chemistry B*, 2002, **107**, 668-677.

72. S. Eustis and M. A. El-Sayed, *Chemical Society Reviews*, 2006, **35**, 209-217.

References

73. J. R. Lombardi and R. L. Birke, *Accounts of Chemical Research*, 2009, **42**, 734-742.

74. K. Faulds, R. P. Barbagallo, J. T. Keer, W. E. Smith and D. Graham, *Analyst*, 2004, **129**, 567-568.

75. M. Umadevi, S. R. Kavitha, P. Vanelle and T. Terme, *Plasmonics*, 2013, **8**, 859-867.

76. L. A. Dick, A. D. McFarland, C. L. Haynes and R. P. Van Duyne, *The Journal of Physical Chemistry B*, 2001, **106**, 853-860.

77. R. C. Ambrosio and A. A. Gewirth, *Analytical Chemistry*, 2010, **82**, 1305-1310.

78. P. Hildebrandt and M. Stockburger, *The Journal of Physical Chemistry*, 1984, **88**, 5935-5944.

79. G. Schmid, *Nanoparticles: From Theory to Application*, Wiley-VCH Verlag GmbH & Co. KGaA, Weinheim, 2nd edn. edn., 2010.

80. S. Thobhani, S. Attree, R. Boyd, N. Kumarswami, J. Noble, M. Szymanski and R. A. Porter, *Journal of Immunological Methods*, 2010, **356**, 60-69.

81. S. G. Spain, L. Albertin and N. R. Cameron, *Chemical Communications*, 2006, 4198-4200.

82. A. MacAskill, D. Crawford, D. Graham and K. Faulds, *Analytical Chemistry*, 2009, **81**, 8134-8140.

83. K. Faulds, F. McKenzie, W. E. Smith and D. Graham, *Angewandte Chemie International Edition*, 2007, **119**, 1861-1863.

84. P. Douglas, K. M. McCarney, D. Graham and W. E. Smith, *Analyst*, 2007, **132**, 865-867.

85. V. V. Mody, R. Siwale, A. Singh and H. R. Mody, *J Pharm Bioallied Sci*, 2010, **2**, 282-289.

86. H. Jans, K. Jans, P.-J. Demeyer, K. Knez, T. Stakenborg, G. Maes and L. Lagae, *Talanta*, 2011, **83**, 1580-1585.

References

87. S. K. Nune, P. Gunda, P. K. Thallapally, Y.-Y. Lin, M. L. Forrest and C. J. Berkland, *Expert opinion on drug delivery*, 2009, **6**, 1175-1194.

88. J. Turkevich, P. C. Stevenson and J. Hillier, *Discussions of the Faraday Society*, 1951, **11**, 55-75.

89. P. C. Lee and D. Meisel, *The Journal of Physical Chemistry*, 1982, **86**, 3391-3395.

90. S. Gross, in *Materials Syntheses*, eds. U. Schubert, N. Hüsing and R. Laine, Springer Vienna, 2008, ch. 21, pp. 155-161.

91. L. Mulfinger, S. D. Solomon, M. Bahadory, A. V. Jeyarajasingam, S. A. Rutkowsky and C. Boritz, *Journal of Chemical Education*, 2007, **84**, 322.

92. K. Song, S. Lee, T. Park and B. Lee, *Korean Journal of Chemical Engineering*, 2009, **26**, 153-155.

93. N. Leopold and B. Lendl, *The Journal of Physical Chemistry B*, 2003, **107**, 5723-5727.

94. S. kheybari, N. Samadi, S. V. Hosseini, A. Fazeli and M. R. Fazeli, *DARU Journal of Pharmaceutical Sciences*, 2010, **18**, 168-172.

95. Z. S. Pillai and P. V. Kamat, *The Journal of Physical Chemistry B*, 2003, **108**, 945-951.

96. E. Rodriguez-Leon, R. Iniguez-Palomares, R. E. Navarro, R. Herrera-Urbina, J. Tanori, C. Iniguez-Palomares and A. Maldonado, *Nanoscale Res Lett*, 2013, **8**, 318.

97. J. H. F. E. Hutter, *Adv. Mater.*, 2004, **16**, 1685-1706.

98. E. Petryayeva and U. J. Krull, *Analytica Chimica Acta*, 2011, **706**, 8-24.

99. G. Emmerich, Surface Plasmon Resonance: Technology Overview and Practical Applications, https://gregemmerich.wordpress.com/2012/11/16/surface-plasmon-resonance-technology-overview-and-practical-applications/).

100. G. Mie, *Annalen der Physik*, 1908, **330**, 377-445.

References

101. M. M. Alvarez, J. T. Khoury, T. G. Schaaff, M. N. Shafigullin, I. Vezmar and R. L. Whetten, *The Journal of Physical Chemistry B*, 1997, **101**, 3706-3712.

102. S. K. Ghosh and T. Pal, *Chem Rev*, 2007, **107**, 4797-4862.

103. S. Nath, S. Ghosh, S. Kundu, S. Praharaj, S. Panigrahi and T. Pal, *Journal of Nanoparticle Research*, 2006, **8**, 111-116.

104. S. Schlücker, *ChemPhysChem*, 2009, **10**, 1344-1354.

105. I. Lee, S. W. Han and K. Kim, *Journal of Raman Spectroscopy*, 2001, **32**, 947-952.

106. A. O. Pinchuk, A. M. Kalsin, B. Kowalczyk, G. C. Schatz and B. A. Grzybowski, *The Journal of Physical Chemistry C*, 2007, **111**, 11816-11822.

107. B. V. Derjaguin and L. Landau, *Acta Phys. Chim. URSS*, 1941, **14**, 633-662.

108. C. E. Marshall, *Journal of Polymer Science*, 1949, **4**, 413-414.

109. R. Lévy, N. T. K. Thanh, R. C. Doty, I. Hussain, R. J. Nichols, D. J. Schiffrin, M. Brust and D. G. Fernig, *Journal of the American Chemical Society*, 2004, **126**, 10076-10084.

110. X. Wang, O. Ramstrom and M. Yan, *Analyst*, 2011, **136**, 4174-4178.

111. Y. Fan, Z. Liu, L. Wang and J. Zhan, *Nanoscale Research Letters*, 2009, **4**, 1230-1235.

112. H. Huang and X. Yang, *Carbohydrate Research*, 2004, **339**, 2627-2631.

113. J. Sagiv, *Journal of the American Chemical Society*, 1980, **102**, 92-98.

114. R. G. Nuzzo and D. L. Allara, *Journal of the American Chemical Society*, 1983, **105**, 4481-4483.

115. C. Vericat, M. E. Vela, G. Benitez, P. Carro and R. C. Salvarezza, *Chemical Society Reviews*, 2010, **39**, 1805-1834.

116. V. Dugas, A. Elaissari and Y. Chevalier, in *Recognition Receptors in Biosensors*, ed. M. Zourob, Springer New York, 2010, ch. 2, pp. 47-134.

References

117. Z. Li, R. Jin, C. A. Mirkin and R. L. Letsinger, *Nucleic Acids Research*, 2002, **30**, 1558-1562.

118. S. D. Schwab, R. L. McCreery and F. T. Gamble, *Analytical Chemistry*, 1986, **58**, 2486-2492.

119. K. Faulds, F. McKenzie, W. E. Smith and D. Graham, *Angewandte Chemie*, 2007, **119**, 1861-1863.

120. T. Chen, H. Wang, G. Chen, Y. Wang, Y. Feng, W. S. Teo, T. Wu and H. Chen, *ACS Nano*, 2010, **4**, 3087-3094.

121. K. L. Rule and P. J. Vikesland, *Environmental Science & Technology*, 2009, **43**, 1147-1152.

122. R. A. Halvorson and P. J. Vikesland, *Environmental Science & Technology*, 2010, **44**, 7749-7755.

123. X. Huang and J. Barchi Joseph, eds., *Petite and Sweet: Glyco-Nanotechnology as a Bridge to New Medicines*, American Chemical Society, 2011.

124. S. Gelperina, K. Kisich, M. D. Iseman and L. Heifets, *Am J Respir Crit Care Med*, 2005, **172**, 1487-1490.

125. D. C. Hone, A. H. Haines and D. A. Russell, *Langmuir*, 2003, **19**, 7141-7144.

126. M. J. Marin, A. Rashid, M. Rejzek, S. A. Fairhurst, S. A. Wharton, S. R. Martin, J. W. McCauley, T. Wileman, R. A. Field and D. A. Russell, *Organic & Biomolecular Chemistry*, 2013, **11**, 7101-7107.

127. K. R. Lim, J.-M. Park, H. N. Choi and W.-Y. Lee, *Microchemical Journal*, 2013, **106**, 154-159.

128. L. Ding, R. Qian, Y. Xue, W. Cheng and H. Ju, *Analytical Chemistry*, 2010, **82**, 5804-5809.

129. G. V. P. Kumar, *Journal of Nanophotonics*, 2012, **6**, 064503-064501-064503-064520.

130. J. Wang, T. Duan, L. Sun, D. Liu and Z. Wang, *Analytical Biochemistry*, 2009, **392**, 77-82.

References

131. A. Sharma, S. Sharma and G. K. Khuller, *J Antimicrob Chemother*, 2004, **54**, 761-766.

132. G. Obaid, I. Chambrier, M. J. Cook and D. A. Russell, *Angewandte Chemie International Edition*, 2012, **51**, 6158-6162.

133. Y. C. Liu, H. Y. Yen, C. Y. Chen, C. H. Chen, P. F. Cheng, Y. H. Juan, K. H. Khoo, C. J. Yu, P. C. Yang, T. L. Hsu and C. H. Wong, *Proc Natl Acad Sci U S A*, 2011, **108**, 11332-11337.

134. R. Pacis, M. Pilat, K. Yamazaki and K. Pienta, *Int J Oncol*, 1995, **7**, 1349-1354.

135. V. E. Bischel, L. A. Liotta and E. F. Petricoin, *Cancer J.*, 2001, **7**, 69.

136. M. J. Garnett, J. Edelman, S. J. Heidorn, C. D. Greenman, A. Dastur, K. W. Lau, P. Greninger, I. R. Thompson, X. Luo, J. Soares, Q. S. Liu, F. Iorio, D. Surdez, L. Chen, R. J. Milano, G. R. Bignell, A. T. Tam, H. Davies, J. A. Stevenson, S. Barthorpe, S. R. Lutz, F. Kogera, K. Lawrence, A. McLaren-Douglas, X. Mitropoulos, T. Mironenko, H. Thi, L. Richardson, W. J. Zhou, F. Jewitt, T. H. Zhang, P. O'Brien, J. L. Boisvert, S. Price, W. Hur, W. J. Yang, X. M. Deng, A. Butler, H. G. Choi, J. Chang, J. Baselga, I. Stamenkovic, J. A. Engelman, S. V. Sharma, O. Delattre, J. Saez-Rodriguez, N. S. Gray, J. Settleman, P. A. Futreal, D. A. Haber, M. R. Stratton, S. Ramaswamy, U. McDermott and C. H. Benes, *Nature*, 2012, **483**, 570.

137. W. N. Hait, *Cancer Res.*, 2009, **69**, 1263.

138. J. N. Andersen, S. Sathyanarayanan, A. Di Bacco, A. Chi, T. Zhang, A. H. Chen, B. Dolinski, M. Kraus, B. Roberts, W. Arthur, R. A. Klinghoffer, D. Gargano, L. Li, I. Feldman, B. Lynch, J. Rush, R. C. Hendrickson, P. Blume-Jensen and C. P. Paweletz, *Sci Transl Med*, 2010, **2**, 43ra55.

139. A. Fadiel and F. Naftolin, *Int. Arch. Biosci*, 2003, 1111-1121.

140. M. Schena, D. Shalon, R. W. Davis and P. O. Brown, *Science*, 1995, **270**, 467-470.

141. M. Raitio, K. Lindroos, M. Laukkanen, T. Pastinen, P. Sistonen, A. Sajantila and A.-C. Syvänen, *Genome Research*, 2001, **11**, 471-482.

142. S. Sun, Y.-W. Huang, P. Yan, T. Huang and S. Lin, *BioData Mining*, 2011, **4**, 13.

References

143. S. Pillai and S. Chellappan, in *Chromatin Protocols*, ed. S. P. Chellappan, Humana Press, 2009, vol. 523, ch. 23, pp. 341-366.

144. R. Rappuoli, *Proceedings of the National Academy of Sciences*, 2000, **97**, 13467-13469.

145. N. M. Jawhar, *Ann Saudi Med*, 2009, **29**, 123-127.

146. B. B. Haab, *Proteomics*, 2003, **3**, 2116-2122.

147. S. Park, J. C. Gildersleeve, O. Blixt and I. Shin, *Chem Soc Rev*, 2013, **42**, 4310-4326.

148. *Microarrays on the slide*, Macmillan Magazines Ltd., 2000.

149. Z.-l. Zhi, A. K. Powell and J. E. Turnbull, *Analytical Chemistry*, 2006, **78**, 4786-4793.

150. J. Heimburg-Molinaro, X. Song, D. F. Smith and R. D. Cummings, in *Current Protocols in Protein Science*, John Wiley & Sons, Inc., 2001.

151. L. Ban, N. Pettit, L. Li, A. D. Stuparu, L. Cai, W. Chen, W. Guan, W. Han, P. G. Wang and M. Mrksich, *Nat Chem Biol*, 2012, **8**, 769-773.

152. M. Fais, R. Karamanska, S. Allman, S. A. Fairhurst, P. Innocenti, A. J. Fairbanks, T. J. Donohoe, B. G. Davis, D. A. Russell and R. A. Field, *Chemical Science*, 2011, **2**, 1952-1959.

153. J. Stevens, O. Blixt, T. M. Tumpey, J. K. Taubenberger, J. C. Paulson and I. A. Wilson, *Science*, 2006, **312**, 404-410.

154. L. M. Chen, P. Rivailler, J. Hossain, P. Carney, A. Balish, I. Perry, C. T. Davis, R. Garten, B. Shu, X. Xu, A. Klimov, J. C. Paulson, N. J. Cox, S. Swenson, J. Stevens, A. Vincent, M. Gramer and R. O. Donis, *Virology*, 2011, **412**, 401-410.

155. S. E. Tully, M. Rawat and L. C. Hsieh-Wilson, *Journal of the American Chemical Society*, 2006, **128**, 7740-7741.

156. O. Blixt, I. Boos and U. Mandel, in *Anticarbohydrate Antibodies*, eds. P. Kosma and S. Müller-Loennies, Springer Vienna, 2012, ch. 12, pp. 283-306.

References

157. J. Hirabayashi, M. Yamada, A. Kuno and H. Tateno, *Chemical Society Reviews*, 2013, **42**, 4443-4458.

158. H. H. Wandall, O. Blixt, M. A. Tarp, J. W. Pedersen, E. P. Bennett, U. Mandel, G. Ragupathi, P. O. Livingston, M. A. Hollingsworth, J. Taylor-Papadimitriou, J. Burchell and H. Clausen, *Cancer Res*, 2010, **70**, 1306-1313.

159. D. Graham, B. J. Mallinder, D. Whitcombe, N. D. Watson and W. E. Smith, *Analytical Chemistry*, 2002, **74**, 1069-1074.

160. L. L. Jantzie, V. A. M. I. Tanay and K. G. Todd, in *Handbook of Neurochemistry and Molecular Neurobiology*, eds. A. Lajtha, G. Baker, S. Dunn and A. Holt, Springer US, 2007, ch. 8, pp. 193-218.

161. A. Huefner, W.-L. Kuan, R. A. Barker and S. Mahajan, *Nano Letters*, 2013, **13**, 2463-2470.

162. T. Donnelly, W. E. Smith, K. Faulds and D. Graham, *Chemical Communications*, 2014, **50**, 12907-12910.

163. A. Tiwari and A. Tiwari, CRC Press, Boca Raton, FL, USA, 2013.

164. G. McAnally, C. McLaughlin, R. Brown, D. C. Robson, K. Faulds, D. R. Tackley, W. E. Smith and D. Graham, *Analyst*, 2002, **127**, 838-841.

165. G. T. Hermanson, in *Bioconjugate Techniques (Third edition)*, ed. G. T. Hermanson, Academic Press, Boston, 2013, pp. 549-587.

166. D. Bartczak and A. G. Kanaras, *Langmuir*, 2011, **27**, 10119-10123.

167. A. J. Lomant and G. Fairbanks, *Journal of Molecular Biology*, 1976, **104**, 243-261.

168. J. V. Staros, R. W. Wright and D. M. Swingle, *Analytical Biochemistry*, 1986, **156**, 220-222.

169. Z. Grabarek and J. Gergely, in *Anal Biochem*, United States, 1990, vol. 185, pp. 131-135.

170. Q. P. Lei, D. H. Lamb, A. G. Shannon, X. Cai, R. K. Heller, M. Huang, E. Zablackis, R. Ryall and P. Cash, *Journal of Chromatography B*, 2004, **813**, 103-112.

References

171. W. P. Wuelfing, S. M. Gross, D. T. Miles and R. W. Murray, *Journal of the American Chemical Society*, 1998, **120**, 12696-12697.

172. J. P. Camden, J. A. Dieringer, Y. Wang, D. J. Masiello, L. D. Marks, G. C. Schatz and R. P. Van Duyne, *Journal of the American Chemical Society*, 2008, **130**, 12616-12617.

173. M. Ghosh, B. K. Bachhawat and A. Surolia, *Biochemical Journal*, 1979, **183**, 185-188.

174. B. Kim, G. S. Cha and M. E. Meyerhoff, *Anal Chem*, 1990, **62**, 2663-2668.

175. A. Pusztai, *Plant Lectins*, Cambridge University Press, 1991.

176. S. Rao, F. Kelly, A. Woodruff, Y. Agroskin and C. Pohl, *Dionex Corporation*, 2011.

177. A. A. Jeyaprakash, S. Katiyar, C. P. Swaminathan, K. Sekar, A. Surolia and M. Vijayan, *J Mol Biol*, 2003, **332**, 217-228.

178. C. P. Stowell and Y. C. Lee, in *Advances in Carbohydrate Chemistry and Biochemistry*, Academic Press, 1980, vol. Volume 37, pp. 225-281.

179. Z. Barghouthi and S. Amereih, *Water SA*, 2012, **38**, 543-548.

180. B. Cummins, J. Simpson, Z. Gryczynski, T. J. Sørensen, B. W. Laursen, D. Graham, D. Birch and G. Coté, *SPIE Conference Proceedings (2014)*, 2014, 89510-89517.

181. K. Aslan, J. R. Lakowicz and C. D. Geddes, *Analytical Biochemistry*, 2004, **330**, 145-155.

182. G. Danaei, M. M. Finucane, Y. Lu, G. M. Singh, M. J. Cowan, C. J. Paciorek, J. K. Lin, F. Farzadfar, Y. H. Khang, G. A. Stevens, M. Rao, M. K. Ali, L. M. Riley, C. A. Robinson and M. Ezzati, *Lancet*, 2011, **378**, 31-40.

183. C. D. Mathers and D. Loncar, *PLoS Med*, 2006, **3**, e442.

184. K. Tonyushkina and J. H. Nichols, *J Diabetes Sci Technol*, 2009, **3**, 971-980.

185. S. Vaddiraju, D. J. Burgess, I. Tomazos, F. C. Jain and F. Papadimitrakopoulos, *Journal of Diabetes Science and Technology*, 2010, **4**, 1540-1562.

References

186. F. J. Arregui, *Sensors Based on Nanostructured Materials*, Springer US, 2010.

187. K. Tian, M. Prestgard and A. Tiwari, *Mater Sci Eng C Mater Biol Appl*, 2014, **41**, 100-118.

188. J. Luo, S. Jiang, H. Zhang, J. Jiang and X. Liu, *Analytica Chimica Acta*, 2012, **709**, 47-53.

189. D. Zhai, B. Liu, Y. Shi, L. Pan, Y. Wang, W. Li, R. Zhang and G. Yu, *ACS Nano*, 2013, **7**, 3540-3546.

190. B. M. Cummin, J. Lim, E. E. Simanek, M. V. Pishko and G. L. Coté, *Biomedical Optics Express*, 2011, **2**, 1243-1257.

191. B. Cummins, J. Simpson, Z. Gryczynski, T. J. Sørensen, B. W. Laursen, D. Graham, D. Birch and G. Coté, 2014.

192. R. G. Spiro, *Journal of Biological Chemistry*, 1960, **235**, 2860-2869.

193. H. Otsuka, Y. Akiyama, Y. Nagasaki and K. Kataoka, *Journal of the American Chemical Society*, 2001, **123**, 8226-8230.

194. W. Ma, M. Sun, L. Xu, L. Wang, H. Kuang and C. Xu, *Chemical Communications*, 2013, **49**, 4989-4991.

195. I.-B. Kim, J. N. Wilson and U. H. F. Bunz, *Chemical Communications*, 2005, **0**, 1273-1275.

196. J. G. Kenimer, P. G. Probst, A. B. Karpas, D. L. Burns and H. R. Kaslow, *Dev Biol Stand*, 1991, **73**, 133-141.

197. CDC, Centre for Disease Control and Prevention - Laboratory Testing for Cholera, 1993, pp. 62-88.

198. D. L. Evers, J. He, J. T. Mason and T. J. O'Leary, *Journal of Clinical Microbiology*, 2010, **48**, 4620-4622.

199. C. Kaittanis, S. Santra and J. M. Perez, *Advanced Drug Delivery Reviews*, 2010, **62**, 408-423.

References

200. J. Simpson, D. Craig, K. Faulds and D. Graham, *Nanoscale Horizons*, 2016, **1**, 60-63.

201. J. H. Seo, C. S. Kim and H. J. Cha, *Analyst*, 2013, **138**, 6924-6929.

202. M. Bergstrom, S. Liu, K. L. Kiick and S. Ohlson, *Chem Biol Drug Des*, 2009, **73**, 132-141.

203. U. Tuteja, S. Kumar, J. Shukla, J. Kingston and H. V. Batra, *Journal of Medical Microbiology*, 2007, **56**, 1340-1345.

204. V. L. Schmit, R. Martoglio and K. T. Carron, *Analytical Chemistry*, 2012, **84**, 4233-4236.

205. A. R. de Boer, C. H. Hokke, A. M. Deelder and M. Wuhrer, *Glycoconj J*, 2008, **25**, 75-84.

206. M. D. Disney and P. H. Seeberger, *Chem Biol*, 2004, **11**, 1701-1707.

207. D. Wang, G. T. Carroll, N. J. Turro, J. T. Koberstein, P. Kovac, R. Saksena, R. Adamo, L. A. Herzenberg and L. Steinman, *Proteomics*, 2007, **7**, 180-184.

208. Matthias A. Oberli, M.-L. Hecht, P. Bindschädler, A. Adibekian, T. Adam and Peter H. Seeberger, *Chemistry & Biology*, 2011, **18**, 580-588.

209. O. Oyelaran, Q. Li, D. Farnsworth and J. C. Gildersleeve, *J Proteome Res*, 2009, **8**, 3529-3538.

210. J. L. de Paz, D. Spillmann and P. H. Seeberger, *Chem Commun (Camb)*, 2006, 3116-3118.

211. X. Song, Y. Lasanajak, B. Xia, J. Heimburg-Molinaro, J. M. Rhea, H. Ju, C. Zhao, R. J. Molinaro, R. D. Cummings and D. F. Smith, *Nat Methods*, 2011, **8**, 85-90.

212. X. Zhou, C. Turchi and D. Wang, *Journal of proteome research*, 2009, **8**, 5031-5040.

213. D. Wang, S. Liu, B. J. Trummer, C. Deng and A. Wang, *Nat Biotechnol*, 2002, **20**, 275-281.

References

214. L. Moni, G. Pourceau, J. Zhang, A. Meyer, S. Vidal, E. Souteyrand, A. Dondoni, F. Morvan, Y. Chevolot, J.-J. Vasseur and A. Marra, *ChemBioChem*, 2009, **10**, 1369-1378.

215. Y. Guo, H. Feinberg, E. Conroy, D. A. Mitchell, R. Alvarez, O. Blixt, M. E. Taylor, W. I. Weis and K. Drickamer, *Nat Struct Mol Biol*, 2004, **11**, 591-598.

216. F.-T. Liu and G. A. Rabinovich, *Nat Rev Cancer*, 2005, **5**, 29-41.

217. A. Leppanen, S. Stowell, O. Blixt and R. D. Cummings, *J Biol Chem*, 2005, **280**, 5549-5562.

218. J. Stevens, O. Blixt, L. Glaser, J. K. Taubenberger, P. Palese, J. C. Paulson and I. A. Wilson, *J Mol Biol*, 2006, **355**, 1143-1155.

219. C. S. Kim, J. H. Seo and H. J. Cha, *Analytical Chemistry*, 2012, **84**, 6884-6890.

220. Y. Fang, A. G. Frutos and J. Lahiri, *Langmuir*, 2002, **19**, 1500-1505.

221. W. Kim, F. K. Tengra, Z. Young, J. Shong, N. Marchand, H. K. Chan, R. C. Pangule, M. Parra, J. S. Dordick, J. L. Plawsky and C. H. Collins, *PLoS One*, 2013, **8**, e62437.

222. A. Balcht and R. Smith, *Journal*, 1994, 83-84.

223. P. D. Lister, D. J. Wolter and N. D. Hanson, *Clinical Microbiology Reviews*, 2009, **22**, 582-610.

224. B. K. Gorityala, Z. Lu, M. L. Leow, J. Ma and X.-W. Liu, *Journal of the American Chemical Society*, 2012, **134**, 15229-15232.